Flow Dynamics in Human Aorta with Coexisting Models of Bicuspid Aortic Stenosis and Coarctation of the Aorta

Zahra Keshavarz-Motamed

A Thesis

in

the Department

of

Mechanical and Industrial Engineering

Presented in Partial Fulfillment of the Requirement

for the Degree of Doctor of Philosophy

at Concordia University

Montréal, Québec, Canada, 2011

December 2011

CONCORDIA UNIVERSITY
SCHOOL OF GRADUATE STUDIES

This is to certify that the thesis prepared

By: Zahra Keshavarz-Motamed

Entitled: Flow Dynamics in Human Aorta with Coexisting Models of Bicuspid Aortic Stenosis and Coarctation of the Aorta

and submitted in partial fulfillment of the requirements for the degree of

Doctor of Philosophy

complies with the regulations of the University and meets the accepted standards with respect to originality and quality.

Signed by the final examining committee:

Dr. R. Soleymani — Chair

Dr. L. G. Mongeau — External Examiner

Dr. S. Li — External to Program

Dr. G. H. Vatistas — Examiner

Dr. H. D. Ng — Examiner

Dr. L. Kadem — Thesis Supervisor

Approved by

Chair of Department or Graduate Program Director

Dean of Faculty

Flow dynamics in human aorta with coexisting models of bicuspid aortic stenosis and coarctation of the aorta

Zahra Keshavarz Motamed, Ph.D.

Concordia University, 2011

ABSTRACT

Coarctation of the aorta (COA) is an obstruction of the aorta and is usually associated with bicuspid and tricuspid aortic valve stenosis (AS). The main objective of this work is to understand the hemodynamic of COA from different perspectives. This was performed using a global approach including: numerical simulations, mathematical lumped parameter modeling and experimental measurements.

Numerous investigations pointed to a relationship between the genesis and the progression of cardiovascular disease and the locally irregular flow occurring at the diseased zone. Therefore, to examine the relationship between arterial disease and hemodynamics conditions, a joint experimental and numerical investigation was performed to understand physics of fluid flow of COA.

When COA coexists with AS, the left ventricle faces a double hemodynamic load: a valvular load plus a vascular load. First, a formulation describing the instantaneous net pressure gradient through COA was introduced and the predictions compared to *in vitro* results. The model was then used to determine left ventricular work induced by coexisting aortic stenosis and coarctation with different severities. The suggested model can be used to guide the choice of optimal operative procedure (aortic valve replacement and/or coarctation repaired surgery) and to predict the potential outcome for such patients.

Early detection and accurate estimation of COA severity is the most important predictor of successful long-term outcome. However, current clinical parameters used for the evaluation of the severity of COA have several limitations. In this study, first, we evaluated the limitations of current existing parameters (Catheter trans-COA pressure gradients and Doppler echocardiographic trans-COA pressure gradients) for the evaluation of the severity of COA. Then, we suggested a new approach based on COA Doppler velocity index and COA effective orifice area capable of predicting more accurately the severity of COA.

In conclusion, this study investigated the flow dynamics of COA and development of a lumped parameter model, based on non-invasive measurements, capable of accurately investigating the impact of coexisting AS and COA on left ventricular workload. In addition, this study proposed two innovative approaches to evaluate the severity of COA correctly.

Dedicated to the ones

whose unconditional love is absolutely incredible

who are my inspiration in life

who gave me the strength and courage

and without them this could not be a reality

To my beloved parents

Bahram & Eshrat

To my beloved husband

Nima

To my wonderful twin daughters

Armita & Vianna

ACKNOWLEDGEMENT

First I would like to express my gratitude to and respect for Dr. Lyes Kadem for his professional supervision and patient guidance during different phases of my research. He gave me very interesting questions at first and then let me free to find my way to the target. Although I was free in choosing the path, I always had the luxury of his comments and hints. Writing this thesis was definitely not possible without his technical, moral and financial support.

I am very honored to have very distinguished researchers in my PhD defence committee. I would like to thank Dr. Luc Guy Mongeau for accepting to be the external member of my PhD defence committee and for his valuable comments. I would like to thank the committee members of my thesis, Dr. Hoi Dick Ng, Dr. Georgios H. Vatistas and Dr. Samuel Li for their times, support and constructive comments. I especially thank Dr. Hoi Dick Ng for his great comments and his continuous attention and support, Dr. Georgios H. Vatistas for all things that I learned from him and Dr. Samuel Li for his helpful comments.

My thanks to friends and colleagues at Concordia University for making my graduate studies a joyful journey to remember and especially to Julio Garcia with whom I had wonderful collaborations. Mechanical engineering department at Concordia will always be a sweet memory for me because of Leslie, Arlene, Maureen, Sophie, Robert and Rudi.

The last, but of course not the least, my warmest appreciation goes to my family. Words cannot describe my gratitude to my parents, Bahram and Eshrat, for their

sacrifice and their unconditional love. My deepest gratitude goes to my husband, Nima. His incredible love has always been a great source of support and motivation for me. I am very deeply grateful of my brothers, Pejman, Payam and Pouyan for their never ending supports, encouragements and for making the world a much happier place for me. To my family, I owe all that I have ever accomplished.

Praise Lord of Life, God the Wise	به نام خداوند جان و خرد
A worthier notion shall not arise	کزین برتر اندیشه برنگذرد
The God of fame in whom powers reside	خداوند نام و خداوند جای
Provider, Sustainer, the Ultimate Guide.	خداوند روزی ده رهنمای
Creator of the world & the orderly universal run	خداوند کیوان و گردان سپهر
The light giver to the Moon, Mercury and Sun.	فروزنده ماه و ناهید و مهر
Transcends all name, label and notion	ز نام و نشان و گمان برتر ست
Is the author of form and motion	نگارنده ی بر شده پیکر ست
Capable is he who is wise	توانا بود هر که دانا بود
Happiness from wisdom will arise.	ز دانش دل پیر برنا بود
The Epic of the Kings, by Ferdowsi, Persian poet (935-1020),	شاهنامه فردوسی

TABLE OF CONTENTS

LIST OF FIGURES

LIST OF TABLES

NOMENCLATURE

a	Internal radius of the curved tube (cm)
A	Area (cm^2)
C	Compliance (ml/mmHg)
De	Dean number
R	Resistance (mmHg.s/ml)
L	Inductance ($mmHg.s^2/ml$)
$E(t)$	Time varying elastance (mmHg/ml)
R	Radius of curvature (cm)
Q	Flow rate (L/min)
V	Velocity (m/s)
Re	Reynolds number
T	Cardiac cycle period (s)
P	Pressure (mmHg)
S	Rate of strain tensor (s^{-1})
Ω	Rotation tensor (s^{-1})
ω	Frequency (s^{-1})
μ	Dynamic viscosity (Pa.s)
ρ	Density (kg/m^3)

τ, ϕ	Wall shear stress (Pa)
r	Refinement ratio
p	Apparent order
ϕext	Extrapolated value (Pa)
e_a	Apparent error
e_{ext}	Extrapolated error
GCI_{fine}	Fine-grid convergence index
ε	Discretization error

ABBREVIATION

AS	Aortic stenosis
COA	Coarctation of the aorta
BAV	Bicuspid aortic valve
CFD	Computational fluid dynamics
CO	Cardiac output
DVI	Doppler velocity index
EOA	Effective orifice area
E_LCo	Valvular energy loss coefficient
ECs	Endothelial cells
HR	Heart rate
LV	Left ventricle
LVEDV	Left-ventricular end-diastolic volume
MRI	Magnetic resonance imaging
PIV	Particle image velocimetry
PtoP	Peak to peak
SW	Stroke work
SV	Stroke volume

SSFP	Steady-state free precession
TAWSS	Time-averaged wall shear stress
TCPG	Trans-coarctation pressure gradient
TPG	Transvalvular pressure gradient
TR/TE	Repetition time/Echo time
VTI	Velocity-time integral
WSS	Wall shear stress
WSSG	Spatial gradient of wall shear stress
OSI	Oscillatory shear index

Chapter 1

1. Introduction

Oxygen-rich blood enters the aorta, the largest artery in the body, from the left ventricle. Blood flow crosses the aortic valve and is directed towards the aortic arch arteries and the descending aorta. The aortic arch arteries include brachiocephalic, left common carotid, and left subclavian arteries which supply blood to the head and upper body. Figure 1.1 illustrates a healthy human aorta with its main anatomic features.

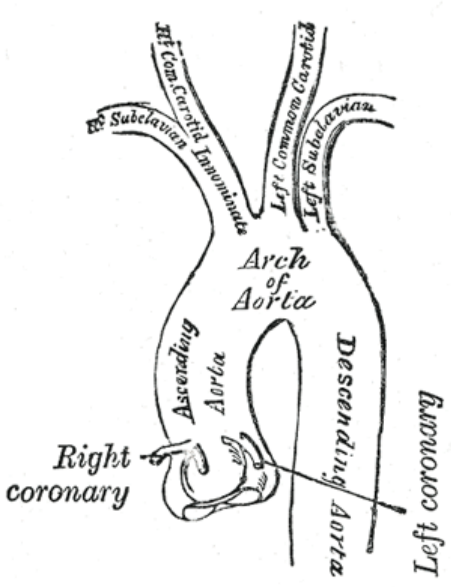

Figure 1.1. Main features of healthy human aorta (http://www.theodora.com/anatomy/the_aorta.html)

Coarctation of the aorta (COA) is a congenital heart disease characterized by a narrowing of the isthmus zone, the section of the descending aorta distal to the left subclavian artery (Fig 1.2). Coarctation of the aorta accounts for 5%-10% of all

congenital heart diseases, represents 7% of critically ill infants with heart disease (Secchi et al., 2009) and is more common in males than in females (2:1 ratio).

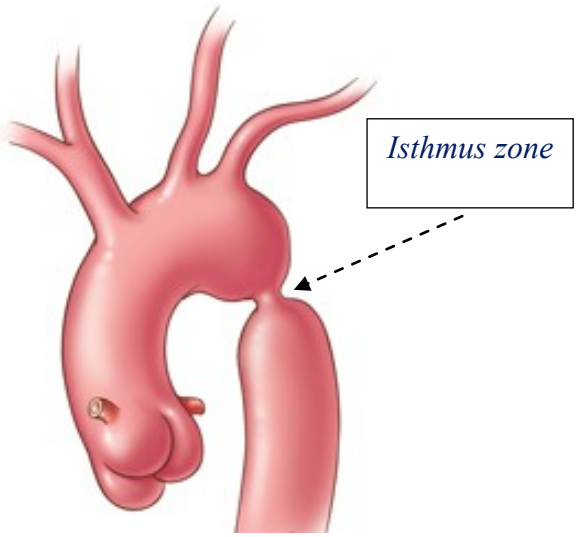

Figure 1.2. Coarctation of the aorta

Figure 1.3. Aneurysm

(http://www.uth.tmc.edu/cvs/patient-care/aortic-surgery.html)

The most common symptoms associated with congenital aortic coarctation are hypertension in the vasculature proximal to the coarctation and insufficient blood flow distal to the coarctation. Long standing hypertension in the upper vasculature may cause headaches, dizziness, blurred vision as well as more severe cerebrovascular and cardiac events. Reduced blood flow distal to the coarctation can lead to leg weakness, pain when exercising and underdevelopment of the lower limbs. Thus, early detection and accurate estimation of COA severity are of primary importance. However, some individuals may not present any of these symptoms until later in life. If the lesion is left untreated, life expectancy is shortened considerably. Accordingly, 60% of adults over 40 years old with uncorrected COA have symptoms

of heart failure, 75% of these patients die by the age of 50 and 90% by the age of 60 (Brickner et al., 2000).

Coarctation of the aorta can be simple (isolated defect) or complex (associated with other cardiac defects). In the majority of cases, COA is associated with a bicuspid aortic valve (20 to 85%) (Grotenhuis and Roos, 2011). Bicuspid aortic valve occurs due to inadequate production of fibrillin-1 during valvulogenesis and complex developmental pathology which causes the fusion of two normal cusps (Tadros et al., 2009) (Fig. 1.4). The presence of bicuspid aortic valve significantly increases the risks of aortic dissection. Indeed, when bicuspid aortic valve was present with COA, 50% of patients had a dissection of the aorta.

Depending on the severity of COA, surgery is often the primary method for repairing the coarctation (see section 2). However, patients with coarctation intervention require close follow-up because of postsurgical acute complications, (1) hypertension accompanied by an increase in aortic medial collagen and a decrease in smooth muscle that exists in 11% to 68% of patients after successful repair, (2) recoarctation at the site of surgical repair estimated to occur in up to 40% of patients after intervention (Araoz et al., 2003), (3) aneurysm (aorta enlargement) involving abnormal dilation (Fig. 1.3), thinning of the vessel wall and finally aorta rupture, has been observed, in particular, with those patients previously undergoing surgical treatment.

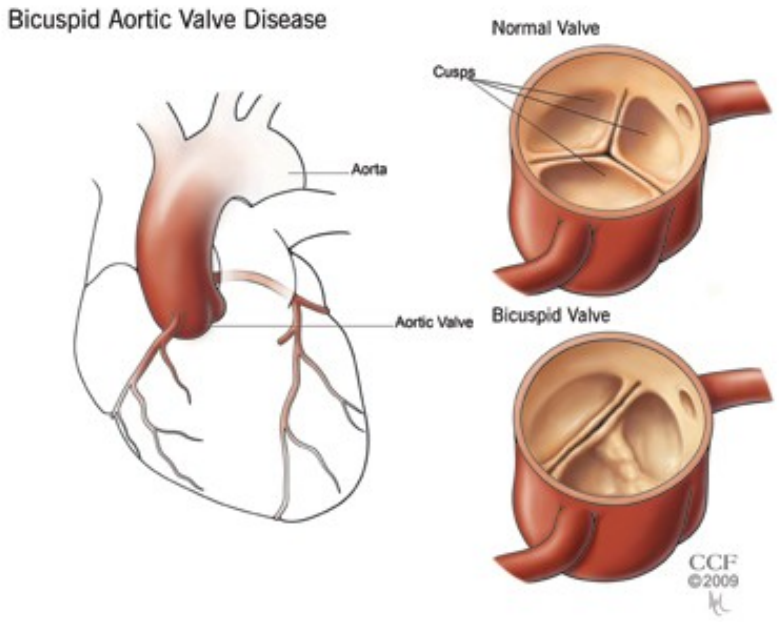

Figure 1.4. normal and bicuspid aortic valve
(http://my.clevelandclinic.org/heart/disorders/congenital/congenvalve.aspx)

1.1. Coarctation of the aorta diagnosis

1.1.1. Arm-to-leg blood pressure difference measured by sphygmomanometry

There is a common agreement that all clinical cases of aortic coarctation are manifest of systolic hypertension above and systolic hypotension below the constriction, therefore, coarctation causes hypertension proximally. In this case, arm-to-leg blood pressure differences measured by sphygmomanometry can provide helpful information. However, it was reported that such measurements may not accurately represent the hemodynamic severity of the coarctation and may change significantly with flow rate (Araoz at al., 2003; Guenthard et al. 1996; Swan et al. 2003).

1.1.2. Doppler echocardiography

The primary method for non-invasive evaluation of the severity of COA is Doppler echocardiography which has introduced several parameters to evaluate the severity of coarctation (peak and mean trans-coarctation pressure gradients). Instantaneous peak trans-coarctation pressure gradients can be estimated using simplified energy equation (the unsteady flow component and the energy losses by turbulence and friction are neglected), as follows:

$$\Delta P = 4(V_2^2 - V_1^2) \tag{1.1}$$

Where V_2 and V_1 are the peak flow velocities in the descending aorta, distal to coarctation (continuous-wave Doppler) and proximal to the coarctation (pulsed Doppler), respectively. Number 4 with the unit of $mmHg.s^2/m^2$ is the product of unit conversion from Pa to mmHg. Peak and mean trans-coarctation pressure gradients can be determined with or without correcting of the pre-coarctation velocity. The Doppler echocardiographic diastolic runoff which represents the magnitude of the antegrade diastolic flow has also been suggested to evaluate the severity of coarctation, typically seen in patients with severe coarctation. However, DeGroff et al. (2003) and Tacy et al. (1999) showed that this parameter is highly dependent on aortic compliance.

Given its non-invasive, radiation-free and low-cost nature, Doppler echocardiography is currently the method of choice to assess coarctation severity. However, it has several theoretical and technical limitations that may contribute to an inaccuracy

about of the actual severity of the COA and consequently the therapeutic management of the patient (Marx and Allen, 1986). These limitations include:

(1) Trans-coarctation pressure gradients are highly dependent on cardiac output and on collateral blood supply limiting their accuracy and their applicability in a wide cohort of patients (Steffens et al. 1994; Carvalho et al. 1990).

(2) The inability to achieve consistent results because of complications in obtaining a clear acoustic window, interference from lung tissue and difficulties in determining the throat diameter of the coarctation.

(3) The potential for underestimation of the flow velocity due to mis-alignment of Doppler beam with flow direction.

(4) Risk of underestimation of upstream coarctation diameter due to inadequate quality and/or positioning of the image plane.

(5) Measurement variability related to manual tracing of flow velocity contours, etc.

These above limitations may significantly alter the performance of Doppler echocardiography to accurately quantify coarctation severity. There is thus an important need for additional non-invasive and accurate methods to confirm the severity of the coarctation in patients for whom Doppler echocardiography does not provide a definitive conclusion.

1.1.3. Cardiac catheterization

Invasively, cardiac catheterization and angiography are considered the gold standard for definitive evaluation of the severity of the COA. Many published reports regard a peak-to-peak trans-coarctation pressure gradient greater than 20 mmHg as an important criterion for the diagnosis of significant COA in the setting of normal cardiac index.

However, all catheter pressure gradients are highly influenced by the flow rate and pressure recovery phenomenon. Peak-to-peak pressure gradient also depends on compliant properties of the aorta (Kadem et al., 2006). Furthermore, the nature of cardiac catheterization is invasive and thus carries a higher risk than other methods. The risks include cardiac arrhythmias, heart attack, bleeding, low blood pressure, stroke and trauma to the artery caused by hematoma. Therefore, using invasive cardiac catheterization could be problematic if multiple follow-up examinations after surgical repair are required. Recoarctation is a common occurrence (up to 40%) after even successful COA repair and the development of aneurysm after patch graft repair are not uncommon (Boxer et al., 1986; Parks et al., 1995; Araoz et al., 2003).

1.1.4. Magnetic resonance imaging

Magnetic resonance imaging (MRI) has been recognized as the noninvasive imaging modality of choice for the evaluation of aortic coarctation before repair and is superior to Doppler echocardiography. Magnetic resonance imaging provides an accurate assessment of the anatomic characteristics of COA (site, degree and extent

of the narrowing of COA) and the collateral blood vessels. Magnetic resonance imaging can also be used to determine the mean and maximal trans-coarctation pressure gradients and the regional flow rate. Furthermore, MRI can provide useful information on the severity of COA by calculation the extent of mismatch between the flow rate in the proximal aorta and the distal descending aorta (an indirect way to evaluate the flow rate in collaterals). However, some patients with severe COA do not develop collaterals and the flow rate entering the descending aorta below the level of the diaphragm is not taken into account.

1.2. Current treatments for coarctation

Current treatment options for coarctation of the aorta include surgical repair, balloon angioplasty, and stent placement.

1.2.1. Surgical repair

There are several open-heart surgical techniques to repair aortic coarctation. The decision on the type of surgical repair depends on age of the patient, the morphology of the coarctation, and the preference of the surgeon. The options include:

1.2.1.1. Resection with end-to-end anastomosis: In this procedure, the aorta is isolated and the aortic isthmus and ductal tissue are resected (Fig. 1.5). The distal aortic arch is incised along its inferior side, the lower aorta is incised along its lateral side, and the two are stitched together. The benefits of the end-to-end method are that

the subclavian artery is not sacrificed, and complete relief of obstruction is easily achieved. Currently, in most patients with coarctation especially in patients beyond the newborn period, repair can be accomplished with end-to-end anastomosis. A variation of the classic end-to-end repair is the extended end-to-end technique. This method is similar to the classic end-to-end COA repair discussed above, but differs in that the aortic arch is incised more proximally along its lesser curvature, and the lower aorta is incised further along its posterior-lateral aspect. The two ends are then brought together and anastomosed. The advantage of this difference is that relief of aortic arch hypoplasia is promising since the aortic arch is more extensively opened, and therefore, obstruction is more readily relieved. Extended end-to-end repair may prove to be the operation of choice since aortic arch hypoplasia is now thought to be more widespread than previously recognized.

(a) (b)

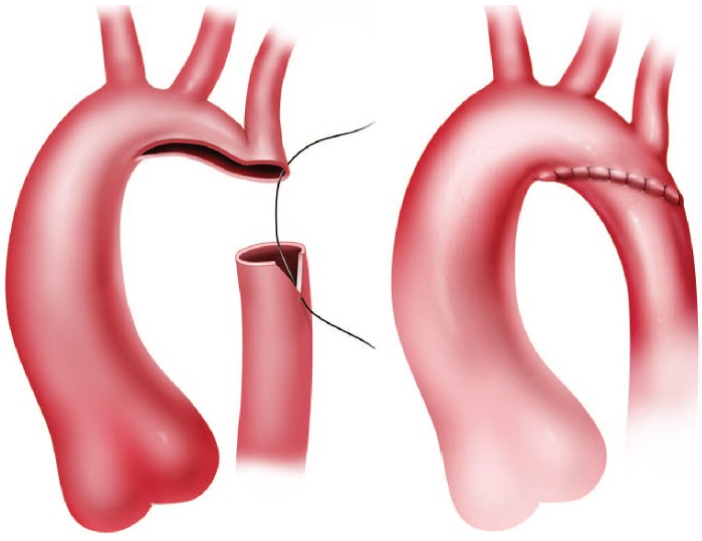

Figure 1.5. Illustrations show extended end-to-end anastomosis for repair coarctation of aorta: (a) Incision for extended end-to-end repair, (b) Coarctation repaired by means of extended end-to-end anastomosis (Gaca et al., 2008)

1.2.1.2. Patch aortoplasty

In some patients, there may be a rather lengthy section of coarctation; if the coarctation section is excised, the two ends of the aorta would be too far apart. In this situation, repair with a prosthetic patch could be accomplished (Fig. 1.6). In this procedure, the aorta is isolated, the site of coarctation is opened with proximal and distal extension of the incisions, and a patch of synthetic material or homograft is stitched into place. This method of repair has the advantage of being technically simple, relatively quick, offers a low rate of recurrence, and provides excellent relief of the obstruction. The use of prosthetic material has been associated with late aneurysm formation. It is thought that newer materials may decrease the potential for this difficulty.

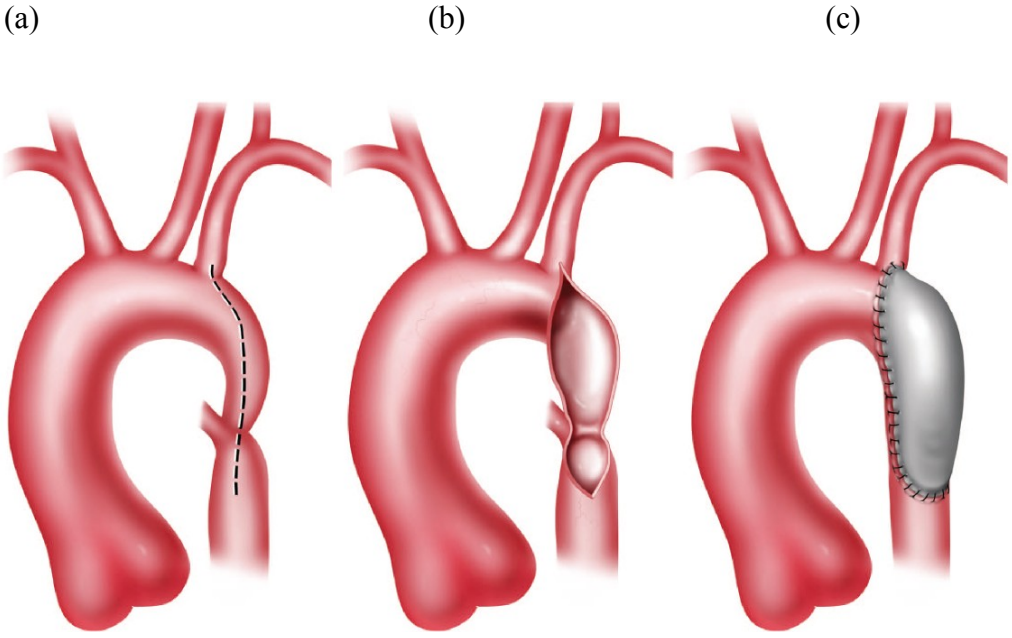

Figure 1.6. Illustrations show patch aortoplasty for repair of coarctation: (a) Incision site for patch repair, (b) Incision has been performed prior to patch placement, (c) Patch repair of coarctation (Gaca et al., 2008)

1.2.1.3. Left subclavin flap aortoplasty

An alternative to a prosthetic patch is the subclavian artery patch repair. In this procedure, the left subclavian artery is isolated and divided (Fig. 1.7). The vessel is then opened longitudinally. The subclavian artery flap is then folded down over the area of aortic narrowing and stitched into place. This method is simple, it allows using the patient's own tissue, it has a low recurrence rate, and it provides excellent relief of the COA. A disadvantage is that the subclavian artery is sacrificed in the subclavian flap angioplasty technique. Transient decreased perfusion to the left arm has been reported in older patients who have undergone COA repair using this method, but limb threatening ischemia is rare.

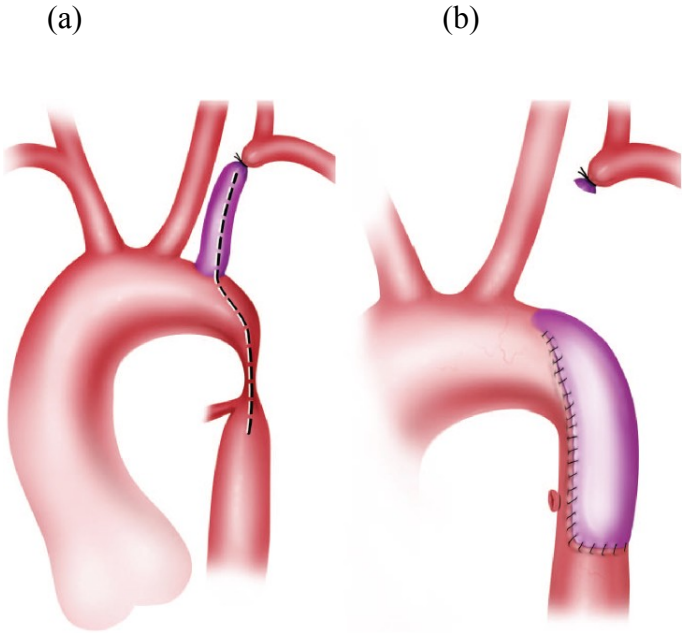

Figure 1.7. Illustrations show Left subclavin flap aortoplasty for repair of coarctation: (a) Incision site before repair coarctation, (b) coarctation has been repaired (Gaca et al., 2008)

1.2.2. Balloon angioplasty

Balloon angioplasty is often used in the treatment of recurrent coarctation, with good results. For this procedure, a special balloon tipped catheter is inserted into COA. The balloon is inflated and causing the artery to widen (Figure 1.8 (a)). Balloon angioplasty is considered a safe alternative to surgery for adolescents and adults with native coarctation because of supportive postsurgical scar tissue at the site of dilation. Studies have, however, shown a higher incidence of recoarctation and aneurysm formation (Rao et al., 1996; Fawzy et al., 2004). The complications of balloon angioplasty, whether for native coarctation or recoarctation, are similar. Excluding arterial access–site injury, most early complications of balloon angioplasty, including aortic intimal tears and flaps and cerebrovascular accidents, are rare, occurring in fewer than 2% of procedures. Aneurysm formation at the site of dilation is both an early and a late complication and has been described in patients who had undergone angioplasty more than 5 years. Early recoarctation has been described in patients undergoing balloon angioplasty of both native coarctation and recoarctation (Fawzy et al., 2004). As with surgical correction, a late complication of balloon angioplasty is the development of hypertension in 30%–40% of patients.

(a) (b)

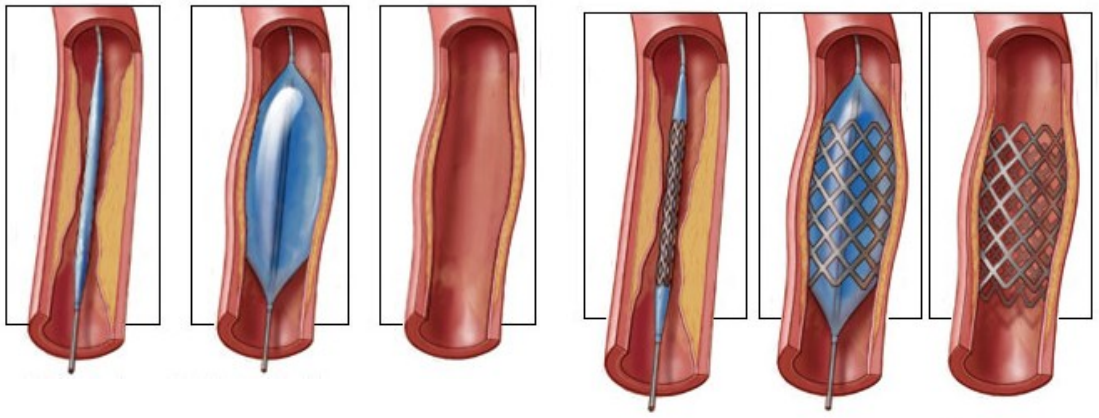

Figure 1.8. (a) Balloon angioplasty (http://www.qualitycardiaccare.com), (b) Stent placement (http://health.msn.com)

1.2.3. Stent placement

The newest treatment for coarctation is stent placement. A stent is a small, coiled wire-mesh tube. During a procedure called angioplasty, the stent is inserted into a blood vessel and expanded using a small balloon (Figure 1.8 (b)). The stent is left in place to help keep the artery open while the balloon is removed. This procedure has generally been reserved for patients who have recoarctation after previous surgical repair or balloon angioplasty, who have unfavorable anatomy for balloon angioplasty (such as long segment narrowing), or who are at high risk for surgical repair (Thanopoulos et al., 2000). A potential advantage to stent implantation is the treatment of any aneurysms present at the time of catheterization. The use of stents is generally avoided in small children due to the large size of the delivery system and the need for repeat procedure as the child grows. The most important complications of stent placement include acute rupture or extensive dissection of the aorta

(Mahadevan and Mullen, 2004). Additional complications include stent fracture, incomplete stent expansion, stent migration, and thromboembolic events. Aneurysm formation has been described in up to 11% of patients as a late complication (Suarez de Lezo et al., 1999). Long-term follow-up is still required to more completely evaluate the outcome of this endovascular treatment for coarctation.

1.3. Objectives and outline of the current work

The main objective of this work is to understand the hemodynamics of coarctation of the aorta from different perspectives. This was performed using a comprehensive approach including: numerical simulations, mathematical lumped parameter modeling and experimental measurements. The objectives of this study were achieved by realizing four specific aims as described below.

Specific Aim 1: To investigate numerically, steady and pulsatile flow in a three-dimensional curved tube with two constrictions simulating aortic stenosis and coarctation. The simple geometry in this study allows exploring effects of coarctation of the aorta and aortic stenosis independent from sophisticated curvatures of the real aorta which impose difficulties in drawing clear conclusions.

Specific Aim 2: To identify hemodynamic factors that lead to acute and gradual changes in the function and health of the vessels through a joint experimental and numerical investigation of blood flow dynamics in the aorta. For this purpose, aortas with realistic geometries in healthy condition and coarctation of the aorta coexisted with normal tricuspid and bicuspid aortic valves were explored.

Specific Aim 3: To investigate respective impacts of aortic stenosis and coarctation of the aorta on the left ventricular load by developing a new lumped parameter model, solely based on non-invasive parameters.

Specific Aim 4: (1) To evaluate the current clinical method for coarctation of the aorta and (2) to propose novel and non-invasive parameters for the evaluation of coarctation severity.

Chapter 2

Literature review

2.1. Flow in curved pipes

In order to investigate the flow dynamics of the complex geometry of the human aorta, it is imperative to understand idealized flow models in simple models like curved pipes.

Theoretical and experimental studies of flow in curved pipes started with the investigation of Thomson (1876) on the effect of curvature in open channels. In 1902, Williams et al. observed that the location of the maximum axial velocity is shifted towards the outer wall of a curved tube. Later, Eustice (1910) proved the presence of secondary flow by injecting ink into water flowing through a coiled pipe. The presence of secondary flows is another interesting phenomenon associated with curvature effects. Secondary flow is attributed to the physical fact that the fluid elements experience a variation in centrifugal force along their position in the arch. Dean (1927) developed analytical solutions of fully developed, steady flow in a curved tube of circular cross section. The results explained that as the flow moves around the curved tube, an imbalance between centrifugal forces and the inwardly directed radial pressure gradient results in secondary flow developed within the tube cross section. The fluid in the core moves towards the outer wall of curvature and returns to the inner wall along the tube wall resulting in two symmetric vortices. As a result of secondary motion, the axial velocity is skewed with a maximum axial velocity magnitudes found more towards the outer wall with increasing curvature

(Dean 1927; 1928) (Fig. 2.1). Dean number: $De = 2(a/R)^{1/2}\sqrt{\mathrm{Re}}$, where *De, a, R* and *Re* are Dean number, the pipe radius, the radius of the curvature of the pipe and Reynolds number, respectively.

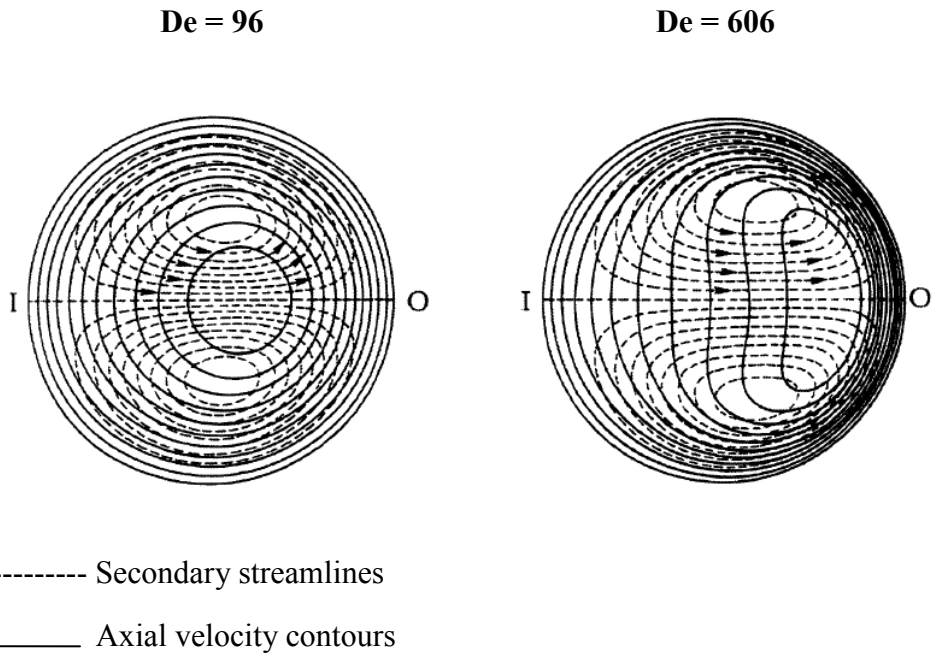

Figure 2.1. Secondary flow pattern for steady flow in curved pipe (Dean 1927), the effect of the Dean number on secondary flow patterns can be seen ($De = 2(a/R)^{1/2}\sqrt{\mathrm{Re}}$, where *De, a, R* and *Re* are Dean number, the pipe radius, the radius of the curvature of the pipe and Reynolds number, respectively)

After initial studies on steady flow by Dean (1927, 1928), Womersley (1957) tackled the question of time periodicity on the laminar flow in curved and elastic pipes. Womersley used a simplified model based on linearization of the pulsatile flow in the form of a sinusoidal wave. The non-dimensional parameter (Womersley number) is defined as follows,

$$\alpha = R\sqrt{\omega\rho / \mu} \tag{2.1}$$

Where R, ω, μ and ρ are vessel radius, angular frequency of the oscillation, dynamic viscosity and density, respectively. Womersley applied this linear analysis to a straight tube with a pulsatile flow in the form of a simple sinusoidal wave. The Womersley number can be considered the Reynolds number of oscillatory flows.

The study of the combined effect of flow pulsation and curvature was the next step which various researchers worked on theoretically, computationally and experimentally (Yao and Berger, 1975; Zalosh et al., 1991; Agrawal et al., 1978; Naruse and Tanishita, 1996; Qiu and Tarbell, 2000). These studies have provided great insight into the complexity of flow pattern in curved tube geometries and have demonstrated the skewness in the velocity profiles, toward the outer wall, as well as the structure of secondary flow patterns within these geometries. Consequently, these studies demonstrated that the curvature as is the cause of the spiral flow patterns already reported by Dean (1928). Furthermore, these studies established the dependence of flow in curved tubes on various geometric and flow parameters including the extent of vessel curvature, blood flow rate and pulsatility. The results of Hamakiotes and Berger (1988) are the most celebrated simulation of pulsatile flow in curved pipes. Figure 2.2 shows a typical result for the secondary flow pattern from direct numerical simulations of pulsatile flow through a curved vessel (Hamakiotes and Berger, 1988).

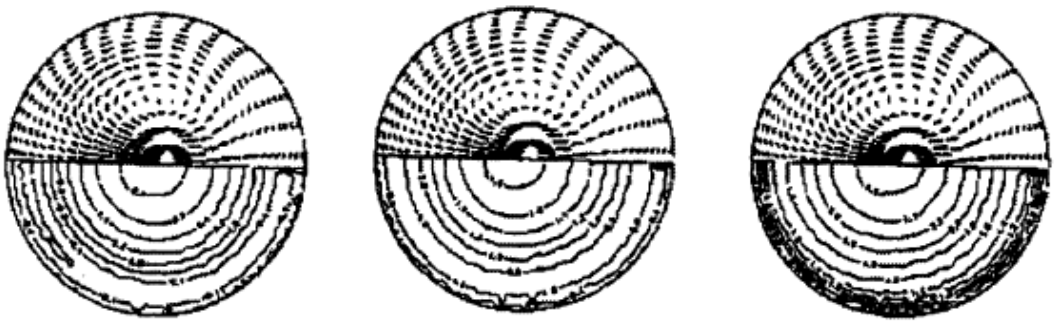

Figure 2.2. Secondary flow pattern for the pulsatile flow through a 180-degree curved pipe (Hamakiotes and Berger (1988, 1990))

In biofluid dynamics, the issue of secondary flow arises again since the blood supply system is mainly composed of curved vessels. For physiological applications, the correct understanding of such flows is required not only for mapping the flow velocity field but also for determining the shear stress values alongside the vessel walls. This is important for understanding phenomena such as atherosclerosis which depend on the filtration properties through the endothelial cells linings and the precipitation of large lipoproteins in this region. The largest vessel in the human body, which is responsible for delivering blood to the whole body, is the aorta, which is highly curved. Therefore, many researchers are interested in understanding the physics of fluid flow in a curved vessel and its relation to certain disease such as atherosclerosis.

Chang and Tarbell (1985) simulated flow in the aortic arch using a numerical model of an ideal curved tube with periodical sinusoidal inlet waveforms. Their results revealed a wide variety of flow phenomena including detailed descriptions of the velocity distribution of the rotating flow patterns and the wall shear stress distributions produced by the spiral flow, data which are difficult to obtain by

experimental methods. Komai and Tanishita (1997) investigated the flow in a similar numerical model that had a fully developed inlet flow with a waveform consisting of a pulsatile systolic flow period followed by a stationary diastolic period. Although the inlet velocity waveform of their modeling was different from that of Chang and Tarbell (1985), the results were quite similar.

Hoogstraten (1996) carried out simulation of flow in an artery with two consecutive bends using finite element method. The study showed that, although the bends in the model are relatively gentle, the axial and secondary flow patterns, computed for four selected values of the Reynolds number: Re = 120, 240, 480 and 960, showed strong and complex three-dimensional flow effects. In particular, the secondary flow pattern in the second bend for relatively small values of Re (Re < 240) turned out to be significantly altered from that for larger Re-values.

Dash (1999) obtained an analytical solution of blood flow in a catheterized curved artery with stenosis for the case of small curvature and mild stenosis. The effect of catheterization on various physiologically important flow characteristics (i.e., the pressure drop, impedance and the wall shear stress) was studied for different values of catheter size and Reynolds number. The study showed that flow characteristics vary significantly across a stenotic lesion. Furthermore, it was found that the effect of stenosis is more dominant than that of the curvature. Due to the combined effect of stenosis, curvature and catheterization, secondary flow streamlines were significantly modified.

Yao (2000) investigated a computational model of three-dimensional blood flow in curved arteries with elliptic stenosis. The study investigated different angles of curvature (0^o, 60^o, 120^o) and different degrees of stenosis (40%, 60% and 80% by area), under typical conditions for stenosed coronary artery. The study demonstrated the significant presence of secondary flow in a curved artery. In addition, the secondary flow in a curved artery caused elevated shear stress on the vessel wall. These results indicated that both curvature and stenosis should be considered together by cardiologists to assess the severity of the stenosis.

2.2. Flow through the aorta

The aorta is the major blood vessel transporting blood pumped by the left ventricle to the systemic circulation. The aorta is a vessel with complex geometry including curvature in multiple planes, branches and taper. A better knowledge of the flow in the aorta is essential for a better understanding of the origin of some common cardiovascular disease and possible ways of overcoming them. This knowledge is also indispensible to the designers of artificial organs for optimizing their design without damaging arterial walls.

2.2.1. Flow through healthy aorta

Rotation of blood flow *in vivo* was detected early by Doby and Lowman (1961) who used a radiopaque streamer technique. Their studies demonstrated circular motion that persisted in the same direction throughout both systole and diastole in the aorta. Lynch and Bove (1969) used water-soluble radiopaque droplets and cineradiography

to observe blood flow in the canine heart and aorta. They found that radiopaque droplets trailed a helical path in the aortic arch during systole. Caro et al. (1994) studied blood flow patterns in patients using magnetic resonance angiography, and reported anti-clockwise rotational flow patterns occupying the right common iliac artery while there was clockwise rotation in the left.

Studies by Segadal and Matre (1987) observed bi-directional flow in the ascending aorta from late systole to middle diastole. Blood flow rotated in a clockwise direction when observed from a left anterior position. Frazin et al. (1990) distinguished rotational blood flow by using color-flow Doppler in the transverse aorta and proximal aorta in 53 patients. By using a transesophageal color-flow Doppler, he demonstrated diastolic counterclockwise rotation and systolic clockwise helical flow in patients. These results suggest that rotational flow begins in the proximal aorta and continues in the descending aorta where flow is asymmetric with systolic clockwise and diastolic counterclockwise direction.

Magnetic resonance velocity mapping is a very powerful techniques allowing *in vivo* blood flow 3D visualization in large vessels. Klipstein et al. (1987) investigated blood flow patterns in the human aorta using this method. Their study showed that velocity profiles in the ascending aorta were skewed in systole. During diastole, flow was reversed along the posterior left wall of the ascending aorta while it continued forward at the anterior right wall. Based on the results, they concluded that turbulent flow did not occur in the ascending or descending aorta of any healthy subjects. Kilner et al. (1993) used magnetic resonance velocity mapping to study the complex flow found in the healthy aortic arch (Fig. 2.3). They found that a skewed velocity

profile develops in early systole in the aortic arch where higher velocities occur closer to the inner curvature of the arch. As systole progresses, the peak axial velocities travel outwards and a counter helical flow develops through the arch.

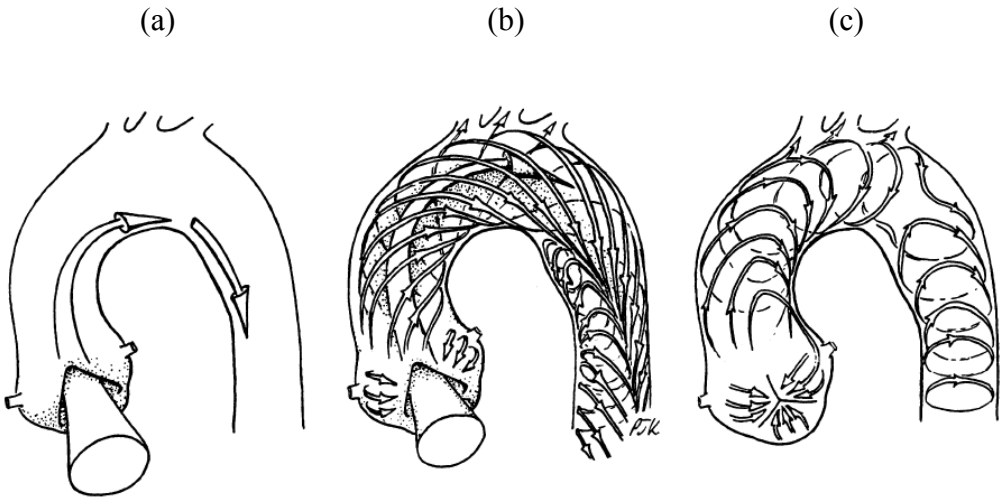

Figure 2.3. The blood flow patterns in the aorta, (a) during flow acceleration phase, (b) during flow deceleration phase, (c) during diastolic phase. (from Kilner et al., 1993)

These secondary flows were also found in other magnetic resonance velocity mapping studies done by Bogren et al. (1994). The results from this study however contain large uncertainties (ranging from 10% to 40%) which arise from the lack of high temporal resolutions and noise. The study found that reverse flow exists and is confined to certain areas of the aorta during different periods of the cardiac cycle. Backward flow always exists in the left posterior part of the ascending aorta and along the aortic arch. Reversing flow is anteriorly located and is much smaller in the proximal descending aorta and continues to diminish towards the distal descending aorta (Bogren et al., 1994). Magnetic resonance velocity mapping was used on healthy aorta by Suzuki et al. (1998) to create baseline values for *in vivo* shear

stresses found in the ascending and descending aorta. The mean age of the normal volunteers in this study was 28+4 years (Table 2.1 and 2.2).

TABLE 1 Time-Averaged Mean Wall Shear Rate (Sec^{-1})

Location	Length	Axial	Nonaxial	Nonaxial/Length[a]
Ascending aorta				
At inner wall of curvature of aortic arch	135 ± 46	121 ± 46	43 ± 17	0.32 ± 0.13
At outer wall of curvature of aortic arch	120 ± 72	115 ± 73	23 ± 6	0.24 ± 0.13
Proximal portion of aortic arch				
At inner wall of curvature of aortic arch	108 ± 30	95 ± 28	47 ± 16	0.44 ± 0.11
At outer wall of curvature of aortic arch	90 ± 22	84 ± 20	30 ± 7	0.34 ± 0.10
Distal portion of aortic arch				
At inner wall of curvature of aortic arch	74 ± 32[b]	48 ± 25[c]	43 ± 28	0.53 ± 0.31
At outer wall of curvature of aortic arch	137 ± 67	122 ± 77	31 ± 33	0.28 ± 0.34
Descending aorta				
At inner wall of curvature of aortic arch	107 ± 32	97 ± 29	27 ± 20	0.25 ± 0.18
At outer wall of curvature of aortic arch	171 ± 59[d]	170 ± 43[d]	22 ± 34	0.12 ± 0.14
Total	118 ± 53	106 ± 55	33 ± 23	0.32 ± 0.22
Analysis of variance	$p = .041$	$p = .007$	$p = .366$	

Note.—Values are mean ± SD.

[a] Represents degree of contribution of nonaxial element to wall shear rate vector.

[b] Significant differences ($p < .05$) versus ascending aorta at inner wall and distal portion of aortic arch and descending aorta at outer wall.

[c] Significant differences ($p < .05$) versus ascending aorta at inner and outer walls and distal portion of aortic arch and descending aorta at outer wall.

[d] Significant differences ($p < .05$) versus proximal portion of aortic arch at inner and outer walls and descending aorta at inner wall.

Table 2.1. Time-averaged mean wall shear rate (1/sec) (from Suzuki et al., 1998)

Shahcheraghi et al. (2002) performed numerical pulsatile blood flow in a human aortic arch. The results demonstrated that the primary flow velocity is skewed towards the inner aortic wall in the ascending aorta, but this skewness shifts to the outer wall in the descending thoracic aorta. They reported that significant secondary flow motion was observed in the aorta, and the structure of these secondary flows was influenced considerably by the existence of the branches. The study also showed that wall shear stress was generally high along the outer

wall in the vicinity of the branches and low along the inner wall.

TABLE 2 Peak Values of Wall Shear Rate (Sec^{-1})

Location	Length	Axial	Nonaxial
Ascending aorta			
At inner wall of curvature of aortic arch	605 ± 334	586 ± 334	237 ± 126
At outer wall of curvature of aortic arch	682 ± 639	660 ± 655	142 ± 48
Proximal portion of aortic arch			
At inner wall of curvature of aortic arch	475 ± 118	446 ± 123	176 ± 43
At outer wall of curvature of aortic arch	396 ± 106	384 ± 107	162 ± 24
Distal portion of aortic arch			
At inner wall of curvature of aortic arch	370 ± 150	237 ± 80[a]	267 ± 191
At outer wall of curvature of aortic arch	711 ± 356	596 ± 392	232 ± 191
Descending aorta			
At inner wall of curvature of aortic arch	540 ± 178	528 ± 178	172 ± 88
At outer wall of curvature of aortic arch	671 ± 258	684 ± 219	145 ± 174
Total	556 ± 316	515 ± 326	192 ± 127
Analysis of variance	$p = .406$	$p = .245$	$p = .575$

Note.—Values are mean ± SD.

[a] Significant differences ($p < .05$) versus ascending and descending aortas at outer wall.

Table 2.2. Peak values of wall shear rate (1/sec) (from Suzuki et al., 1998)

In another study, Jin et al. (2003) performed magnetic resonance imaging and velocity mapping to develop a computational model to examine the effects of curvature and wall movement on the aorta. The study showed that differences in the magnitude of wall shear stress (WSS) between the rigid and full motion models are not notable and results are very close to each other. However, the computed results were in better agreement with the MRI data when full wall motion was included in the model.

Liu (2007) investigated the influence of stenosis on pulsatile blood flow patterns in curved arteries with varying levels of stenosis in the inner wall to examine the effect of the stenosis on hemodynamic characteristics such as secondary flow, flow

separation, wall shear stress and pressure drop. Results demonstrated that secondary flow, wall shear stress and pressure drop downstream of the artery with stenosis at the inner wall show a dramatic change compared to that of a curved artery with no stenosis. The study further reported a flow separation area at the inner wall of the post stenosis region in curved arteries with a stenosis.

Another study by Huo et al. (2008) investigated numerically the detailed distribution of hemodynamic parameters such as wall shear stress and oscillatory wall shear index (OSI) (defined as $OSI = 1/2\left(1 - \frac{\int_0^T \tau dt}{\int_0^T |\tau| dt}\right)$, where T and τ are cardiac cycle period and wall shear stress, respectively) in the entire length of the mouse aorta. It was found that complex flow patterns occur at bifurcations between the main trunk and the branches. The major branches of the terminal aorta, with the highest proportion of atherosclerosis, have the lowest WSS, and the relatively atherosclerotic-prone aortic arch has much more complex WSS distribution and higher OSI value than other sites.

2.2.2. Flow through coarctation of the aorta

Seifert et al. (1999) performed an *in vitro* study on the coarctation of the aorta with three different stiffnesses of the proximal descending aorta. They evaluated pressure gradients using continuous wave Doppler and catheter methods. The study concluded that the stiffness of the proximal aorta has a significant influence on aortic pressure and pressure gradients through the coarctation. A stiff aortic precoarctation segment

is associated with higher catheter pressure measurements, greater continuous wave Doppler gradients, and increased pressure dropoff across the coarctation. Furthermore, acceleration of flow in the proximal descending aorta toward the coarctation was also affected by the stiffness of the aorta. This study did not consider aortic arch branches. This is an important issue since a substantial fraction of blood flow crossing the aortic valve does not pass through the coarctation and is redirected towards the aortic arch arteries.

Recently, DeGroff et al. (2003) used three models of coarctation with high, low, and no wall compliance to perform numerical simulations. Flow simulations were run representing high and low-flow states. They determined that increased aortic compliance leads to greater dilatation of the precoarctation aorta in systole, resulting in a persistence of stored upstream energy. This stored energy, released downstream in diastole as the pre-coarctation aortic walls contract, leads to higher diastolic runoff. However, certain simplifications were considered for the geometry in this study which may not completely reflect the physiological conditions found in a patient with coarctation of the aorta. The study did not consider aortic arch branches (Fig. 2.4). This is an important issue since a substantial fraction of blood flow crossing the aortic valve does not pass through the coarctation and is redirected towards the aortic arch arteries.

In the other study, particle image velocimetry (PIV) was used to obtain 3D velocity maps of flow distal to the coarctation (Miller, 2007). Results showed that the formation of high speed jets at the exit of the coarctation which induced a symmetric recirculation zone along the lateral and medial walls where the average shear rates

were significantly higher than the normal *in vivo* values and in the opposite direction. In addition, the turbulent nature of the flow caused the areas of reattachment to fluctuate creating an oscillatory shear at the walls. However, the study did not consider three aortic arteries (the brachiocephalic, left common carotid and left subclavian artery) (Fig. 2.5). Additionally, the coarctation did not represent a realistic constriction and its location was not at the isthmus.

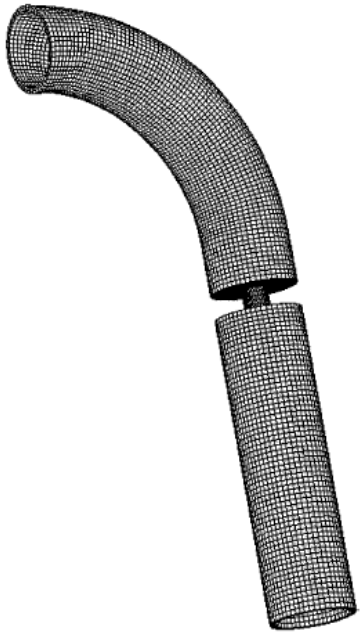

Figure 2.4. Model used by DeGroff et al. (2003)

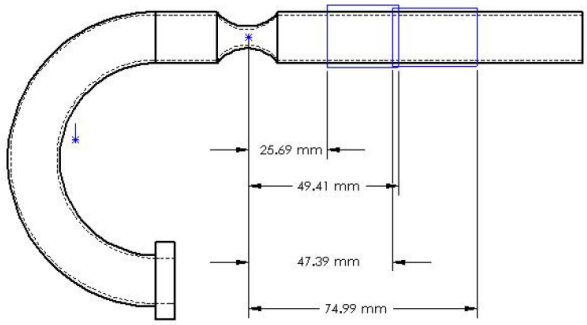

Figure 2.5. Model used by Miller (2007)

Kim et al. (2009) considered the interactions between the heart and the arterial system by utilizing a lumped parameter model as an inflow boundary condition for three dimensional finite element simulations of aortic blood flow and vessel wall dynamics. When the aortic valve is open, the coupled multi-domain method is used to strongly couple the lumped parameter heart model and the three-dimensional arterial models

and compute the ventricular volume, ventricular pressure, aortic flow and aortic pressure. The study was carried out in a patient-specific model of a normal human thoracic aorta under rest and exercise conditions and an aortic coarctation model under pre and post interventions. The results showed that interactions between the heart and the systemic circulation can be studied using this approach. The method can also be utilized to predict outcomes of cardiovascular interventions as demonstrated with the patient-specific thoracic aorta model with an aortic coarctation.

Tan et al. (2009) investigated numerical simulations in a patient-specific aorta associated with both coarctation and aneurysm. The study concluded that laminar–turbulent transition in the dilated vessel can alter significantly the flow structure, shear stress and pressure distribution.

Lately, Hope et al. (2010) used time-resolved, 3D phase contrast magnetic resonance imaging (MRI) to assess blood flow in the thoracic aorta of 34 individuals: 26 patients with coarctation (22 after surgery or stent placement) and 8 healthy volunteers. Abnormal blood flow patterns were demonstrated at peak systole with 4D Flow visualization methods in the descending thoracic aorta of patients but not healthy volunteers. Marked helical flow was seen in 9 of 13 patients with angulated aortic arch geometries even after coarctation repair. Also vortical flow was seen in regions of post-stenotic dilation.

2.2.1.1. Diagnosis of coarctation of the aorta

Several invasive and non-invasive modalities have been used in order to detect and assess the severity of COA. Invasively, cardiac catheterization is considered the reference standard for definitive evaluation of COA severity (Yetman et al., 1997; Maheshwari et al., 2000). It requires the invasive determination of trans-coarctation pressure gradients (TCPGs) (peak-to-peak; peak and mean pressure gradients). However, all catheter pressure gradients are highly influenced by the flow rate and pressure recovery phenomena. Peak-to-peak pressure gradient also depends on compliant properties of the aorta (Kadem et al., 2006). Furthermore, using invasive cardiac catheterization might be problematic if multiple follow-up examinations after surgical repair are required knowing that recoarctation is a common occurrence (up to 40%) after COA repair (Boxer et al., 1986; Parks et al., 1995; Araoz et al., 2003). Arm-to-leg blood pressure difference measured by sphygmomanometry can provide helpful information, but it has been reported that it may not accurately represent the hemodynamic severity of the stenosis and may change significantly with flow rate (Araoz at al., 2003, Guenthard et al., 1996, Swan et al., 2003). Doppler echocardiography is a more robust non-invasive technique which has been used to introduce several parameters to evaluate the severity of COA. Maximal and mean TCPGs can be determined with or without correcting for the pre-COA velocity (De Mey et al., 2001). However, TCPGs are highly dependent on cardiac output and on collateral blood supply (Steffens et al., 1994; Carvalho et al., 1990). This limits their accuracy and their applicability in a wide cohort of patients. Doppler echocardiographic diastolic runoff, the magnitude of the antegrade diastolic flow, has

also been suggested to evaluate the severity of COA. However, DeGroff et al. (2003) and Tacy et al. (1999) showed that this parameter is highly dependent on aortic compliance.

Another Doppler echocardiographic parameter uses the velocity ratio defined as the ratio of angle-corrected distal (abdominal aorta) velocity and COA jet velocity (Teien et al. 1993), a velocity ratio lower than 0.27 represents a severe COA (COA index < 0.25). However, since this parameter uses the distal velocity, it is highly influenced by the shape of the abdominal aorta (post-stenotic dilatation) and the amount of the collateral flow.

Summary of the literature review

1. A previous study (Jin et al., 2003) showed that the rigid wall assumption in simulation of the aorta is acceptable. The results showed that the overall behavior for wall shear stress at each point is similar for the rigid and elastic walls with an average root mean squared error of 1.232%. Furthermore, the velocity distributions, computed in both elastic and rigid models, showed good agreement with magnetic resonance imaging (MRI) measurements.

2. There are a limited number of numerical studies on coarctation in the literature. Furthermore, certain geometric simplifications were considered in most studies (i.e., different studies on coarctation ignored aortic arch branches). This is an important consideration since a substantial fraction of blood flow crossing the aortic valve does not pass through the coarctation and is redirected towards the aortic arch arteries.

3. The existing parameters to evaluate the severity of COA have significant limitations making it difficult to accurately predict COA severity.

We started our investigations by analysis of the flow in a curved tube as a simplified model of the aorta. The simple geometry of this model enabled us to explore the effects of coarctation of the aorta and aortic stenosis independently from sophisticated curvatures of the real aorta. An experimentally validated numerical model from the literature was used and baseline results were validated against it. Details of this exploration are presented in the following chapter.

Chapter 3

Article 1

3. 3D Pulsatile Flow in a Curved Tube with Coexisting Model of Aortic Stenosis and Coarctation of the Aorta

Z. Keshavarz-Motamed, L. Kadem

Mechanical and Industrial Engineering, Concordia University, Montréal, Canada

Journal of Medical Engineering & Physics: Published 2010

Abstract

Coarctation of the aorta is a congenital heart disease defined as an obstruction of the aorta distal to the left subclavian artery (between the aortic arch and descending aorta). It is usually associated with other diseases such as bicuspid and tricuspid aortic stenosis. If the coarctation remains uncorrected it can lead to hypertension, left ventricular failure and aortic dissection. Numerous investigations pointed out that there is a relationship between the genesis and the progression of cardiovascular disease and the locally irregular flow occurring at the diseased zone. Therefore, to examine the relationship between arterial disease and hemodynamics conditions, detailed quantitative studies on flow dynamics in arterial models are clearly required. In this study we numerically investigate pulsatile blood flow in a simplified model of the aorta (curved pipe) with coexisting coarctation of the aorta and aortic stenosis. Three severities of aortic stenoses (0.61 cm^2, 1.0 cm^2 and 1.5 cm^2) coexisting with

aortic coarctations (50%, 75% and 90% by area) are investigated. An experimentally validated numerical model from literature is used and baseline results are validated against it. To ensure having a physiologically relevant model using this geometry, flow properties are set so that the Dean number falls in the physiological range for the aorta. The results show that the coexistence of these pathologies significantly modifies the flow in a curved pipe. The maximal velocity is shifted towards the outer wall and can reach values as high as 5 m/s just downstream of the coarctation. The wall shear stress distribution is significantly modified compared to the normal, unobstructed case. Finally, a clinically significant pressure gradient is induced by the curvature of the tube (up to 36 mmHg). This can lead to an overestimation of the severity of the coarctation using catheterization.

3.1. Introduction

Coarctation of the aorta (COA) is a congenital heart disease that consists of an obstruction of the aorta just distal to the left subclavian artery, more specifically at the site of the aortic ductal attachment (ligamentum arteriosum). COA is encountered in 0.1% of newborns (De Mey et al., 2001). In severe cases, COA can result in serious complications such as hypertension, left ventricular failure and aortic dissection. As a consequence, 60% of adults over 40 years with uncorrected COA have symptoms of heart failure and 75% die by the age of 50, and 90% by the age of 60 (Brickner et al., 2000).

COA can be simple (isolated defect) or complex (associated with other cardiac defects). Complex COA is, in the majority of cases, associated with bicuspid aortic stenosed valve (BAV) (30% to 50%) and with tricuspid aortic stenosis (AS) (15%) (Brickner et al., 2000; Braverman et al., 2005, Hamdan, 2006). The presence of BAV and AS increases significantly the risks of aortic dissection. Indeed, when BAV was present with COA, 50% of patients had a dissection of the aorta. Furthermore, the presence of BAV was the strongest clinical predictor of wall complications in patients with COA (Oliver et al., 2004).

The diagnosis of COA is mainly based, non-invasively, on the determination of a higher systolic pressure in the arms compared to the legs. Doppler echocardiographic assessment is then performed to confirm the presence of COA and to determine its severity. Typically, the trans-coarctation pressure gradient is measured, despite its dependence upon the cardiac output. The diastolic runoff, the magnitude of the antegrade diastolic flow as measured by Doppler echocardiography, can also be used. However, DeGroff et al. (2003) showed that this parameter is highly dependent on aortic compliance. Finally, MRI can also be used to give a better insight on the geometry of the COA, mainly using the coarctation index. This index is defined as the ratio between the diameters at the location of the coarcation to the normal section in the descending aorta. An index of 0.5 indicates a severe narrowing and requires surgical repair. An index of 0.65 indicates a mild coarctation and does not necessitate intervention (Carvalho et al., 1990). Invasively, the most common parameter used to assess COA is the peak-to-peak pressure gradient (mild COA < 20 mmHg; and moderate COA > 20 mmHg), this is despite its high dependence upon the systemic

compliance (Kadem et al., 2006). If the peak-to-peak transcoartation pressure is higher than 30 mmHg, a surgical repair is recommended.

It is important to note that surgical repair still has, however, a limited long term success, mainly due to post-surgery systemic hypertension or recurrent coarctation (Abbruzzese and Aidala, 2007; Maia et al., 2000). Depending on the study, re-coarctation occurs in 5% to 60% of patients and post-surgical hypertension exists in 11% to 68% of patients (Maia et al., 2000). Despite their significant preponderance, the exact mechanisms of re-coarctation and post-surgery hypertension are still not completely understood. It is, however, hypothesized that hypertension may still remain post-surgery because of the baromechanical induced changes to chemical output of the aortic endothelial cells (ECs) (Barton et al., 2001) and these problems are a result of shear rate changes that occur as an effect of the coarctation.

Indeed, from a fluid mechanics point of view, centrifugal forces resulting from the curvature of the aorta induce secondary flows pushing the flow towards the outer wall. These secondary flows are expected to be more significant with irregular patterns if constriction, such a coarctation of the aorta, is present downstream of the curvature (Liu, 2007). Furthermore, if this constriction is associated with another constriction upstream of the curvature, such a valvular stenosis, the flow is completely modified and might lead to a secondary recirculation pattern different from the typical Dean-type flow (Maia et al., 2000), and results in significant difference in the shear rate affecting the aortic wall.

Since re-coarctation and post-surgical hypertension are not well understood, it is beneficial to investigate the effects of coarctation on the hemodynamics in the aorta. The objective of the present study is, therefore, to investigate using a numerical model, steady and pulsatile flow in a three dimensional curved tube with two constrictions, one simulating an aortic stenosis (or a bicuspid aortic stenotic valve) and one a coarctation of the aorta. The interaction between these two constrictions will be studied and their impacts on the development of secondary flows, wall shear stress and their clinical relevance will be investigated.

3.2. Methods

3.2.1. Geometrical model

Figure 3.1(a) shows the schematic diagram of the model used in the experimental and numerical study of Boiron et al. (2007). The same model was used in this study as baseline geometry for the curved tube without any obstruction (case 0-0 in Table 3.1). This choice allowed us to validate our results for the unobstructed case against their experimental data. The simulation was conducted in a U-shaped tube with an internal radius (*a)* of 1.1 cm and an aspect ratio of $\delta = a/R$ equal to 0.073 (slight curvature). The inlet length is equal to ten radii and the outlet length is twenty radii from the bend outlet.

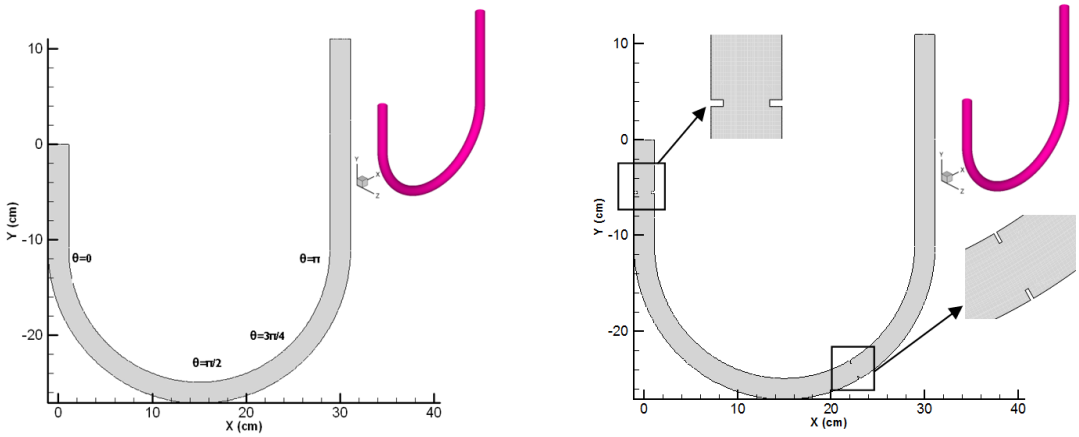

(a)

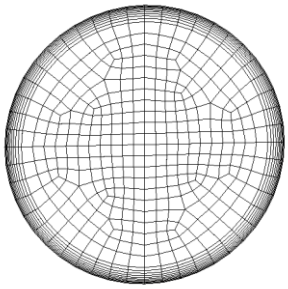

(b)

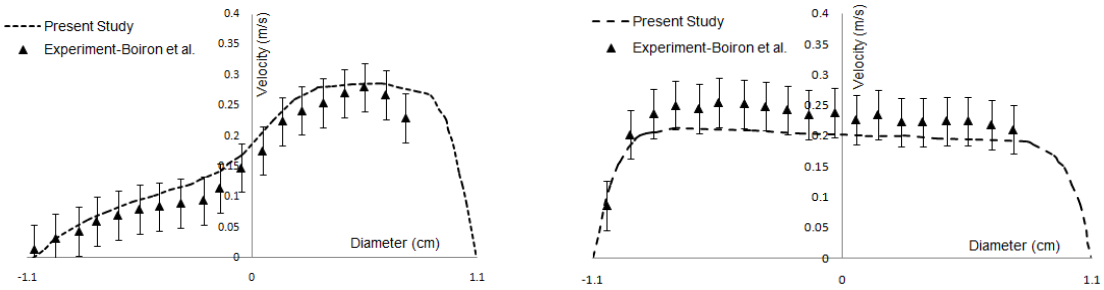

(c)

Figure 3.1. (a) Schematic diagram of the curved tube, (left) with no obstructions, (right) with both stenosis and coarctation, (b) Face Mesh, (c) Velocity profiles along diameter at $\theta = \pi/2$ for validation, Case 0-0. (left) t = 0.3s. (right) t = 1s. The same flow waveform as Boiron et al. (2007) was used to validate against their experimental measurements

CASE 0-0	Tube without obstructions (healthy aorta)
CASE 1.5 cm^2-50%	Tube with EOA of stenosis 1.5 cm^2 and coarctation 50%
CASE 1.5 cm^2-75%	Tube with EOA of stenosis 1.5 cm^2 and coarctation 75%
CASE 1.5 cm^2-90%	Tube with EOA of stenosis 1.5 cm^2 and coarctation 90%
CASE 1 cm^2-50%	Tube with EOA of stenosis 1 cm^2 and coarctation 50%
CASE 1 cm^2-75%	Tube with EOA of stenosis 1 cm^2 and coarctation 75%
CASE 1 cm^2-90%	Tube with EOA of stenosis 1 cm^2 and coarctation 90%
CASE 0.61 cm^2-50%	Tube with EOA of stenosis 0.61 cm^2 and coarctation 50%
CASE 0.61 cm^2-75%	Tube with EOA of stenosis 0.61 cm^2 and coarctation 75%
CASE 0.61 cm^2-90%	Tube with EOA of stenosis 0.61 cm^2 and coarctation 90%

Table 3.1. Definition of the cases.

Dean number (*De*) is the ratio of the effective centrifugal inertial forces to the viscous forces, defined as $De = 2\sqrt{\delta}\,\mathrm{Re}$, where δ and *Re* are aspect ratio and Reynolds number respectively. Dean Number (Dean, 1927) is a dimensionless number that makes curved tubes of the same Dean number with different geometries mathematically interchangeable. In order to investigate the physiological condition, geometrical and flow properties as described above and in section 2.4 were set so that the Dean number is in the physiological range. With this strategy the experimentally validated model was used to further investigate aimed pathologies.

In order to investigate the combined effects of a stenosis and a coarctation on the flow field in a rigid curved pipe, a 3D object with a stenosis at a distance of five radii from the inlet and a coarctation at $\theta = 2\pi/3$ (120 degree) from bend start were created. Both

aortic stenosis and coarctation were simulated as sharp-edge orifices. For aortic stenoses, this is a realistic approach since two (calcified thickened valve and thin fused valve) among the four more preponderant morphological shapes of aortic stenoses can be represented by sharp-edge orifices (Cape et al., 1996). Furthermore, this approach has already been used in several *in vitro* studies (DeGroff et al., 2003; Kadem et al., 2006; Voelker et al., 1995; Niederberger et al., 1996). The same approach can be applied to coarctation of the aorta (De Mey et al., 2001; Seifert et al., 1999). In order to investigate the effects of co-existence of coarctation and aortic stenosis, various cases were considered: coarctations of 50%, 75% and 90% by area (coarctation indexes of 0.70 (mild COA), 0.50 (severe COA) and 0.31 (very severe COA), respectively) and aortic stenoses with effective orifice areas (EOAs) of 0.61, 1.00 and 1.50 cm^2, simulating severe, moderate and mild stenoses, respectively. All the cases investigated in this study are listed in Table 3.1.

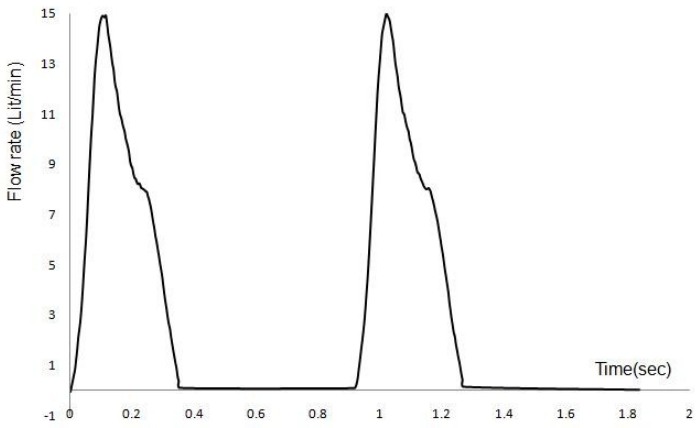

Figure 3.2. Experimental pulsatile velocity profile used as inlet condition for the numerical simulations

It is important to mention that several authors have previously simulated the flow through physiological aorta with or without coarctation. However, to the best of our knowledge, so far no work has been done including simulations of both pathologies (aortic stenosis + coarctation of the aorta) despite the elevated preponderance of such associations. Under such conditions, patient-specific simulations will not necessarily contribute to improve our knowledge on such complex flows, since patient variability and the lack of experimental validation would have limited the clear conclusion from the results.

3.2.2. Numerical model

This study was performed using commercially available software for fluid flow finite-volume simulations (FLUENT 6.3, Lebanon, NH). In the absence of obstructions (case 0-0) or for undiseased vessels, the blood flow is usually laminar and does not experience transition to turbulence, therefore the solution was obtained by simulating a laminar flow inside the domain (Ryval et al., 2004).

The obstruction resulting from a stenosis and/or coarctation can lead to disturbed flow regions in the aorta. Meanwhile, in the presence of a sufficiently severe stenosis, turbulence could be generated during part of the cardiac cycle (i.e., $Re > 1000$) (Ryval et al., 2004). Ghalichi et al. (1998) presented numerical results for transitional and turbulent flow through moderate and severe arterial stenoses by applying a k-ω turbulence model. It was concluded that this model is suitable for blood flow studies where both laminar/transitional and turbulent flow regimes coexist. Hence, in this

study the nine simulated cases with both stenosis and coarctation have been investigated using a $\kappa - \omega$ turbulence model.

3.2.3. Numerical strategy

For the unobstructed case (no stenosis–no coarctation: case 0-0), the mesh (Figure 3.1(b)) was based on the model already used and reported by Boiron et al. (2007). In their study, the final grid consisted of 451,472 hexahedral elements. They determined the velocity field numerically and validated the results against experimental measurements performed using hot-wire anemometry. In our work, we employed a similar numerical methodology and validated our unsteady results for the unobstructed case against their experimental data, using the same inlet flow waveform they reported in their study (Figure 3.1(c)). Figure 3.1(c) shows that there is a relatively good agreement between our numerical results and experimental measurements performed by Boiron et al. obtained for a velocity profile along the diameter at $\theta = \pi/2$.

For obstructed cases (nine cases in Table 1), several tests with different grid spacing were performed to determine the optimal mesh configuration. This was achieved by dividing the model into 7 sub-volumes and then generating a mesh by sweeping the mesh node pattern of a source face through each volume along the curved axis. We also used an adaptive mesh refinement technique to obtain the most accurate solution. For each case, the volume was meshed with four different mesh definitions of increasing density and then through an adaptation of $y^+ \leq 1$ as criterion, as required by

$\kappa-\omega$ model, which yielded an average y^+ value of 0.2381 for all obstructed cases. The best mesh considering accuracy and computation time was selected. In all cases, hexahedral elements were used and the governing equations were discretized using second order schemes. The mass-momentum equations were solved using the PISO solver.

Mesh independency was judged by two criteria: velocity and wall shear stress. Mesh definition was considered as acceptable when no significant difference (lower than 5%) between successive meshes was noticed in wall shear stress along the inner and outer wall, and also in velocity profiles at two locations ($\theta=0$ and $\theta=3\pi/4$ for obstructed cases). Mesh independency was achieved for these two criteria for all cases with 1,380,000 to 1,486,000 elements for all obstructed models.

For time independency, several time steps were tested: 0.001 s, 0.002 s and 0.0025 s and 0.005 s. The solution marched in time with a time step 0.002 s and three cycles were performed to ensure that the flow was truly periodic. Convergence was obtained when all residuals reached a value lower than 10^{-5}.

Additionally CFD uncertainty and error in the study were found according to (Celik et al., 2008). Table 3.2 shows the calculations for the discretization error for wall shear stress and velocity, where N, r, p ,ϕ, ϕ_{ext}, e_a, e_{ext} and GCI_{fine} are the number of elements, the refinement ratio, the apparent order, wall shear stress, the extrapolated value, the apparent error, the extrapolated error and the fine-grid convergence index, respectively (Celik et al., 2008). It should be mentioned that in this study ϕ was the wall shear stress (Pa) at the outer wall. These computations

indicate that the numerical uncertainty for the fine mesh (1,410,231 elements), for case $1cm^2$ - 75%, is 2.3%.

N_1, N_2, N_3	1410231, 1150021, 930125
r_{21}	1.561
r_{32}	1.495
ϕ_1	300.15 Pa
ϕ_2	297.051 Pa
ϕ_3	282.42 Pa
p	3.768
ϕ_{ext}	305.683 Pa
e_a	1.032%
e_{ext}	1.8%
GCI_{fine}	2.3%

ε_{32}=-14.6310, ε_{21}=-3.099

Table 3.2. Calculation of discretization errors for case $1cm^2$-75%

Severityof the stenosis 0.6 cm²; coarctation severity from 50% to 90%
Severityof the stenosis 1.5 cm²; coarctation severity from 50% to 90%
Normal case
Case 0.6cm²-90%
Case 0.6cm²-75%
Case 0.6cm²-50%
Case 1.5cm²-90%
Case 1.5cm²-75%
Case 1.5cm²-50%
Case 0-0
θ=π/2
θ=3π/4
θ=π
Y (cm)
X (cm)
θ=0
θ=π/2
θ=3π/4
θ=π

Figure 3.3. Secondary flow for steady simulation at three different sections ($\theta = \pi/2$, $3\pi/4$ and π) for the normal case and the cases with both aortic stenosis (1.5 cm^2 and 0.6 cm^2) and coarctation of the aorta (50%, 75% and 90%)

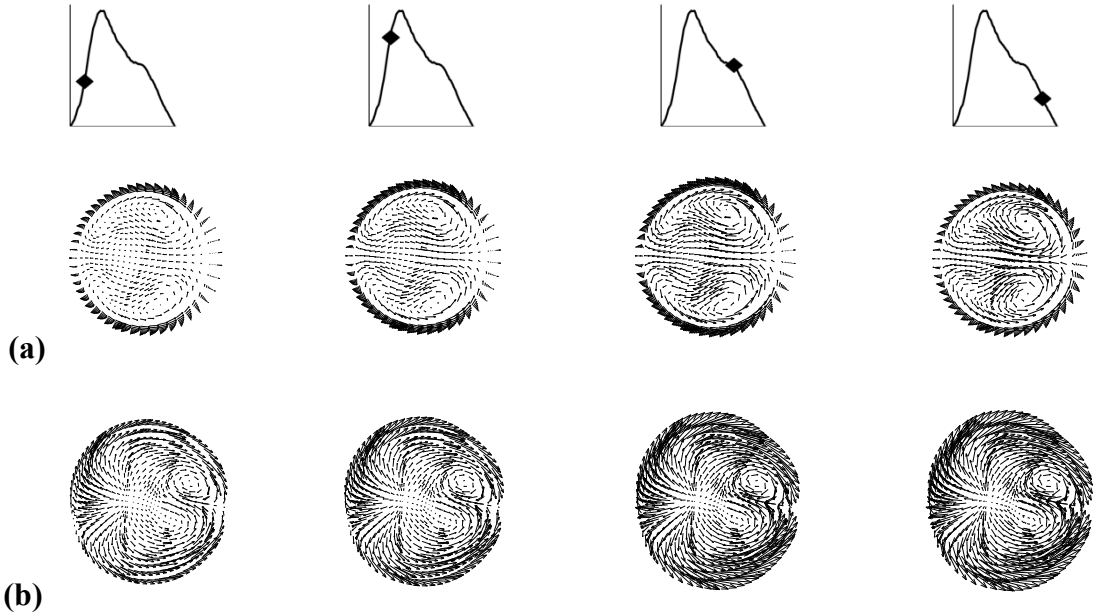

Figure 3.4. Evolution of the secondary flow at $\theta = 3\pi/4$ cross section at t = 0.04 s, 0.08 s, 0.2 s, 0.26 s. (a) Case 0-0, (b) Case 0.61cm^2-75%

3.2.4. Boundary conditions and model properties

Blood was assumed to be incompressible and Newtonian with density 1050 kg/m^3 and constant viscosity 0.0035 Pa ·s (Morris et al., 2005). Although human blood tends to exhibit non-Newtonian behavior at shear rates under 100 s^{-1} near the vessel walls, the shear rates in like the aorta are generally observed to be greater than 100 s^{-1} and hence it is reasonable to assume a Newtonian fluid in the simulation (Fung 1981; Shahcheraghi et al., 2002; Morris et al., 2005). The vessel wall was considered to be

rigid, this can be justified by: 1) Jin et al. (2003) showed that rigid wall assumption for the aorta is realistic. Their results showed that the overall behavior for WSS (wall shear stress) at each point is similar for the rigid and elastic walls with average root mean squared error of 1.232%. Furthermore, their velocity distribution, computed in both elastic and rigid models, showed a good agreement with magnetic resonance phase contrast velocity measurements; 2) patients with both coarctation and aortic stenosis are usually hypertensive and characterized by reduced compliance and elevated stiffness index (Vitarelli et al., 2007; Xu et al., 1997). No-slip boundary condition was also applied at the rigid walls. The mean cardiac output was 5 L/min.

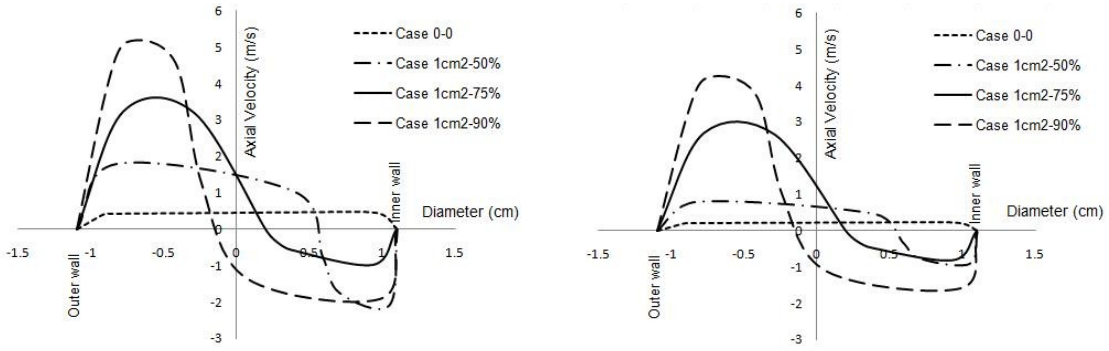

(a) (b)

Figure 3.5. Axial velocity profiles along a diameter for θ=3π/4 cross section, (a) t = 0.08 s, (b) t = 0.2 s. Note the shift of the maximal velocity towards the outer wall as well as the significant increase in the maximal velocity

In order to start the pulsatile cycle calculations, a steady state solution at the peak of the systolic phase (corresponding to an inlet Reynolds number of 4356) was first obtained. This steady state solution was then used as the initial condition for the unsteady computations. For the unsteady simulations, an experimental pulsatile flow rate was applied at the inlet (Figure 3.2). The unsteady simulations were performed

with a systolic duration of 300 ms (intermittency parameter = 0.35) and the heart rate was 70 bpm. This corresponded to a mean systolic inlet Reynolds number of 2310, a Dean number of 1248 and a frequency parameter of 16.3, all in a range close to physiological values in the aorta (Zarandi, 2000).

3.3. Results and discussions

3.3.1. Steady flow conditions

In curved tubes, under steady state conditions, the fluid near the tube axis moves away from the center of curvature whereas the fluid near the walls moves towards it. Secondary flow forms as a result of the superposition of these movements on the primary axial flow. This can be explained physically by the pressure gradient across the tube that has to balance the centrifugal force acting on the fluid which is forced to follow a curved trajectory (Cuming , 1952). This secondary flow appears in the tube cross section as two symmetrical helical vortices with respect to the plane of curvature. Figure 3.3 shows secondary flow in unobstructed (Case 0-0) and obstructed tubes (valvular stenosis + coarctation; for the sake of clarity only mild (1.5 cm^2) and severe stenosis (0.6 cm^2) are displayed) at different locations along the tube. It appeared that the flow became more complex with increasing both valvular stenosis and coarctation severities. At $\theta = \pi/2$ (upstream from the coarctation), the secondary flows became stronger leading to a transition from confined vortices in the regions close to the lateral walls to vortices occupying almost the whole section, as a result of increasing valvular stenosis severity. Downstream of the stenosis, it clearly appeared

that a severe coarctation further amplified the secondary flows. For a very severe coarctation a strong jet-like flow directed from the inner wall towards the outer wall can be noticed.

3.3.2. Unsteady flow conditions

The evolution of the secondary flow for unsteady flow conditions for the unobstructed case (Case 0-0) is shown in figure 3.4(a). The emergence of a viscous layer can be observed during the acceleration phase which results in the appearance of two weak counter-rotating vortices. Under these conditions, the maximum axial velocity does not occur on the centerline anymore but instead a skewed profile develops where higher velocities occur near the inner wall during systole as reported by Boiron et al. (2007). Figure 3.4(b) shows the secondary flow downstream of the coarctation when a 0.61 cm^2 valvular stenosis coexists with a 75% coartcation (Case 0.61 cm^2-75%). It appeared that as a result of elevated axial velocity and centrifugal force, the counter-rotating vortices developed under obstructed conditions are convected towards the inner wall and are confined close to the centerline of the tube. This new configuration of the secondary flow has a significant impact on the wall shear stress distribution at the inner wall.

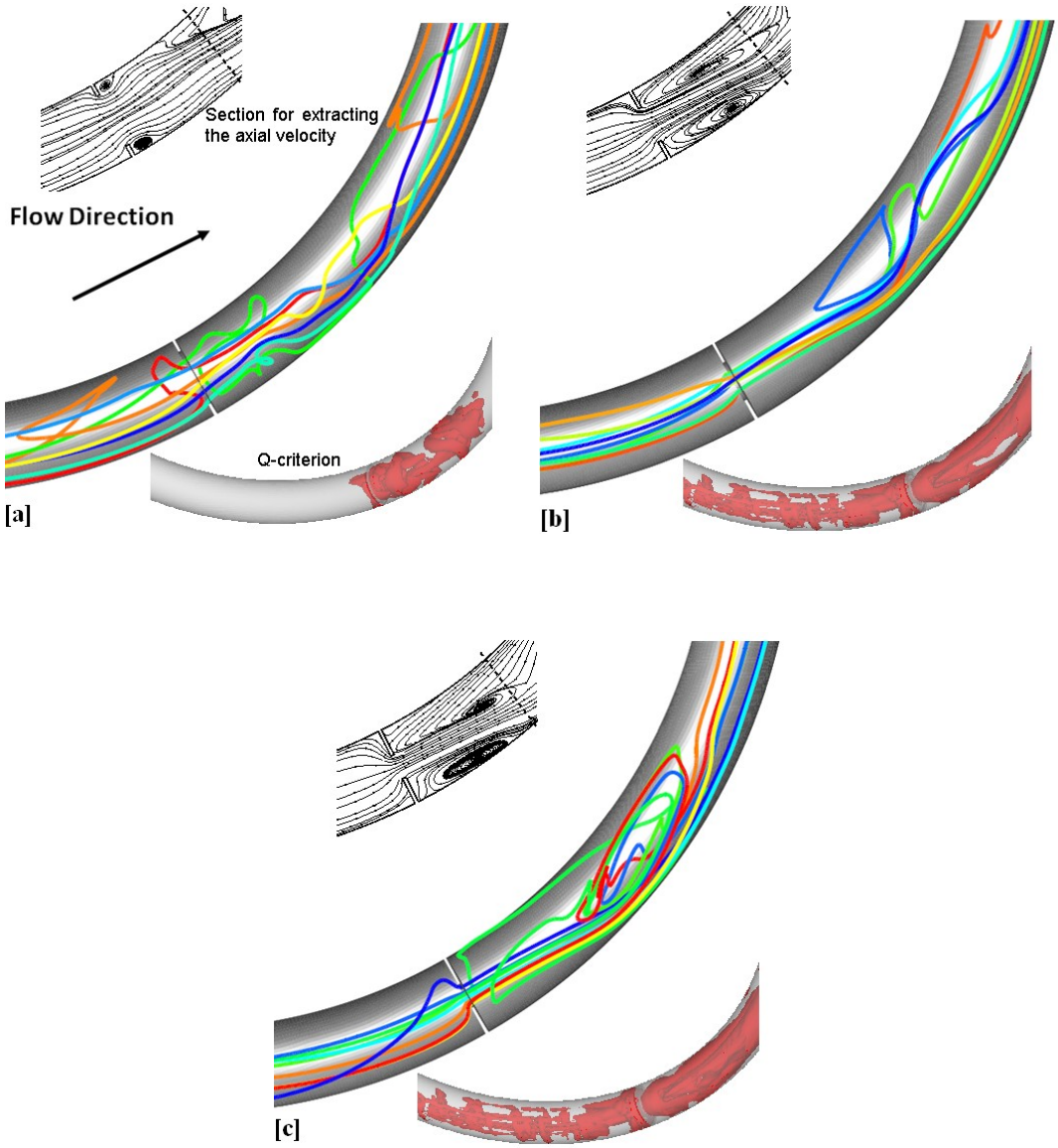

Figure 3.6. Instantaneous streamlines, particle tracking and Q criterion for (a) case1cm^2-50%, (b) case1cm^2-75% and (c) case1cm^2-90%. Note the loss in symmetry of the trans-coarctation jet

Figures 3.5(a) and 3.5(b) show the combined effects of a fixed valvular stenosis (1.0 cm^2) and different coarctation severities (50% to 90%) on the axial velocity profile downstream of the coarctation (at section: $\theta = 3\pi/4$) during the acceleration (t = 0.08 s) and deceleration phase (t = 0.2 s). For the unobstructed case the magnitude of the axial velocity profile was relatively low (almost 0.5 m/s at t = 0.08s and 0.29 m/s at t=0.2s). If severe valvular stenosis and coartctation are added, it can be noticed that the maximum of the axial velocity profile is shifted towards the outer wall and its magnitude increases significantly (from 1.98 m/s up to 5 m/s at t = 0.2s and from 0.99 m/s up to 4 m/s at t = 0.2s, for different severities of the coarctation), leading to a skewed axial velocity profile. As an example, Figure 5(a) shows a value of 5.14 m/s for the maximum of the axial velocity in 90% coarctation demonstrating 10 times the normal value (0.5 m/s). This shift of the maximum of the axial velocity towards the outer wall can be explained by the redistribution of the secondary flow resulting from the presence of the coarctation downstream of the tube curvature. The above mentioned shift is further demonstrated by plotting the instantaneous velocity streamlines and particle tracking, using a stochastic model (Gosman and Ioannides, 1981; Smadi et al., 2009; Bluestein et al., 2000) downstream of the coarctation (Figure 3.6). It clearly appears that an increase in coartcation severity (from 50% to 90%) leads to a loss of symmetry of the jet resulting in a skewed axial velocity profile with a maximum directed towards the outer wall. This loss of symmetry of the jet might have implications in terms of the evaluation of the severity of the coarctation using Doppler echocardiography, since Doppler echocardiographic measurements are based on the assumption that the maximal velocity is at the center of tube.

In figure 3.6, secondary flows upstream from and downstream of the coarctation are investigated using the Q criterion (Hunt et al., 1988) during the deceleration phase (t = 0.24 s) for a valvular stenosis of 1 cm^2 and coarctation severities ranging from 50% to 90%. Q is defined as the second invariant of ∇U by $Q = -\frac{1}{2}\frac{\partial U_i}{\partial x_j}\frac{\partial U_j}{\partial x_i} = \frac{1}{2}(\Omega_{ij}\Omega_{ij} - S_{ij}S_{ij})$, where U is the velocity, S is the symmetric part (rate of strain tensor) by $S_{ij} = \frac{1}{2}(\frac{\partial U_i}{\partial x_j} + \frac{\partial U_j}{\partial x_i})$ and Ω is the asymmetric part (rotation tensor) by $\Omega_{ij} = \frac{1}{2}(\frac{\partial U_i}{\partial x_j} - \frac{\partial U_j}{\partial x_i})$. Thus the Q criterion represents the local balance between shear strain rate and vortices magnitude. The coherent vortex and eddy cores are distinguished as the regions characterized by a positive value of Q, which indicates regions where vorticity overcomes strain in the flow. It allows, thus, a better representation of vortical structures and gives a better insight on flow irregularities occurring around the diseased zone. Upstream from the coarctation, secondary contra-rotating vorticies induced by the tube curvature can be visualized around the core flow. Downstream of the coarctation, the flow is more complex. The jet emerging from the obstruction can be visualized (mainly for 75% and 90% coarctation), however secondary flows are confined close to the outer wall and can hardly be seen.

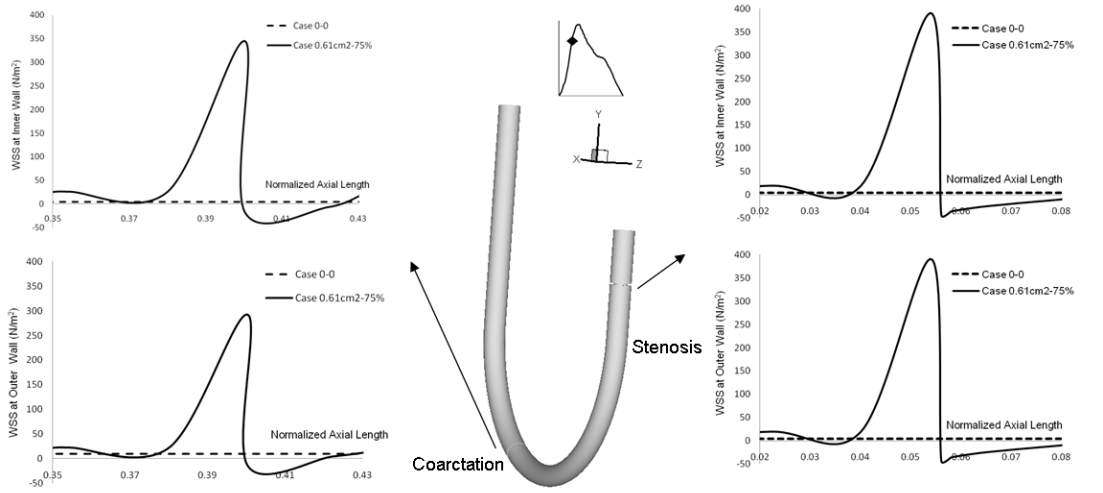

(a)

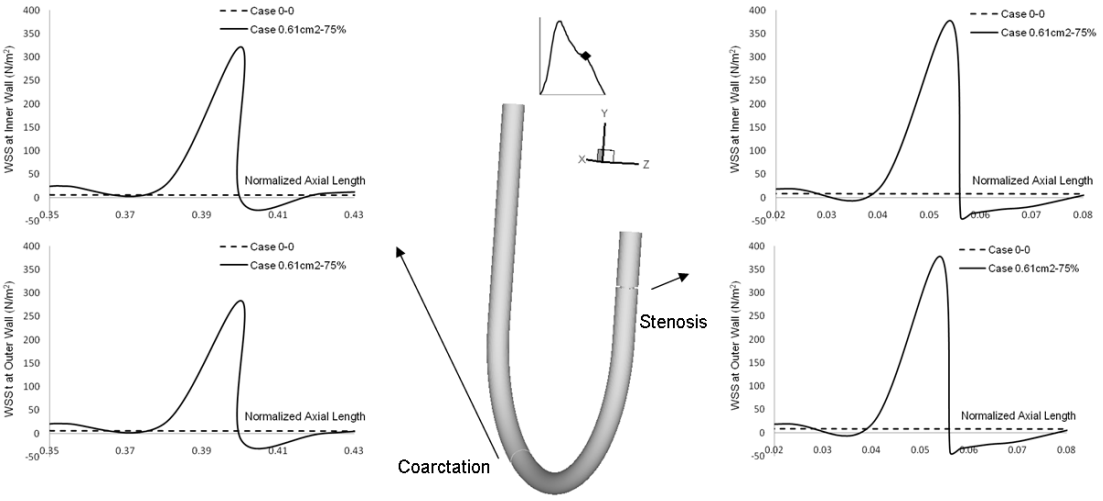

(b)

Figure 3.7. Wall shear stress distribution at the inner/outer walls of coarctation (75%) and stenosis (0.61 cm^2) at (a) t = 0.08 s and (b) t = 0.2 s

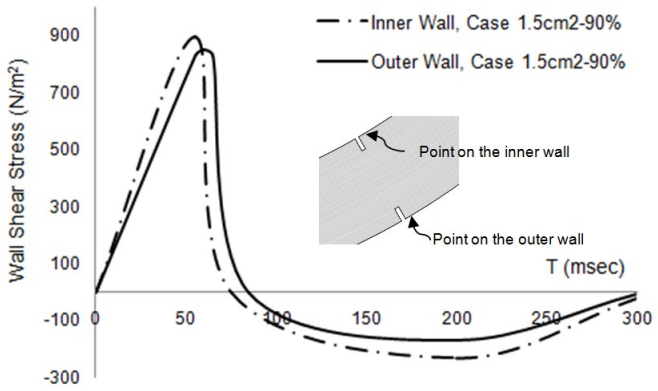

Figure 3.8. Evolution of wall shear stress for two points downstream of the coarctation (90%, aortic stenosis of 1.5 cm^2) during systolic phase

3.3.2.1. Wall shear stress distribution

The fluid mechanical stress that acts directly on the endothelial cells is the wall shear stress. It was pointed out that both high and low oscillating shear stress regions are prone to develop atherosclerosis (Berger and Jou, 2000). Identifying such regions in the flow field is, therefore, essential to understand plaques formation and rupture. Also It is hypothesized that hypertension still exists even after surgery because of the baromechanical induced changes to chemical output of the aortic endothelial cells (ECs) (Barton et al., 2001) which are a result of shear rate changes occurring as an effect of the coarctation. Thus, understanding the shear stresses that are applied to the ECs of the aorta can give insight into how the chemical output from these cells may have been altered.

Figures 3.7(a) and 3.7(b) show the wall shear stress along the inner and the outer walls at two different instants during the cycle (t = 0.08 s and t = 0.2 s) when a coarctation coexists with a valvular stenosis. Significant increase in the WSS on both

inner and outer walls downstream of both the valvular stenosis and the coarctation can be noticed, when compared with the unobstructed case. The maximum of the WSS is located at the locations of the obstructions. However, right downstream of these obstructions, as a result of the presence of recirculation zones, the WSS is locally reduced to a level lower than that of the unobstructed case.

WSS magnitude is an important parameter to investigate, however, due to the pulsatile nature of blood flow in arteries, the oscillatory character of shear stress is even more important to analyze (Ku et al., 1985). For this purpose, Oscillatory Shear Index (OSI) derived from the low shear stress theory has to be computed. It is defined as the degree of deviation of WSS from its average and can be computed as $OSI = \frac{1}{2}\left[1 - \frac{\left|\int_0^T \overrightarrow{\tau_w} dt\right|}{\int_0^T \left|\overrightarrow{\tau_w}\right| dt}\right]$, where T and τ_w are the period of the pulse and the wall shear stress vector respectively. It should be noted that OSI can reach a maximum value of 0.5 in regions with high oscillating shear stress indicating the greater susceptibility of these regions to develop atherosclerosis. Figure 3.8 shows WSS temporal evolution for two points just after the coarctation (3 degrees after the coarctation) at inner and outer walls for 3 different coarctations with a fixed stenosis (1.5 cm^2). Table 3.3 summarizes OSI computed for these two points. It appears that for a coarctation of 50%, WSS is oscillating almost symmetrically (OSI close to 0.2). Then, if the severity of the coarctation is increased, WSS temporal evolution is subject to more violent variations (OSI ranged from 0.27 to 0.49), increasing the risks of endothelial cell damage.

	Case 1.5cm^2-50%	Case 1.5cm^2-75%	Case 1.5cm^2-90%
OSI of Point A (inner wall)	0.1745	0.3977	0.4892
OSI of Point B (outer wall)	0.1431	0.2731	0.3510

Table 3.3. Oscillatory Shear Index (OSI) for two different points downstream of the coarctation for a fixed stenosis (1.5 cm^2) and different coarctation severities (50% to 90%).

3.3.2.2. Pressure distribution

Figure 3.9(a) shows pressure loss distribution along the central line at the peak of the systolic phase for an unobstructed case and for a fixed coarctation severity (75%) associated with different valvular stenosis severities (1.5 cm^2; 1.0 cm^2 and 0.61 cm^2). The problem with coarctation of the aorta is that, as it is commonly associated with a valvular stenosis, the left ventricle experiences a double load. To overcome these loads in series (aortic stenosis + coarctation), the systolic pressure and work of the left ventricle have to increase significantly, thus increasing the risks of heart failure.

Because the obstructions are in series, there is a cumulative effect on the pressure drops. This leads to a significant pressure drop at the outlet (after pressure recovery) for all cases. This pressure drop has to be compensated by the left ventricle as an increase in pressure during the systolic phase. Interestingly, this figure also shows the pressure drop induced by the singularity represented by the curvature of the tube. This pressure drop might have a significant clinical implication since it determines the

position of the catheter upstream from the coarctation when it is evaluated using catheterization.

Figure 3.9(b) shows the upstream pressure drop (relative to the position of the coarctation), the maximal pressure drop (the one that can be obtained by Doppler echocardiography or by positioning the catheter right at the vena contracta downstream of the coarctation) and the pressure drop after pressure recovery, for a constant coarctation of 75% and different aortic stenosis severities (1.5 cm^2 to 0.61 cm^2). It appears that the increase in severity of aortic stenosis induces a slight increase in both maximal pressure drop and pressure drop after pressure recovery. More importantly, the upstream pressure drop is significantly high and dependents on the severity of the upstream obstruction (from 36 mmHg for a 1.5 cm^2 to a 24 mmHg for an AS of 0.61 cm^2). A simple linear fitting shows that the upstream pressure drop is a function of the position of the pressure measurement ($P(x) = 1.34\,x - 13$ mmHg, in average). The clinical consequence is that if the catheter is put far from the coarctation (let's say point 4 instead of point 5 on figure 3.9(c)) there will be a systematic overestimation of the severity of the coarctation.

3.4. Limitations of the study

The first limitation associated with this study is that in a physiological case, a substantial fraction (around 15%) of blood flow crossing the aortic valve does not pass through the coarctation since it is redirected towards the brain and the upper part of the body. Furthermore, in case of a severe coarctation of the aorta, body response is usually to develop a complex pattern of collaterals to limit the impact of the

coarctation on the amount of blood towards the lower parts of the body. However, taking into account these points would have made the study more complex without allowing the determination of the independent impact of the coexistence of coarctation of the aorta and aortic stenosis on the flow within a curved pipe.

Another limitation is that COA is, in the majority of cases, associated with bicuspid aortic stenosed valve (BAV) (30% to 50%) and with tricuspid aortic stenosis (AS) (15%). The stenotic valves simulated in this study are, however, geometrically closer to tricuspid aortic stenoses.

3.5. Conclusions

In our study, three dimensional numerical simulations under unsteady conditions of blood flow in a curved tube with both coarctation and stenosis with various severities have been performed. The results showed that the coexistence of both pathologies has a significant impact on the flow in a curved pipe in terms of secondary flow patterns, wall shear stress and pressure loss.

The results indicate significant variation across the stenotic lesion in the presence of obstructions. The more skewed axial velocity causes more adverse pressure and more reverse flow which is illustrated by the existence of flow separation in the post-stenosis regions. This study also reveals the regions with negative WSS and high OSI which are indicators of atherosclerosis. Furthermore, it appeared that the presence of an aortic stenosis can lead to an overestimation of the severity of the coarctation of the aorta.

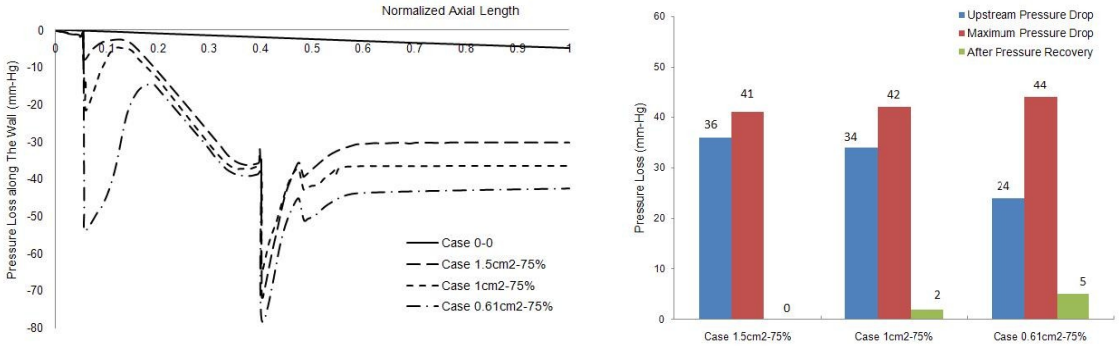

(a) (b)

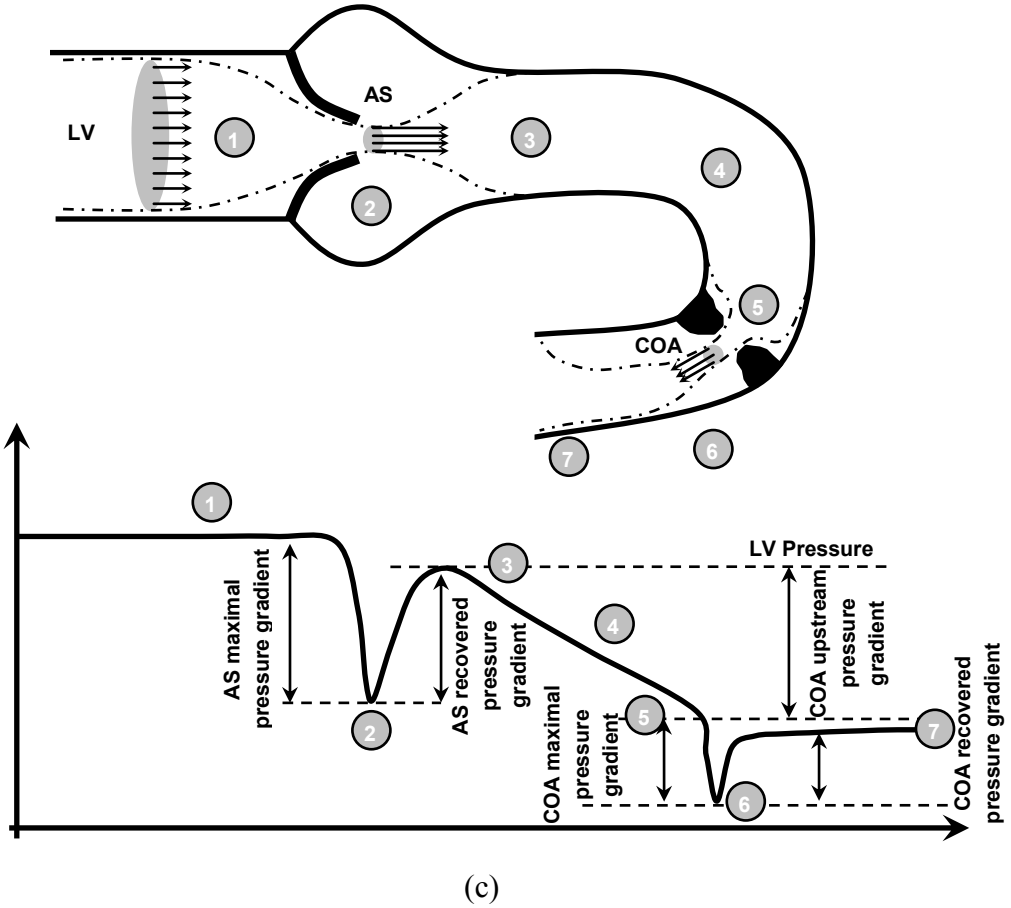

(c)

Figure 3.9. Pressure loss through the normal case and the cases with the same coarctation severity (75%) but different stenosis severities (0.61 cm^2; 1.0 cm^2 and 1.5 cm^2). (a) Pressure drop along the central line of the curved tube. (b) Upstream, maximum and after pressure recovery pressure drops. (c) Sketch of the pressure variation along an aorta with coexisting aortic stenosis and coarctation of the aorta. Note that the severity of the coarctation is overestimated if a catheter is placed far downstream of the location of the coarctation (point 4 instead of point 5)

After completion of the chapter 3, the next logical step was to perform similar analysis on a realistic geometry of the aorta. In the following chapter, aortas (with realistic geometries and curvature) in healthy condition and COA coexisted with normal tricuspid and bicuspid aortic valves (with realistic aortic roots) were explored to identify hemodynamic factors that lead to changes in the function and health of the vessels.

The curved tube model in chapter 3 lacked aortic arch branches. In a healthy aorta a small portion of the total flow rate (15%) is directed towards aortic arch branches. However, when a COA is present in the model, depending on its severity, the portion of the total flow rate bypassing the COA (forwarded towards the aortic branches and potential collaterals) will increase and greatly depends on the severity of COA. This important limitation, which exists in both previous works and the curved tube study (chapter 3), was not present in this study.

Additionally, in the curved tube study (chapter 3), the aortic valve stenosis was investigated by including a simple symmetrical restriction in the flow. The following chapter uses a realistic aortic root with bicuspid aortic valve. Moreover in the previous study coarctation was modeled as a simple sharp restriction in the flow whereas here it has a realistic geometry.

Chapter 4

Article 2

4. Study of Fluid Dynamics through Coarctation of the Aorta and the Effect of Bicuspid Valve

Abstract

Coarctation of the aorta is an obstruction of the aorta (between aortic arch and descending aorta) and is usually associated with bicuspid aortic valve. Numerous investigations pointed out that there is a relationship between the genesis and the progression of cardiovascular disease and the locally irregular flow occurring at the diseased zone. The objective of this study is to investigate the flow in the aorta in the presence of a coarctation (75% by area) and bicuspid aortic valve (EOA = 1.1 cm^2). For this purpose, aorta with realistic geometries in healthy condition and coarctation coexisted with normal and bicuspid aortic valves were explored. The maximal velocity is shifted towards the outer wall and can reach values as high as 3 m/s just downstream of the coarctation. This alteration is more pronounced downstream of the coarctation where negative velocities demonstrating reversed flow are present. The wall shear stress distribution is significantly modified in the presence of a coarctation compared to the normal case. Coarctation caused high wall shear stress at the region of the coarctation and low time-averaged wall shear stress, and high oscillatory wall shear stress index downstream of the coarctation. Finally, when coarctation is

accompanied by bicuspid aortic valve, the maximum velocity downstream of coarctation is greater than coarctation with the same severity in a normal valve. This can lead to an overestimation of the severity of the coarctation using Doppler echocardiography.

4.1. Introduction

Coarctation of the aorta (COA) is a common cardiovascular condition, accounting for 5%–10% of congenital heart disease and represents 7% of critically ill infants with heart disease (Secchi et al., 2009), with significant associated morbidity including hypertension, aortic aneurysm and dissection, heart failure as well as hemorrhage. COA can be either simple (isolated defect) or complex (associated with other intracardiac or extracardiac defects). Complex aortic COA is associated with bicuspid aortic valve (BAV) in the majority of cases (20 to 85%) (Grotenhuis and Roos 2011). The presence of a BAV confers a substantially increased risk for aortic dissection. Patients with both COA and BAV are more likely to develop aortic stenosis, aortic regurgitation, and aortic aneurysm (Abbott, 1928). Additionally, when BAV occurs with COA, the risk of aortic complications such as dissection and aneurysm is markedly increased (Oliver at al., 2004; Ward, 2000).

It is hypothesized that hypertension may still remain post-surgery because of the baromechanical induced changes to the chemical output of the aortic endothelial cells (ECs) (Barton et al., 2001) as an effect of the coarctation. Endothelial cells lining the inner wall of blood vessels are constantly exposed to biomechanical stimuli ranging

from hydrostatic pressures and cyclic strains, to frictional wall shear stresses. Hemodynamics has been proposed as a factor regulating blood vessel structure and influencing the development of vascular pathology (Fry, 1969; Zarins et al., 1983; Kerber et al., 1996). Considerable attention has been given to wall shear stress (WSS), one of the most important biomechanical stimuli, which is known to alter EC morphology and their complex biological activities (Barton et al., 2001). The ECs lining the interior wall of blood vessels have mechano-sensors consisting of membrane components such as membrane proteins, ion channels, caveolae and the cytoskeleton which can detect changes in shear stress lie on the cell membrane (Fisher et al., 2001; Li et al., 2005). As a result of the changes in shear stress to ECs, the ECs can change structurally and functionally in cellular production of a range of chemicals that carry out cellular functions as well as systemic functions (Malek et al., 1999; Hsiai et al., 2002).

Hemodynamics of the normal adult-scale aorta is a classical topic of cardiovascular fluid dynamics and has been extensively studied (Wood et al., 2001; Mori and Yamaguchi, 2002; Shahcheraghi et al., 2002; Jin et al., 2003; Wen et al., 2010). Interestingly, only limited studies have been dedicated to simulate coarctation of the aorta (Kim et al. , 2009; Keshavarz-Motamed and Kadem, 2010).

The objective of this study, therefore, is to identify hemodynamic factors that lead to acute and gradual changes in the function and health of the vessels through a joint experimental and numerical investigation of blood flow dynamics in COA. The interaction between COA and BAV will be studied and their relative impacts on hemodynamics will be investigated. For this purpose, aorta with realistic geometries

in healthy condition and COA coexisted with normal tricuspid and bicuspid aortic valves will be examined.

4.2. Methods

4.2.1. Numerical simulations

4.2.1.1 Numerical model

Computations were performed using computational fluid dynamics open source (OpenFOAM) based on a finite volume method for solving the Navier-Stokes equations. In healthy vessels, the blood flow is usually laminar and does not experience transition to turbulence. Therefore the solution was obtained by simulating a laminar flow inside the domain of healthy aorta (Figure 4.1) (Ryval et al., 2004). Obstruction resulting from a stenosis and/or coarctation can lead to disturbed flow regions in the aorta. Meanwhile, in the presence of a sufficiently severe stenosis, turbulence could be generated during part of the cardiac cycle (i.e., $Re > 1000$) (Ryval et al., 2004). Ghalichi et al. (1998) presented numerical results for transitional and turbulent flow through moderate and severe arterial stenoses by applying a $\kappa-\omega$ turbulence model. It was concluded that this model is suitable for blood flow studies where both laminar/transitional and turbulent flow regimes coexist. Hence, in this study, the models with both COA and/or BAV have been investigated using the transitional version of the $\kappa-\omega$ turbulence model which has been shown to give a better overall representation of both steady and pulsatile flow compare to the standard $\kappa-\omega$ (Ryval et al., 2004).

Mesh independency was achieved for all cases with 1855000 to 2100000 tetrahedral elements with elements concentrated in the region downstream of the COA. Moreover, additional care was taken near the wall to maintain y^+ less than 1, a criterion required by the $\kappa-\omega$ model, which yielded an average y^+ value of 0.523 for all cases. For time independency, several time steps were tested: 0.001 s, 0.002 s, 0.0025 s and 0.003 s. The solution marched in time with a time step of 0.0025 s to satisfy time step independency. Four cardiac cycles were simulated for each flow model to ensure periodicity. The governing equations were discretized using second order schemes. The mass-momentum equations were solved using PISO algorithm. The convergence was obtained when all residuals reached a value lower than 10^{-5}.

Additionally CFD uncertainty and error in the study were found according to (Celik et al., 2008). Table 4.1 shows the calculations for the discretization error for wall shear stress and velocity respectively. The parameters, N, r, p, ϕ, ϕ_{ext}, e_a, e_{ext} and GCI_{fine} represent the number of elements, the refinement ratio, the apparent order, the wall shear stress, the extrapolated value, the apparent error, the extrapolated error and the fine-grid convergence index respectively (Celik et al., 2008). It should be mentioned that in this study ϕ was the wall shear stress (Pa) at the inner wall at the COA region. These computations indicate that the numerical uncertainty for the case where COA coexists with normal valve is 5.51%.

4.2.1.2 Boundary conditions and model properties

Blood was assumed to be a Newtonian and incompressible fluid with dynamic viscosity of 0.0035 Pa·s and a density of 1050 kg/m^3 (Morris et al., 2005). Although human blood tends to exhibit non-Newtonian behavior at shear rates under 100 s^{-1} near the vessel walls, the shear rates in large arteries are generally observed to be greater than 100 s^{-1} and hence it is reasonable to assume a Newtonian fluid in the simulation (Fung 1981; Shahcheraghi et al., 2002; Morris et al., 2005). The arterial wall was treated as solid and rigid, this assumption can be justified by: 1) Jin et al. (2003) showed that the overall behavior for wall shear stress at each point is similar for the rigid and elastic walls with average root mean squared error of 1.232%. Furthermore, their velocity distribution, computed in both elastic and rigid models, showed a good agreement with magnetic resonance phase contrast velocity measurements; 2) It was reported that patients with coarctation are usually hypertensive and characterized by reduced compliance and elevated stiffness index in both proximal and distal aorta (Gardiner et al., 1994; Xu et al., 1997; Brili et al., 1998; Vogt et al., 2005; Vitarelli et al., 2007; Senzaki et al., 2008). Non-permeable and a no-slip boundary condition was applied at the rigid walls. In normal aorta, a small portion of the total flow rate (15%) is directed towards aortic arch branches. However, in aorta with coarctation, depending on its severity, the portion of the total flow rate bypassing the COA (forwarded towards the aortic branches and potential collaterals) is specified as an outlet boundary condition following the predictions from the lumped parameter model (75% COA: 30% of total inlet flow rate was specified at the exit of the branches) (Keshavarz et al., 2011).

For pulsatile flow simulations, at the aortic inlet, a flat inflow velocity profile was adopted in conjunction with a pulsatile waveform. The statement of the flat velocity profile specified at the aortic inlet is justified by *in vivo* measurements using the hot film anemometry technique in various animal models. Results have shown that the velocity profile distal to the aortic valve was relatively flat (Nerem 1992; Shahcheraghi et al., 2002; Gao et al., 2006). The unsteady simulations were performed with a systolic duration of 300 ms (intermittency parameter = 0.35) and a heart rate of 70 bpm. The mean cardiac output was 5 L/min corresponding to a mean systolic inlet Reynolds number of 2110.

N_1, N_2, N_3	2050341, 1686476, 1000446
r_{21}	1.331
r_{32}	1.446
ϕ_1	102.22 Pa
ϕ_2	100.71 Pa
ϕ_3	99.1 Pa
p	4.013
ϕ_{ext}^{21}	106.78 Pa
e_a^{21}	1.47%
e_{ext}^{21}	4.27%
GCI_{fine}^{21}	5.51%

ε_{32} = -1.61, ε_{21} = -1.51

Table 4.1. Calculation of discretization errors for COA coexists with normal valve

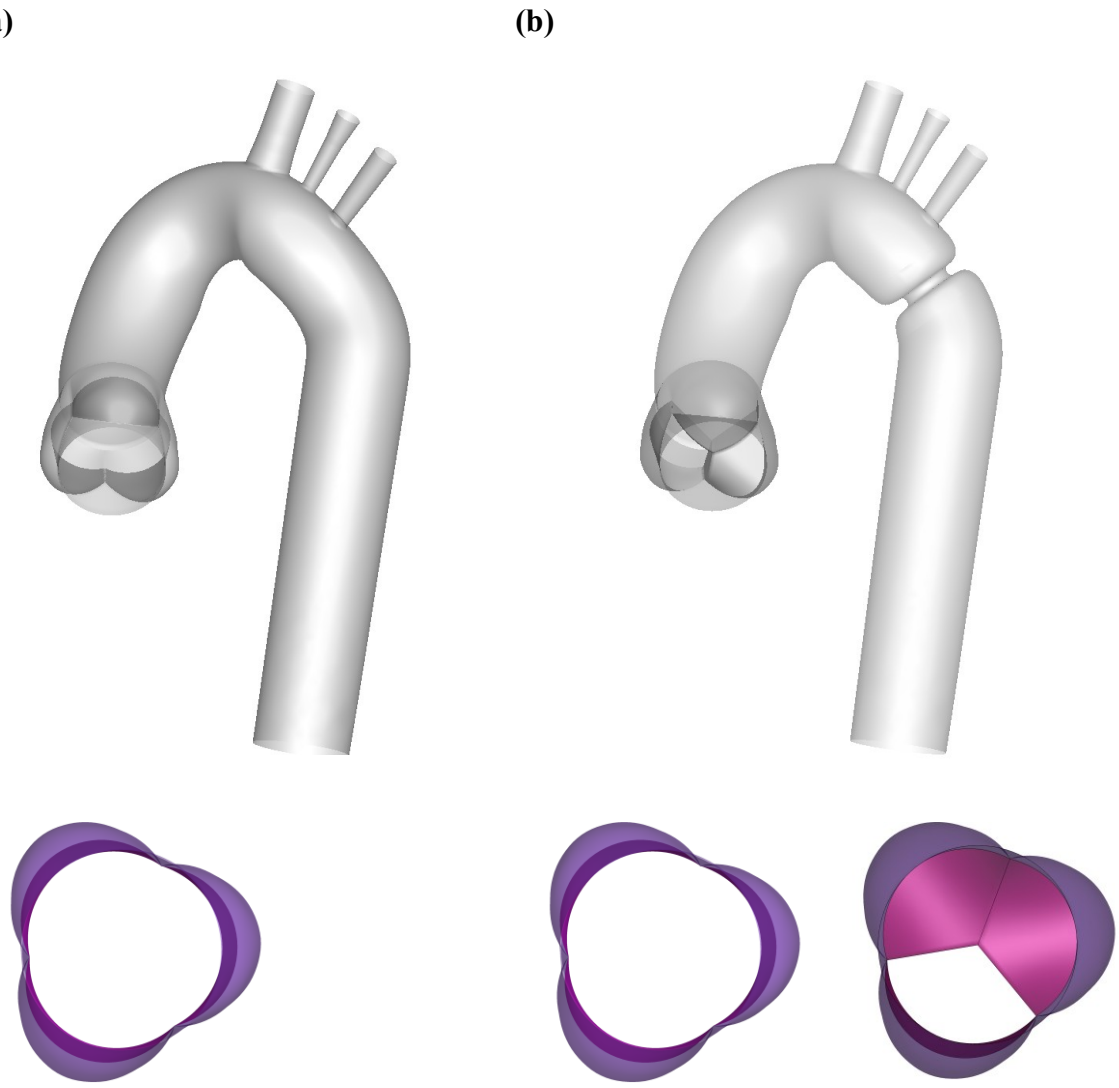

Figure 4.1. Aorta models used for numerical simulations and MRI measurements, (a) Normal aorta and normal valve, (b) COA (75% by area) coexisted with normal valve and BAV

4.2.2. Magnetic resonance imaging measurement protocol

4.2.2.1. *In vitro* setup

The *in vitro* model used for MRI measurements includes a fluid reservoir, a gear pump, an elastic model of the aorta and adjustable systemic arterial resistance and

compliance (Figure 4.2). Three-dimensional models of the human aorta, with anatomical dimensions and orientations, representing healthy aorta and aorta with coarctation (75% by area) were created (Figure 4.1). The completed models are then converted to the stereolithographic (STL) file format from which two molds were manufactured using rapid prototyping techniques and used to fabricate multi-layer silicon elastic models of the aorta. We fabricated elastic models of the aorta (including: ascending aorta, aortic branches and descending aorta) by using a multi–silicone layer method from an anatomically shaped mold.

With the use of this technique, successive layers of silicone were applied on the mold until both radial dilatation of the proximal aorta and total arterial compliance (determined by the ratio of pulse arterial pressure over stroke volume) matched physiological values. The elastic model of the aorta used in this study has a radial dilation of the proximal aorta of 8% (physiological value around 10% (O'Rourke et al., 2008; Herment et al., 2011)) and a total arterial compliance of 1.75 ml/mmHg (physiological value 1.84 ± 0.76 ml/mmHg (Chemla et al., 1998). The fluid (65% saline and 35% glycerine in volume at room temperature) was used to mimic viscous proprieties of blood at 37°C (Sturm et al., 1992). The fluid is pumped from a reservoir, crosses the aortic valve and is then directed towards the aortic branches and the descending aorta. When COA is not present, a small portion of the total flow rate (15%) is directed towards aortic arch branches. However, when a COA is introduced in the experimental model, depending on its severity, the portion of the total flow rate bypassing the COA (forwarded towards the aortic branches and potential collaterals) is adjusted following the predictions from the lumped parameter model (Keshavarz et

al., 2011). Instantaneous flow rates were measured by T206 Transonic flowmeter (Transonic System Inc., Ithaca, NY, USA, accuracy of 1% full scale) at the level of descending aorta and aortic arch arteries. The pressures upstream (10 mm) and downstream (10 mm) of the aortic valve were measured using Truwave disposable pressure transducers (Edwards Lifesciences, Irvine, California, USA, sensitivity of 5 μV/V/mmHg ± 1%) in order to investigate left ventricle and aorta pressures during MRI scanning. The measurements were performed in normal aorta and COA with various aortic valve conditions (biological normal aortic valve and biological bicuspid aortic stenosis) with a pulsatile mean flow rate of 5 L/min.

4.2.2.2. Cardiovascular magnetic resonance imaging

The aortic model was placed at the center of the magnet during the tests and all data were collected with the use of a clinical 3 Tesla magnetic resonance scanner with a dedicated phase-array receiver coil (Achieva, Philips Medical Systems, Best, Netherlands). An ECG patient simulator (model 214B, DNI Nevada Inc, USA) was used to synchronize the scanner's gating with the PC controllable pump. A standard examination was performed by initial acquisition of SSFP cine images in standard longitudinal and transverse planes for acquisition planning.

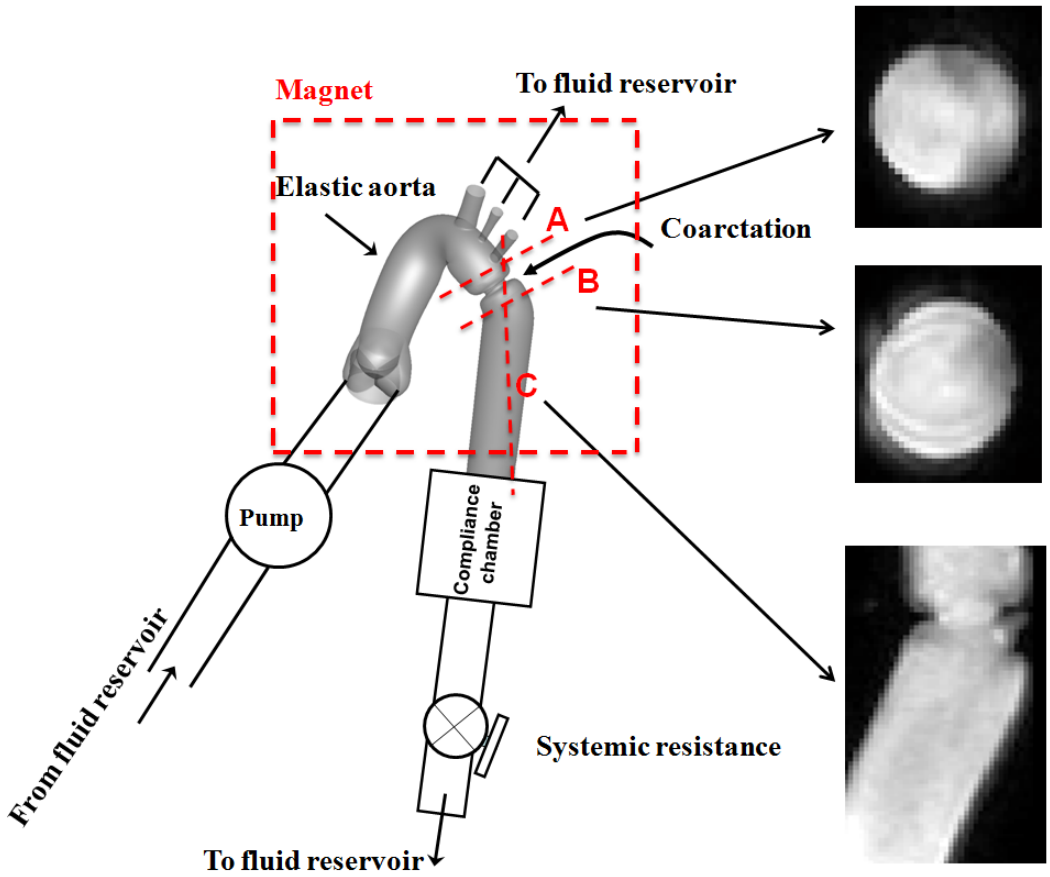

Figure 4.2. Schematic diagram of the *in vitro* flow model used for MRI measurements. Dashed red lines show the planes measured with MRI

Phase-contrast (sQFlow Phase SENSE) retrospective examination was performed on two transverse planes, 12 mm upstream and 10 mm downstream of the aortic valve and the longitudinal plane perpendicular to the leaflets. For coarctation cases, three additional planes were acquired: transverse planes (10 mm) downstream and upstream of the coarctation and a plane perpendicular to the coarctation (Figure 4.2). MRI imaging parameters consisted of: TR/TE (17.99/3.97 ms), flip angle (15°), pixel spacing (1.66 mm), slice thickness (10 mm), acquisition matrix (256 x 256) and encoding velocity (2 × maximal velocity).

A custom-made research application was developed using Matlab software (Mathworks, Natick, MA) to process and analyze MRI images. Spatial resolution of MRI images (initial resolution: 1.66 mm) was artificially improved by a factor of four (final resolution: 0.42 mm) using a bicubic averaged interpolation and themagnitude image stack was processed to filter background noise. All image data was analyzed with specially written Matlab programs (Mathworks, Natick, MA).

4.3. Results and discussions

The results show that COA has significant effects on the fluid dynamics in the aorta. Figure 4.3 shows that as the flow exits the COA, the fluid cannot abruptly change direction and follow the steep curvature after the coarctation. The disturbed flow resulted from COA detaches from the walls and develops into a jet. Under these conditions, the high speed jet induces reverse flow and recirculation areas along both the posterior and anterior walls. As an example, figure 4.3(B_1) shows a peak axial velocity of 3 m/s (demonstrating almost 4 times of the velocity in the normal case: 0.7 m/s in figure 4.5(A_1)) achieved at the peak of the systole downstream of the COA. The flow reversal along the posterior wall reaches a peak axial velocity of -1 m/s (Figure 4.3(B_1)), which is 130% of the average bulk velocity in the normal aorta. This behavior was observed for all instants during both acceleration and deceleration phases. Furthermore maximum axial velocity does not occur on the centerline anymore but instead a skewed velocity profile develops in which higher velocities occur near the wall during systole as observed previously in curved tubes (Keshavarz-

Motamed and Kadem, 2010). The described reversed flow and recirculation areas are further demonstrated by plotting the instantaneous velocity streamlines in figure 4.8. The flow patterns observed here share some common features found in a healthy aorta, such as highly helical flow, but differ in other aspects (e.g. significant recirculation zone) due to the presence of the COA. This is of paramount interest because in the normal aorta, typically the laminar flow is fully attached to the wall and the magnitude of the axial velocity profile is relatively low (with a magnitude of 0.6 to 0.8 m/s) (Figures 4.4 and 4.5). Furthermore, there is almost no flow reversal occurring except at very late systole, which is very minimal.

Figures 4.4 and 4.5 show that the COA has a significant effect on velocity contours upstream and downstream of the COA (planes A and B in Figure 4.2). The presence of the COA changes the rather uniform velocity profile of the normal case (no COA and no AS) to complicated velocity profiles. This alteration is more apparent downstream of the COA where negative velocities demonstrate that reversed flow is present.

Additionally, when the COA coexisted with a bicuspid aortic valve, maximum velocity downstream of the COA becomes significantly higher than COA with the same severity with a normal valve (i.e., Figure 4.3: COA & normal valve: V_{Max} = 1.6 m/s, COA & BAV: V_{Max} = 3 m/s). The same behavior was observed for all instants during systole which causes even stronger reverse flow.

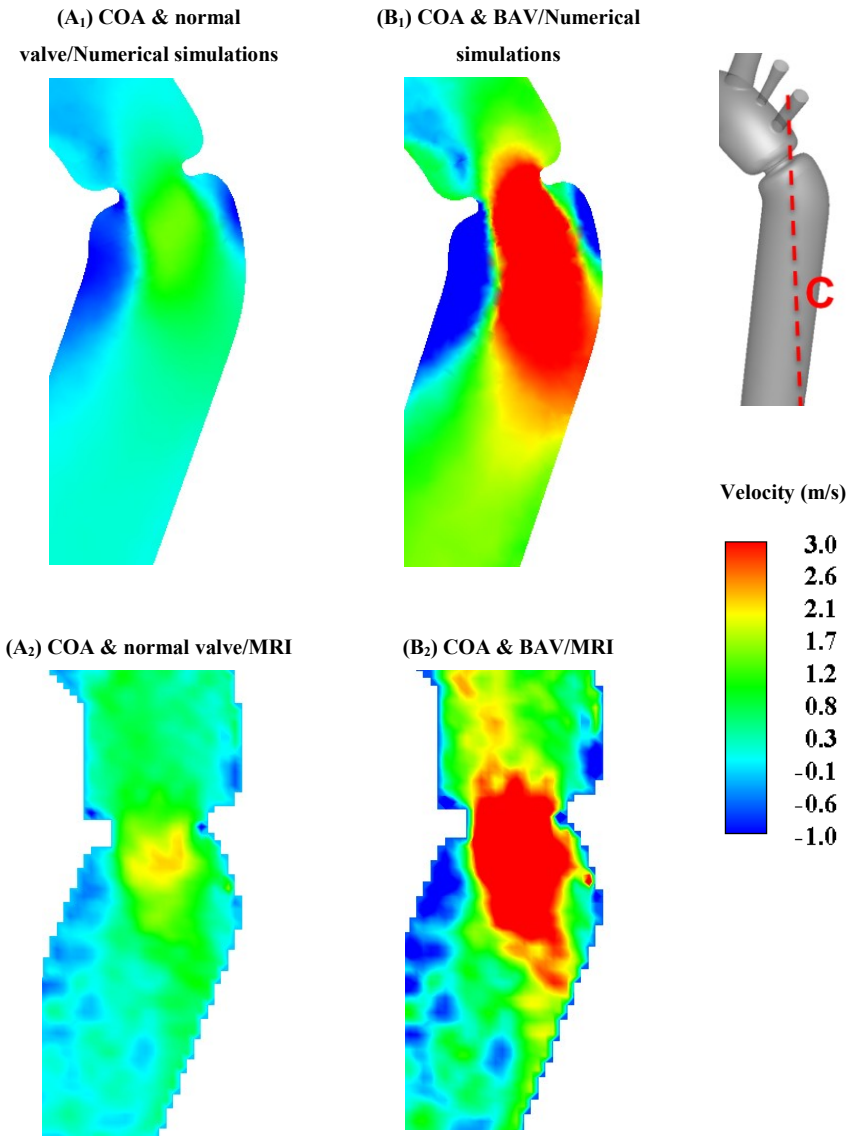

Figure 4.3. Axial velocity contour of the plane C at the peak of the systolic phase

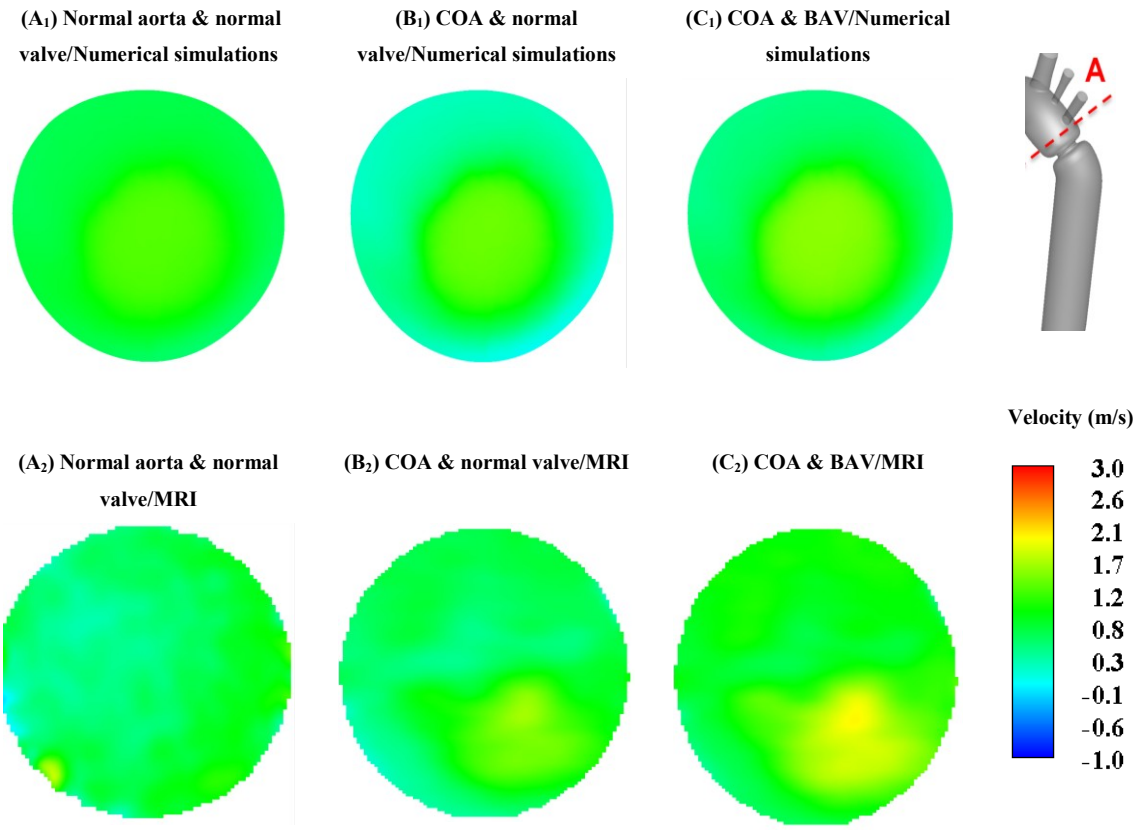

Figure 4.4. Velocity contours of the cross section A at the peak of the systolic phase

Figure 4.6 and 4.7 display the comparison between instantaneous velocity profiles obtained from numerical simulation and MRI measurements along the diameter at cross section A and B. The maximal root mean square error obtained was 0.31 m/s. There is good agreement between the measured and computed velocity. Furthermore, figures 4.3, 4.4 and 4.5 show the velocity contours extracted from the MRI data, compared with the computational results, for cross sections A, B and C, respectively. The CFD results show similar velocity distributions as the MRI measurements. This good overall agreement between the measured and computed velocity permits us to interrogate the numerical solutions with confidence to elucidate flow features that were not accessible by the measurements. This is consistent with the study of Jin et

al. (2003), showed that the overall behaviors for WSS and velocity at each point are similar for the rigid and elastic walls.

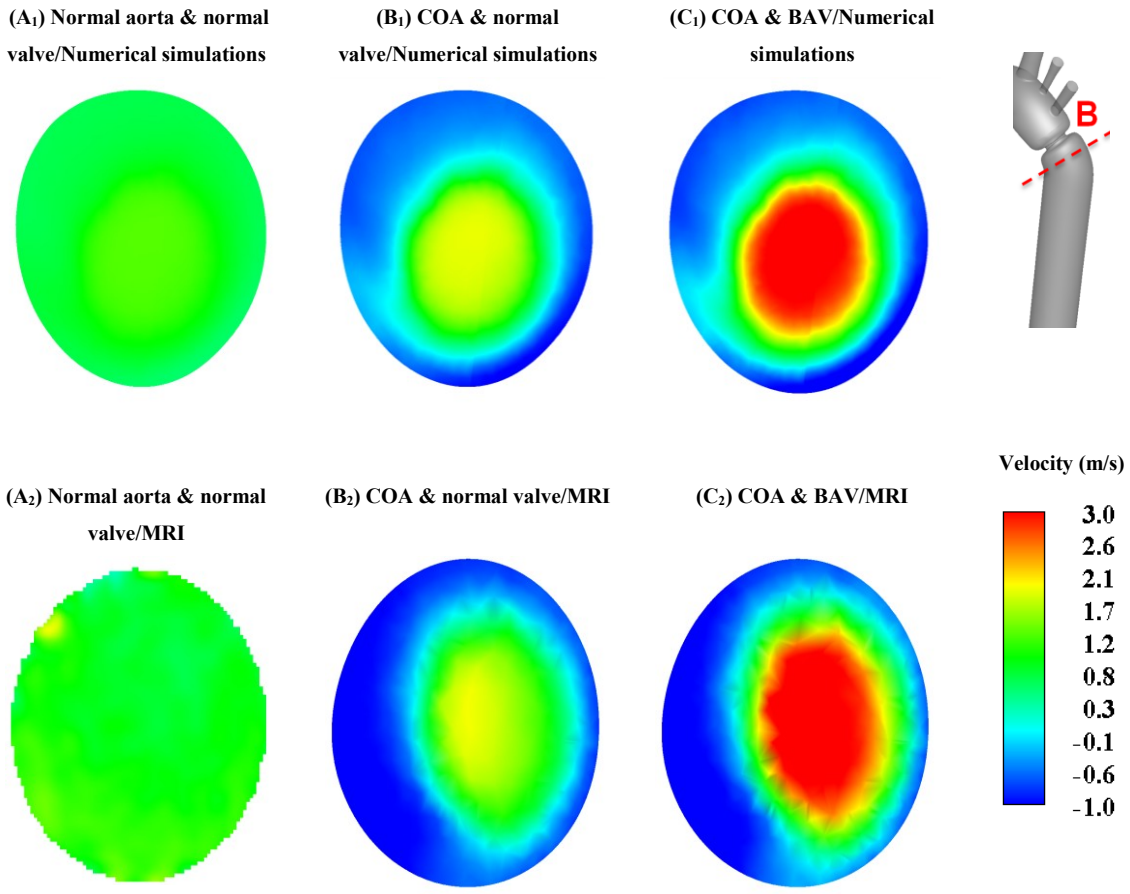

Figure 4.5. Velocity contours of the cross section B at the peak of the systolic phase

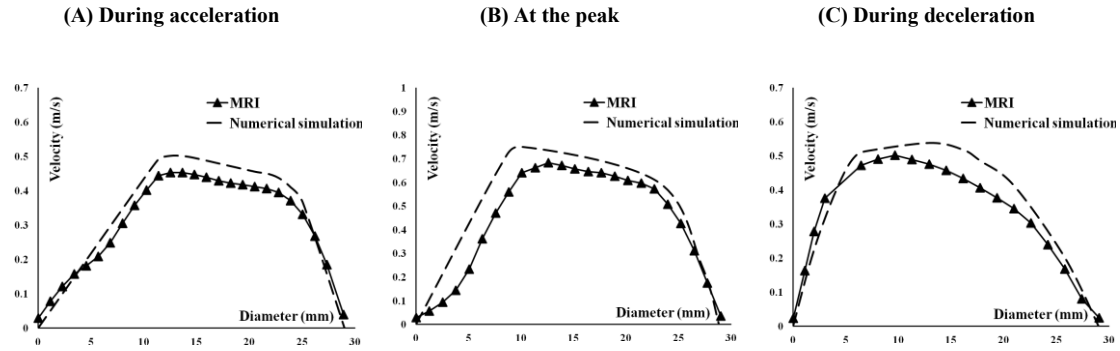

Root mean square error=0.18 m/s Root mean square error=0.21 m/s Root mean square error=0.23 m/s

Figure 4.6. Velocity profile along diameter of the cross section A

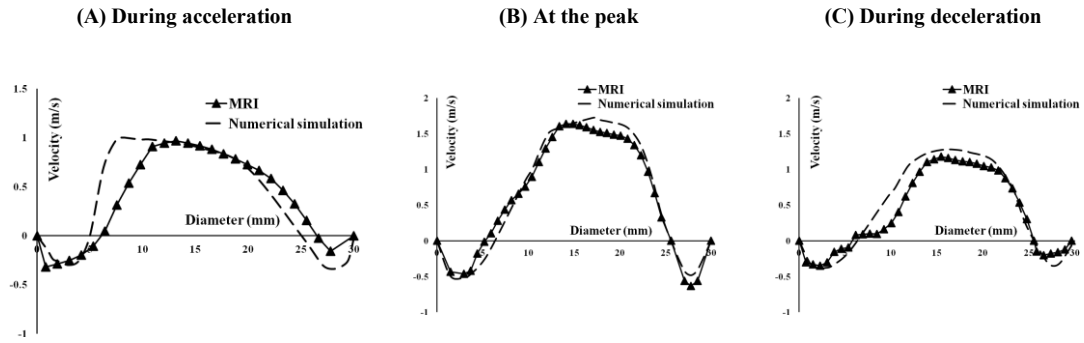

Root mean square error=0.31 m/s Root mean square error=0.17 m/s Root mean square error=0.27 m/s

Figure 4.7. Velocity profile along diameter of the cross section B

The fluid mechanical stress that acts directly on the endothelial cells is the wall shear stress. Berger and Jou (2000) pointed out that both high and low oscillating shear stress regions are prone to develop atherosclerosis. Regions of high WSS are likely to lead to matrix degradation by expression of plasmin, matrix-metalloproteinases and smooth muscle cell apoptosis. This may lead to alteration of the wall thickness and could eventually cause rupture. Furthermore, due to the pulsatile nature of blood flow in arteries, which are considered to be more susceptible to intimal thickening and

plaque formation (Pedersen et al., 1997; Friedman et al., 1981; Zarins et al., 1983; Ku et al., 1985), the oscillatory characteristics of shear stress are even more important to analyze. Identifying such regions in the flow field is, therefore, essential to understand plaque formation and rupture (Pedersen et al., 1997; Friedman et al., 1981; Zarins et al., 1983; Ku et al., 1985). Also, it is hypothesized that hypertension exists even after surgery because of the baromechanical induced changes to the chemical output of aortic endothelial cells (ECs) (Barton et al., 2001) resulting from shear rate changes occurring due to the coarctation effect. Thus, understanding WSS, which cannot be measured directly by current *in vivo* techniques, can give insight into how the chemical output from these cells may have been altered.

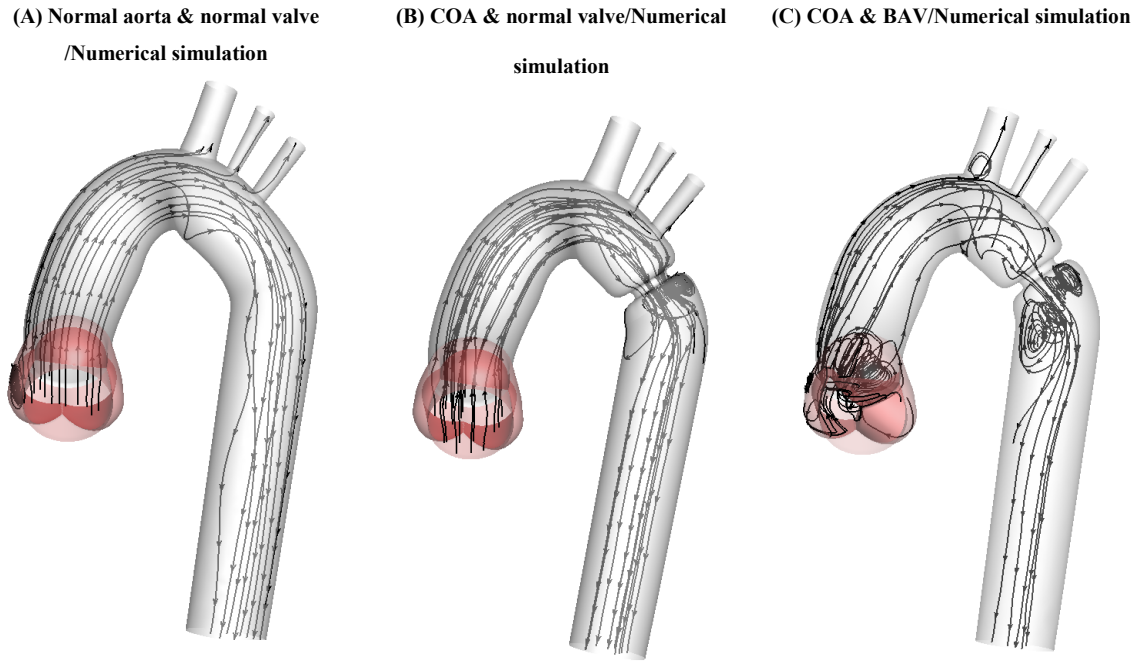

Figure 4.8. Instantaneous streamlines at the peak of the systolic phase

The total shear stress exerted on the wall throughout the cardiac cycle was evaluated using the time-averaged WSS (TAWSS) which is obtained from, $TAWSS = \frac{1}{T}\int_0^T |\tau| dt$ to show the spatial variation of WSS, where T and τ are the cardiac cycle period and instantaneous wall shear stress, respectively. Throughout the cardiac cycle, extremely high levels of TAWSS were found at the COA, where the velocity was high, and a localized part on the posterior wall downstream of COA. Low TAWSS were present in the regions of flow separation and reversal (downstream of COA) (Figure 4.9). The COA region is therefore prone to dilation and eventual rupture.

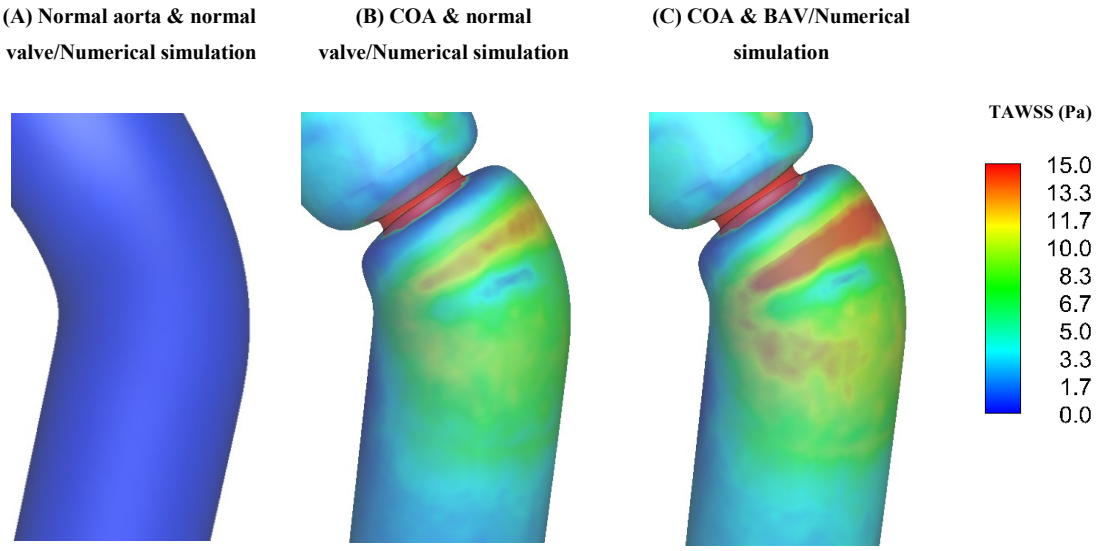

Figure 4.9. Time-averaged wall shear (TAWSS) contours

To evaluate temporal oscillations in WSS, the oscillatory WSS index (OSI) defined as $OSI = 1/2\left(1 - \frac{\int_0^T \tau dt}{\int_0^T |\tau| dt}\right)$ was used, where T and τ are the cardiac cycle period and the wall shear stress, respectively. Figure 4.10 shows the oscillatory shear index (OSI) distribution which has a range between 0 and 0.5, where 0.5 indicates a purely oscillatory flow. The numerical results suggest that high OSI values of up to 0.50 can be seen downstream of the COA. Areas of high OSI (Figure 4.10) lie within the areas of low TAWSS (Figure 4.9) indicating flow reversal or varying flow direction (Figure 4.3) which are considered to be more susceptible to intimal thickening and plaque formation (Pedersen et al., 1997; Friedman et al., 1981; Zarins et al., 1983; Ku et al., 1985).

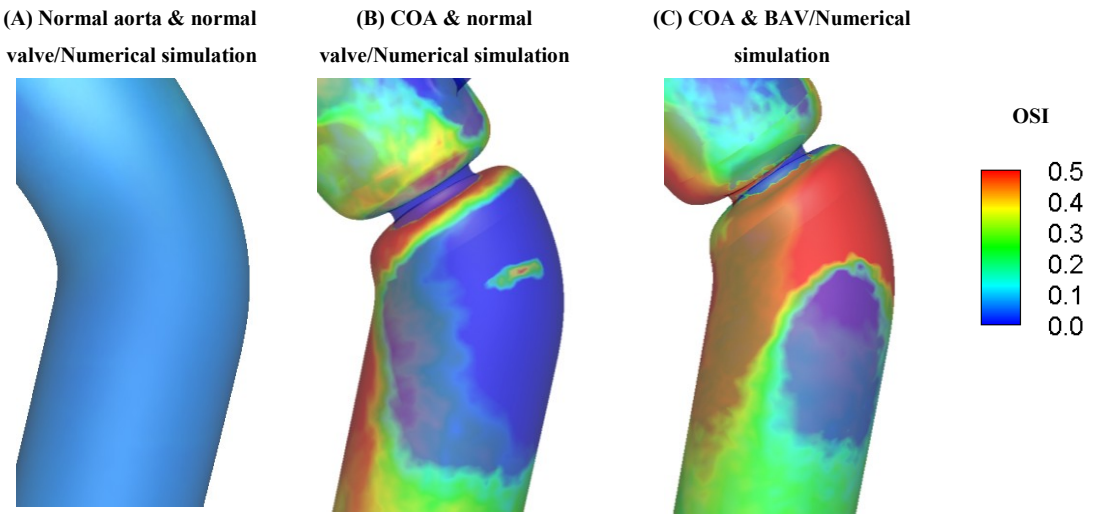

Figure 4.10. Oscillatory shear index (OSI) contours

4.4. Conclusions

The results show that the presence of coarctation of the aorta and bicuspid aortic valve significantly alters fluid dynamics in the aorta. The maximal velocity is shifted towards the outer wall and can reach values as high as 5 times the healthy aorta just downstream of the coarctation. This alteration is more manifested downstream of the COA where negative velocities demonstrating reversed flow are present. WSS distribution, which induces a micro environment of interaction between blood and the endothelial layer, were also analyzed in order to retrieve important information about the effect of the flow pattern on the aorta wall. The presence of a COA caused high WSS in the region of the COA. This study also revealed the regions with low TAWSS and high OSI laying within the areas with flow reversal and varying flow direction. These regions are considered to be more susceptible for atherosclerotic plaque rupture.

The interaction between COA and BAV was also studied. The results showed that when COA coexists with BAV, maximum velocity downstream of COA is significantly greater than when COA coexists with a normal valve. This caused increasing Doppler trans-COA pressure gradients in such cases since Doppler echocardiographic measurements included mean and maximal trans-COA pressure gradients using the simplified Bernoulli equation. This indicated that the presence of bicuspid aortic valve can lead to an overestimation of the severity of the coarctation of the aorta and ignoring this fact may result in major errors in medical diagnosis of patients with both COA and BAV.

Coarctation of the aorta (COA) often coexists with aortic stenosis (AS) (between 30% to 50%). As a result, the left ventricle faces a double-pressure-overload: AS + COA. This leads to a significant increase in systolic pressure and left ventricular work, thus increasing the risk of heart failure. Under such conditions, it is particularly important to determine: 1) Total load supported by the left ventricle and 2) the respective load induced by each pathology independently. This information will contribute to optimization of clinical procedures in terms of the sequence of lesion repair: valve replacement, COA repair or both.

In order to evaluate the global effects of AS and COA on the entire cardiovascular system, we conducted another study and assessed ventricular load. For this purpose, in the following chapter, we developed a lumped parameter model, solely based on non-invasive parameters, allowing the investigation of the respective impacts of AS and COA on the left ventricular load.

Chapter 5

Article 3

5. Modeling the Impact of Concomitant Aortic Stenosis and Coarctation of the Aorta on Left Ventricular Workload

Z. Keshavarz-Motamed[1], J. Garcia[2], P. Pibarot[2], E. Larose[2], L. Kadem[1]

1. Mechanical and Industrial Engineering, Concordia University, Montréal, Canada.

2. Québec Heart and Lung Institute, Laval University, Québec, Canada.

Journal of Biomechanics: Published 2011

Abstract

Coarctation of the aorta (COA) is an obstruction of the aorta and is usually associated with bicuspid and tricuspid aortic valve stenosis (AS). When COA coexists with AS, the left ventricle (LV) is facing a double hemodynamic load: a valvular load plus a vascular load. The objective of this study was to develop a lumped parameter model, solely based on non-invasive data, allowing the description of the interaction between LV, COA, AS, and the arterial system. First, a formulation describing the instantaneous net pressure gradient through the COA was introduced and the predictions were compared to *in vitro* results. The model was then used to determine LV work induced by coexisting AS and COA with different severities. The results show that LV stroke work varies from 0.98 J (no-AS; no-COA) up to 2.15 J (AS: 0.61 cm^2 + COA: 90%). Our results also show that the proportion of the total flow rate that

will cross the COA is significantly reduced with increasing COA severity (from 85% to 40%, for a variation of COA severity from 0% to 90%, respectively). Finally, we introduced simple formulations capable of, non-invasively, estimating both LV peak systolic pressure and workload. As a conclusion, this study allowed the development of a lumped parameter model, based on non-invasive measurements, capable of accurately investigate the impact of coexisting AS and COA on LV workload. This model can be used to optimize the management of patients with COA and AS in terms of the sequence of lesion repair.

5.1. Introduction

Coarctation of the aorta (COA) is a congenital heart disease characterized by a narrowing of the isthmus zone, i.e., the section of the descending aorta distal to the left subclavian artery. COA is encountered in 0.1% of newborns (De Mey et al., 2001) and is the third most prevailing defect in infants and children (5 to 8% of all congenital heart disorders) (Rao, 1995). In severe cases COA can result in serious complications such as hypertension, left ventricular failure, rupture of the aorta and premature coronary artery disease. As a result, 60% of adults over 40 years old with uncorrected COA have symptoms of heart failure and 75% of these patients die by the age of 50 and 90% by the age of 60 (Brickner et al., 2000).

COA often occurs in combination with other congenital cardiovascular diseases. In the majority of cases COA coexists with aortic stenosis (AS) (between 30% to 50%) (Brickner et al., 2000; Braverman et al., 2005; Hamdan, 2006). The left ventricle

(LV) then faces a double-pressure-overload: AS + COA. This leads to a significant increase in left ventricular work and systolic pressure, thus increasing the risk of heart failure. Under such conditions, it is particularly important to determine: 1) the total load supported by the LV and 2) the respective load induced by each pathology independently. This information will contribute to optimize the clinical procedure in terms of the sequence of lesion repair: valve replacement, COA repair or both (Chu et al., 2011). The total load supported by the LV could be better characterized by LV stroke work determination which can be used to assess the inotropic state of the left ventricle (Burkhoff et al., 2005) and represents the work of the left ventricle during each heart beat. Thus, LV stroke work has been shown to effectively characterize patient's outcome (Garcia et al., 2006). However, this parameter requires invasive determination of the instantaneous ventricular pressure and volume, thus limiting its *in vivo* application. An alternative way to estimate LV stroke work and to investigate the impact of pathological conditions on LV performance is to model the cardiovascular system using lumped parameter models. This approach has been extensively used to model both healthy and pathological conditions (Segers et al., 2000-2003; Garcia et al., 2005; Tanné et al., 2008). Interestingly, only a limited number of models have been dedicated to simulate coarctation of the aorta (Engvall et al. 1991 & 1994). More recently, Kim et al. (2009) investigated LV stroke work induced by an isolated COA (without AS) before and after surgery. They coupled a finite-element model to a lumped parameter model, but had to model aorta and COA using a three-dimensional finite-element model.

The limited number of lumped parameter models dedicated to COA can be explained by the following reasons: 1) lack of a mathematical expression that can accurately describe the instantaneous pressure drop (or pressure gradient) across the COA; 2) difficulty to predict mathematically the portion of the total flow rate that crosses the COA.

The objective of this work was to develop a lumped parameter model, solely based on non-invasive parameters, allowing the investigation of the respective impacts of AS and COA on the left ventricular load. For this purpose, a formulation for instantaneous net pressure gradient through the COA was proposed and validated by comparing the results against *in vitro* experiments. The suggested model was then applied to calculate the LV work for different severities of AS and COA. Further validations were performed by comparing the flow rate through COA with *in vivo* MRI measurements published in the literature.

5.2. Lumped parameter model method

A schematic diagram of the lumped parameter model used in this study is presented in figure 5.1. This model includes three different sub-models: 1) left heart-arterial model; 2) AS model; 3) COA model.

(a)

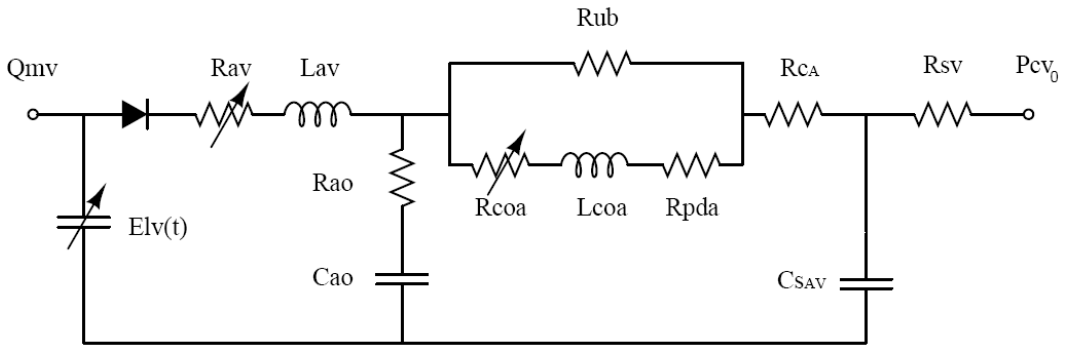

(b)

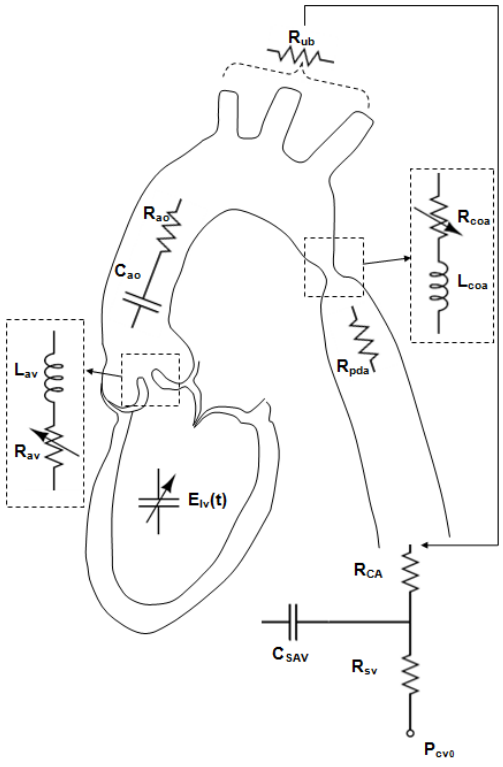

Figure 5.1. Lumped parameter model used to simulate left-sided heart with aortic stenosis and coarctation of the aorta (Please see table 5.1 for more details)

Description	Abbreviation	Value	Maximum relative error*
Ventricular parameters			
Left-ventricular end-diastolic volume	$LVEDV$	150 ml	
Unstressed volume	V_0	-15 ml	
Maximal elastance	E_{max}	Adjusted for stroke volume 75 ml	
Time to maximal elastance	T_{Emax}	0.24s	
Aortic valve parameters			
Effective orifice area	EOA	From 0.6 to 4 cm^2	8.27%
Aortic cross sectional area	A_{ao}	8 cm^2	1.25%
Coarctation of the aorta parameters			
Coarctation severity		From 50% to 90%	
Systematic circulation parameters			
Aortic resistance	R_{ao}	0.05 $mmHg.s.ml^{-1}$	0.41%
Aortic compliance	C_{ao}	0.5 ml/mmHg	0.44%
Systemic vein resistance	R_{SV}	0.05 $mmHg.s.ml^{-1}$	0.47%
Systemic arteries and veins compliance	C_{SAC}	2 ml/mmHg	0.88%
systemic arteries resistance (including arteries, arterioles and capillaries)	R_{SA}	0.8 $mmHg.s.ml^{-1}$	1.28%
Upper body resistance	R_{ub}	Adjusted to have 15% of total flow rate in healthy case (McDonald, 1974)	0.83%
Proximal descending aorta resistance	R_{pda}	0.05 $mmHg.s.ml^{-1}$	0.61%
Output condition			
Central venous pressure	P_{CV0}	4mmHg	
Input condition			
Mitral valve mean flow rate	Q_{mv}		
Other			
Constant blood density		1050 kg/m^3	
Cardiac output	CO	5.2 l/min	
Heart rate	HR	70 beats/min	
Duration of cardiac cycle	T	0.857 s	
* Maximum relative error in the computed left ventricular stroke work from sensitivity analysis in response to independent variation (-/+30%) in each parameter			

Table 5.1. Summary of the cardiovascular parameters used to simulate all cases

5.2.1. The left heart-arterial model

The coupling between LV pressure and LV volume is performed through a time varying elastance *E(t)* and the arterial system is modeled using a 3-element Windkessel model. Heart function is described by time varying elastance which is a measure of cardiac muscle stiffness: low in diastole and elevated in systole.

$$E(t) = \frac{P_{LV}(t)}{V(t) - V_0} \tag{5.1}$$

Where $P_{LV}(t)$, $V(t)$ and V_0 are left ventricular pressure, left ventricular volume and unloaded volume (Suga et al., 1973), respectively. V_0 is considered constant throughout the entire cardiac cycle (V_0 = 15ml).

The amplitude of *E(t)* can be normalized with respect to maximal elastance E_{max}, i.e., the slope of the end-systolic pressure-volume relation, giving $E_N(t_N)=E(t)/E_{max}$. Time then can be normalized with respect to the time to reach peak elastance, T_{Emax} ($t_N=t/T_{Emax}$). Interestingly, it has been shown that this normalized time-varying elastance curves $E_N(t_N)$ have similar shapes in the normal human heart with various inotropic conditions or diseased human hearts despite the presence of differences with regard to etiology of cardiovascular diseases (Suga et al., 1973; Senzaki et al., 1996).

$$E_{\max} E_N(t / T_{E\max}) = \frac{P_{LV}(t)}{V(t) - V_0} \tag{5.2}$$

This normalized curve can easily be described mathematically (Fourier series, polynomial description) and is therefore suitable for computer simulations. Therefore, if $E_N(t_N)$ is given, the relation between $P_{LV}(t)$ and $V(t)$ for any ventricle is determined.

The ventricle is filled by a normalized physiological mitral flow waveform adjusted for a stroke volume of 75 ml (Tanné et al., 2008).

5.2.2. Modeling aortic stenosis

The AS was modeled using the semi-analytical formulation, introduced by Garcia et al. (2005), for the net pressure gradient (TPG_{net}) across the stenotic valve during left ventricle ejection. This formulation expresses the instantaneous net pressure gradient across the stenotic valve (after pressure recovery) as a function of the instantaneous flow rate and the energy loss coefficient.

$$TPG_{net} = P_{LV}(t) - P_A(t) = \frac{2\pi\rho}{\sqrt{E_L Co}} \frac{\partial Q(t)}{\partial t} + \frac{\rho}{2E_L Co^2} Q^2(t) \tag{5.3}$$

and

$$E_L Co = \frac{(EOA)A}{A - EOA} \tag{5.4}$$

Where $E_L Co$, EOA, A and Q are the valvular energy loss coefficient, the effective orifice area, the aortic cross sectional area at the sinotubular junction and the transvalvular flow rate, respectively.

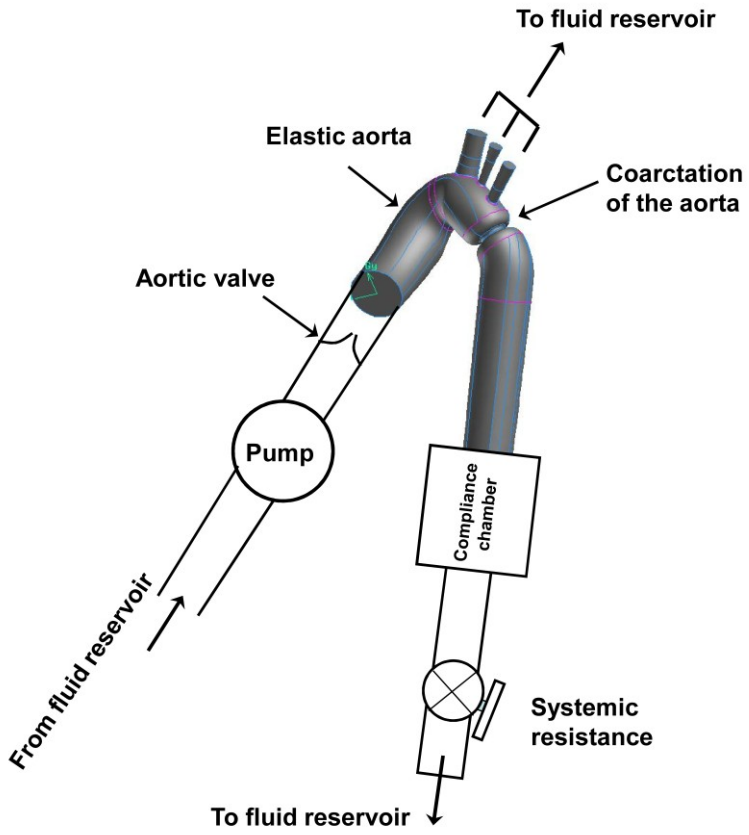

Figure 5.2. Schematic diagram of the *in vitro* model used to validate equation (5.3) and predict net trans-coarctation pressure gradient

5.2.3. Modeling coarctation of the aorta and aortic arch arteries

After crossing the aortic valve, blood flow ejected by the LV is rapidly redirected towards the upper-body (to deliver blood to the head, neck, shoulders and upper limbs) through aortic arch arteries (brachiocephalic truck, left common carotid artery and left subclavian artery) and towards the lower-body through the descending aorta. This characteristic of the arterial system is of primary importance when modeling the COA since only a portion of total flow rate will cross the COA.

To take this into account in the model, two parallel branches are considered. The first branch simulates the flow towards the upper-body, or the flow bypassing the COA (including aortic arch arteries and potential collaterals). The flow crossing the COA and directed towards the descending aorta is simulated in the second branch. This branch includes a resistance for the proximal descending aorta plus a time-varying resistance and an inductance which together represent the net pressure gradient induced by the COA. Since, no formulation has been developed to express the net instantaneous pressure gradient through a COA yet, we elected to use the same formulation as the one used for AS (Eq. (5.3)). The energy loss coefficient is then expressed in terms of the aortic cross section just downstream of the COA and the effective orifice area of the COA. In order to assess the validity of this formulation, *in vitro* experiments were performed in realistic models of the aorta with models of COA (Appendix). The model does not include compliance distal to the COA because patients with coarctation of the aorta are characterized by reduced compliance and elevated stiffness index distal to the COA (Xu et al., 1997).

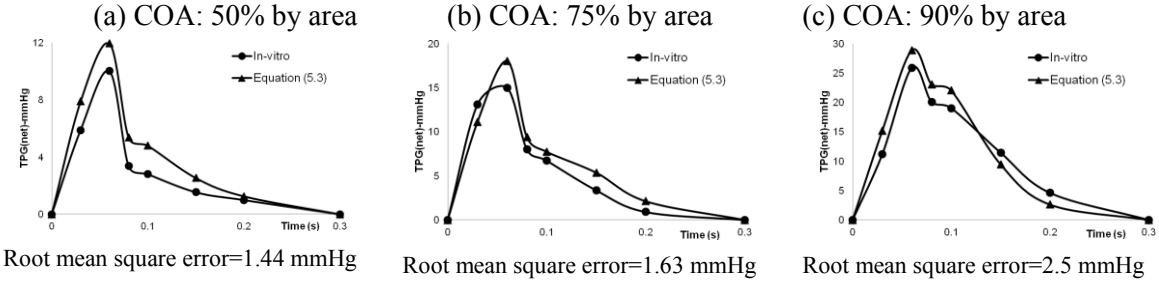

Figure 5.3. Comparison between instantaneous net trans-coarctation pressure gradient obtained *in vitro* and predicted using equation (5.3) for a flow rate of 6 L/min and various coarctation (COA) severities of: (a) 50%; (b) 75% and (c) 90% by area

5.2.4. Parameters used in the simulation

The respective impact of AS and COA on left ventricular work has been investigated under several numerical conditions. Three different severities for AS have been investigated. They correspond to effective orifice areas (EOA) of 0.61 cm^2 (severe AS), 1.0 cm^2 (moderate AS) and 1.5 cm^2 (mild AS). COA severity was varied from 50%, 75% to 90% reduction in aorta cross-sectional area which corresponds to coarctation indexes of 0.7 (mild COA), 0.5 (severe COA) and 0.31 (very severe COA), respectively (Coarctation index is defined as: (narrowest diameter of the descending thoracic aorta)/ (distal diameter of the descending thoracic aorta). All the other parameters are listed in Table 5.1. The values are determined according to the work of Sun et al. (1995) and Tanné et al. (2008).

5.2.5. Computational algorithm

Lumped parameter model illustrated in figure 1 was analyzed numerically by creating and solving system of ordinary differential equations in Matlab Simscape (MathWorks, Inc). Capabilities of this program were enhanced by adding additional codes to meet demands of cardiac model in circuit. Fourier series representation of experimental normalized elastance curve for human adults (Senzaki et al., 1996) was used to generate a signal to be fed into the main program. Equation (5.3), representing the transvalvular pressure gradient across the AS and the COA, was represented by an inductance and a variable resistor as depicted in figure 1. Simulation starts at the onset of isovolumic contraction and elastance signal drives the program by feeding elastance value related to each time step in the cycle to the equation (5.1). Left

ventricle volume $V(t)$ is calculated using left ventricle pressure P_{LV} and elastance values by equation (5.1). P_{LV} used at the beginning of calculation is the initial value assumed across the variable capacitor and is automatically adjusted later by system of equations as solution advances. The left ventricle flow rate subsequently is calculated as the time derivative of the left ventricle volume. After few initial cycles, solution converges. All results presented in this paper were taken at such a state. A diode with very low on resistance and off conductance was used in aortic valve module to prevent backflow from the valve. Matlab's ode23t trapezoidal rule variable-step solver was used to solve system of differential equations with initial time step of 0.1 milliseconds. Convergence residual criterion was set to 10^{-5} and initial voltages and currents of capacitors and inductors set to zero.

	Flow rate: 3 L/min	Flow rate: 4 L/min	Flow rate: 5 L/min
COA: 50% by area	3.6 mmHg	2.7 mmHg	3.1 mmHg
COA: 75% by area	2.8 mmHg	2.11 mmHg	2.2 mmHg
COA: 90% by area	4.5 mmHg	3.8 mmHg	3.5 mmHg

Table 5.2. Root mean square errors resulted from comparison between instantaneous net trans-COA pressure gradient obtained *in vitro* and predicted using equation (5.3) for different flow rates (3, 4 and 5 L/min) and various coarctation of the aorta (COA) severities (50%, 75% and 90% by area)

5.3. Validation of the model

5.3.1. Validation of the formulation for instantaneous trans-COA net pressure gradient

In this study we proposed an equation (5.3) for instantaneous trans-COA net pressure gradient. In order to investigate its validity, *in vitro* experiments were carried.

Briefly, we designed and constructed an *in vitro* model including a fluid reservoir, a gear pump, an elastic model of the aorta and adjustable systemic arterial resistance and compliance (Figure 5.2). We fabricated elastic models of the aorta (including: ascending aorta, aortic branches and descending aorta) by using a multi–silicone layer method from an anatomically shaped mold. With the use of this technique, successive layers of silicone were applied on the mold until both radial dilatation of the proximal aorta and total arterial compliance (determined by the ratio of pulse arterial pressure over stroke volume) match physiological values. The elastic model of the aorta used in this study has a radial dilation of the proximal aorta of 8% (physiological value around 10% (O'Rourke et al., 2008; Herment et al., 2011)) and a total arterial compliance of 1.75 ml/mmHg (physiological value 1.84±0.76 ml/mmHg (Chemla et al., 1998)). The fluid (a mixture of 60% water and 40% glycerol, dynamic viscosity of 3.6 cP) is pumped from an open tank (reservoir), crosses the aortic valve (a bioprosthetic valve or silicone models of AS) and then is directed towards the aortic branches and the descending aorta. When COA is not present, a small portion of the total flow rate (15%) is directed towards aortic arch branches. However, when a COA is introduced in the experimental model, depending on its severity, the portion of the total flow rate bypassing the COA (forwarded towards the aortic branches and potential collaterals) is adjusted following the predictions from the lumped parameter model. Flow control and data acquisition were performed using a custom-made application running under Labview (LabView, National Instruments, Austin, TX, USA). Instantaneous flow rates were measured by electromagnetic flowmeters (Carolina Medical Electronics, East Bend, NC, USA, 600 series, accuracy of 1% full

scale) at the level of ascending aorta and aortic arch arteries. The pressures upstream (20 mm) and downstream (20 mm) of the aortic valve, and the pressures upstream (20 mm) and downstream (20 mm) of the COA were measured using Millar catheters (Millar Instruments, Houston, Tx, USA, SPC 360S, accuracy of 0.5% full scale). The validation of the expression for trans-COA net pressure gradient (eq. 3) was performed under the following experimental conditions: heart rate = 70 bpm; systolic blood pressure = 120 mmHg; diastolic blood pressure = 70 mmHg; three different COA severities (50%, 75% and 90% by area) and various aortic valve conditions (normal aortic valve, bicuspid AS and trileaflet AS) under 4 different flow rates: 3, 4, 5 and 6 L/min.

The difference between pressure measurements upstream and downstream of the COA (net trans-COA pressure gradient) was determined and compared to the analytical predictions using eq. 3. Figure 5.3 displays the comparison between instantaneous trans-COA net pressure gradients obtained from *in vitro* and the ones predicted by equation (5.3) for a flow rate of 6 L/min and various COA severities (50%, 75% and 90% by area). Table 5.2 summarizes the root mean square errors for all the cases tested. The maximal root mean square error obtained was 4.5 mmHg for the most severe COA (90% by area) and a flow rate of 3 L/min.

5.4. Verification of the lumped parameter model in presence of AS and COA using *in vivo* published MRI data

Verification was done using the case study reported by Markl et al. (2009). In their study, the authors present findings from a 36-year-old male patient with coexistent COA and mild AS which was revealed with standard contrast-enhanced magnetic resonance angiography. Data resulting from this case study consists of the flow rate in the ascending aorta, at the COA, after COA and in the descending aorta. As expected with COA, the authors found a significant decrease in the flow rate between the ascending and the descending aorta because more flow is redirected towards aortic arch arteries. Mean blood flow (area under curve) in the ascending aorta, at the COA, in the descending aorta were 125.5 ml, 77.5 ml, and 77.5 ml, respectively.

Data resulting from our mathematical simulations with the same severity for COA and AS mentioned in this case study (COA severity = 62%) were consistent with Markl et al. findings. Mean blood flows in the ascending aorta, at the COA, and in the descending aorta are 125.5 ml, 74.8 ml, and 74.8 ml, respectively.

The error calculated between mean blood flows at the COA, after COA and in the descending aorta was 3.5% throughout the cardiac cycle.

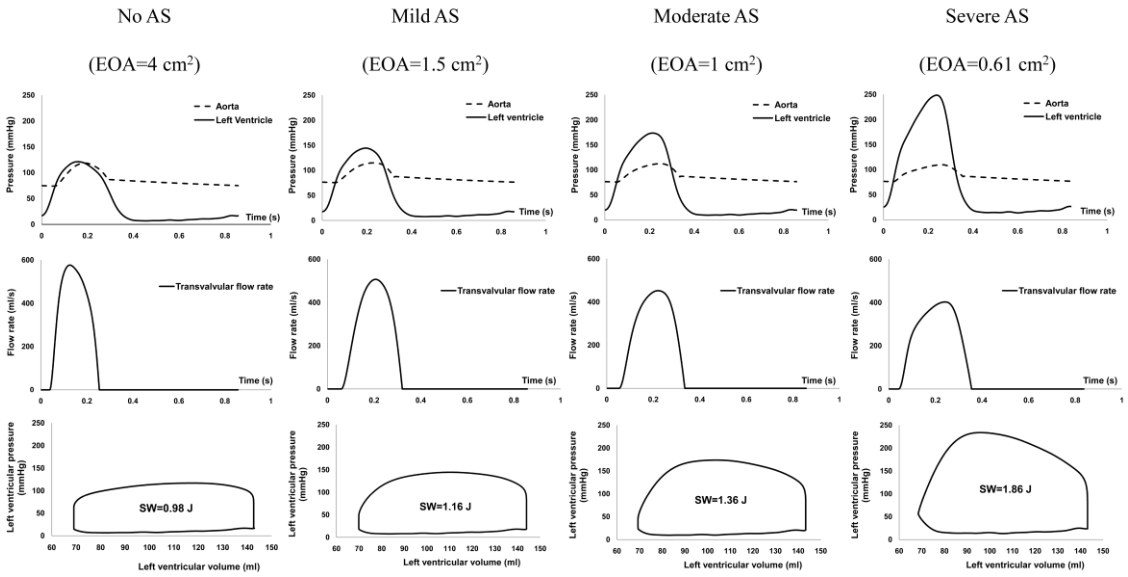

Figure 5.4. Simulated left ventricular and aortic pressure, transvalvular flow waveform and LV stroke work in the case of isolated aortic stenosis (AS). The severity of AS was varied from 0.61 to 4 cm^2. For all cases, stroke volume, heart rate and cardiac output are 75 ml, 70 beats/min and 5.2 l/min, respectively

5.4. Results

5.4.1 Simulation in the presence of an aortic stenosis

Figure 5.4 illustrates four cases simulated using current model: 1) no AS (EOA = 4 cm^2); 2) mild AS (*EOA* = 1.5 cm^2); 3) moderate AS (*EOA* = 1 cm^2); and 4) severe AS (*EOA* = 0.61 cm^2).

As aortic stenosis severity increases, LV peak pressure progressively increases and can reach values as high as 250 mmHg with severe AS. The results also show that, with increasing AS severity, ejection time lengthens and peak transvalvular flow rate occurs later during the ejection phase, which is consistent with previous *in vivo*

studies (Kligfield et al., 1984; Chambers et al., 2005 and Zoghbi et al., 2009). Figure 5.4 also illustrates how LV stroke work varies with AS severity. It can be observed that LV stroke work remains relatively constant about 1 J for $EOA > 1.5$ cm^2. However, when the AS becomes moderate to severe, LV stroke work increases rapidly: moderate AS (1.36 J; increase of 39% with respect to healthy case) and severe AS (1.86 J; increase of 90% with respect to healthy case).

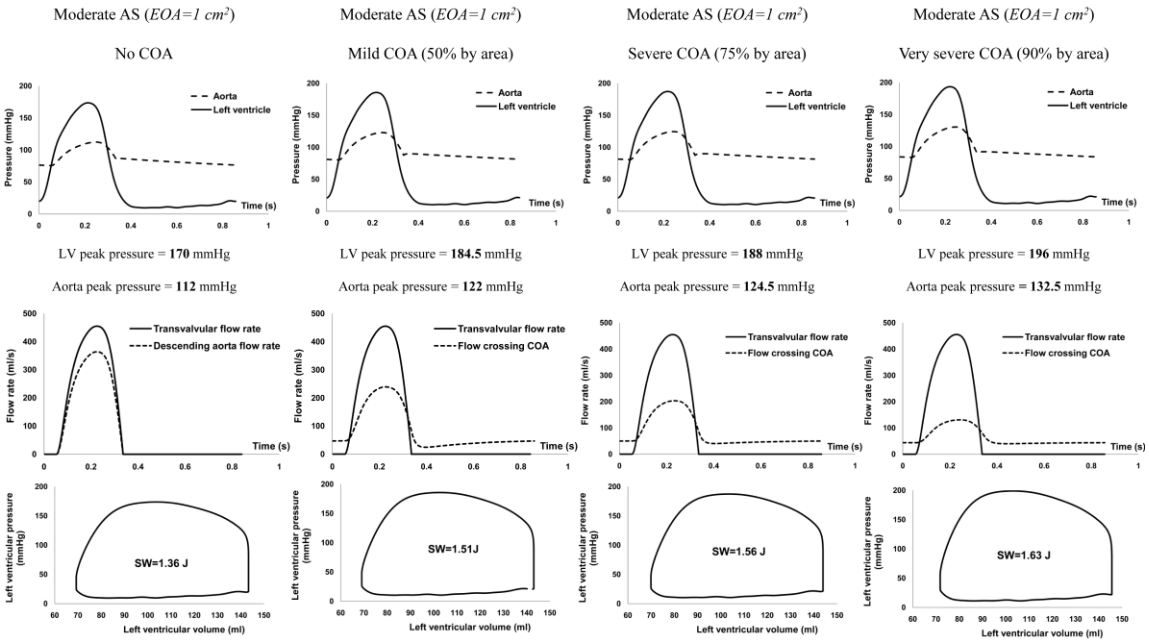

Figure 5.5. Simulated left ventricular and aortic pressure, flow waveforms and stroke work in the case of concomitant aortic stenosis (AS) and coarctation of the aorta (COA). The severity of AS was held constant (EOA = 1.0 cm^2) and the severity of COA was varied from 50% to 90% by area. For all cases, stroke volume, heart rate and cardiac output are 75 ml, 70 beats/min and 5.2 l/min, respectively

5.4.2 Simulation in the presence of coexistent aortic stenosis and coarctation of the aorta

In the majority of cases, COA coexists with aortic stenotic valve (Brickner et al., 2000; Braverman et al., 2005; Hamdan, 2006). Therefore, we performed simulations in order to analyze the effects of both AS and COA on LV stroke work. Figure 5.5 illustrates the effect of progressive narrowing of COA (50%, 75% and 90%) on the pressure waveforms, flow waveforms and LV stroke works for a fixed moderate AS (EOA = 1 cm^2). These simulations reveal that COA will act like a localized resistance by shifting up the pressure waveforms. A severe COA increases both LV and aortic pressures by around 20 mmHg. This has an immediate impact on the LV stroke work which increases from 1.36 J to 1.63 J (increase by 20% compared with the case No-COA and by 66% compared with the healthy case). Figure 5.5 also shows how a COA impacts on the flow distribution between the ascending and descending aorta (Harreveld et al., 1949; Markl et al., 2009). When COA is not present, a small portion of total flow rate (15%) is directed towards aortic arch arteries. However, when a severe COA is present up to 60% of total flow rate is redirected towards upper body including aortic arch branches and potential collaterals. These results are consistent with the results obtained by Riehle et al. (2006) where they showed flow volumes can increase up to 59% from the location of the COA to the diaphragm in patients with severe COA. As a consequence, a large portion of the flow bypasses the COA and the distal perfusion is maintained through collateral vessels (in our study, this is represented by the branch bypassing COA model).

Figure 5.6 illustrates hypothetical cases with normal cardiac output flow conditions (stroke volume = 75 mL, heart rate = 70 bpm, cardiac output = 5.2 L/min). LV stroke work will then only depend upon AS and COA severities. It appears that COA has a smaller impact on LV stroke work than AS with *EOA* = 1 cm^2. Indeed, even a severe COA (90%) induces less additional stroke work (0.27 J) compared to a moderate AS (0.36 J). This can be explained by the fact that an increase in COA severity is compensated partially by a decrease in trans-COA flow rate (see figure 5.5) which is not the case for aortic stenosis, where necessarily the whole blood volume ejected by the heart must pass though the aortic valve (if no major mitral regurgitation is present).

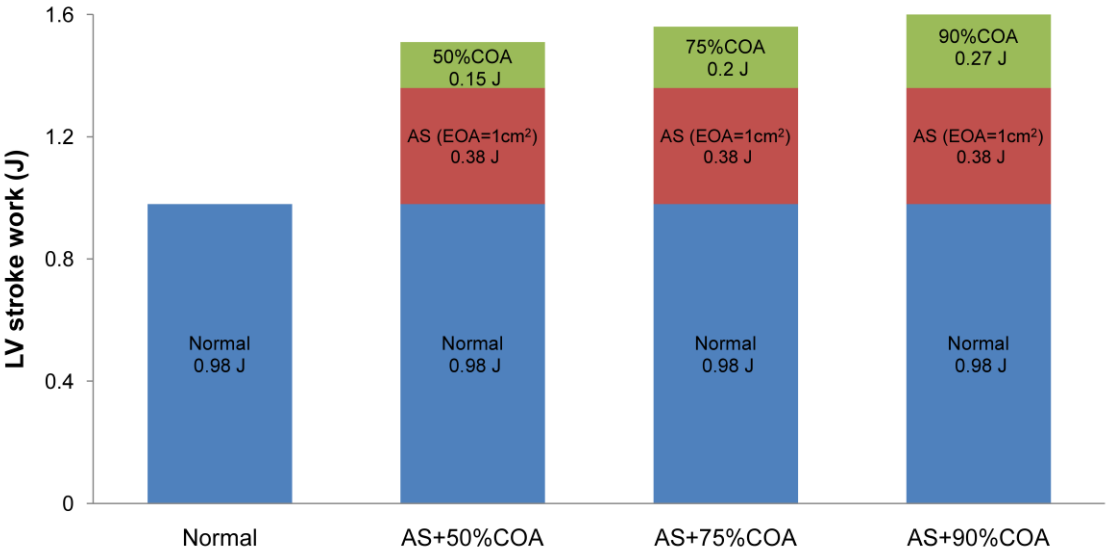

Figure 5.6. Respective contribution of aortic stenosis (AS) and coarctation of the aorta (COA) to the total stroke work. The severity of AS was held constant (effective orifice area (*EOA*) = 1.0 cm^2); and the severity of COA was changed from 50% to 90% by area. For all cases, stroke volume, heart rate and cardiac output are 75 ml, 70 beats/min and 5.2 l/min, respectively

Figure 5.7 better represents the expected influence of AS and COA on left ventricle stroke work. If two hypothetical scenarios (Severe AS + Moderate COA, and Moderate AS + Severe COA) are considered, this plot might help clinicians to provide potential outcomes of the surgery. Indeed, in the case of severe AS (0.61 cm^2) + moderate COA (75%), the estimated LV stroke work will be 2.08 J. Under such conditions, if the valve is replaced, bringing the EOA to around 2.00 cm^2 (typical EOA for high performance prosthetic heart valves) without repairing the COA, LV stroke work will remain around 1.28 J (which is equivalent to the stroke work generated by an AS of EOA = 1.2 cm^2). The benefit of aortic valve replacement is then limited by the persistent overload induced by COA**.** Now, if the COA is repaired without aortic valve replacement, LV stroke work will only decrease from 2.08 J to 1.86 J. A patient under such conditions would not fully benefit from COA surgery, since LV stroke work would remain abnormally elevated (increase by 0.88 J (89.7%) in LV stroke work compared to the healthy case).

For a case with moderate AS (1.0 cm^2) + severe COA (90%), repairing solely the COA will lead only to a decrease in the LV stroke work from 1.63 J to 1.36 J. This operation corrects the vascular component of the left ventricular afterload but not its valvular component related to AS (an increase of 0.38 J (39%) in LV stroke work compared with the healthy case). The benefit of repairing the COA is then limited by the persistent overload induced by AS. Under the same conditions, if now the aortic valve is replaced (bringing the EOA to around 2.00 cm^2) without repairing the COA, LV stroke work will remain around 1.34 J (which is equivalent to the stroke work

generated by an isolated AS of *EOA* = 1 cm^2), limiting then the benefit of aortic valve replacement.

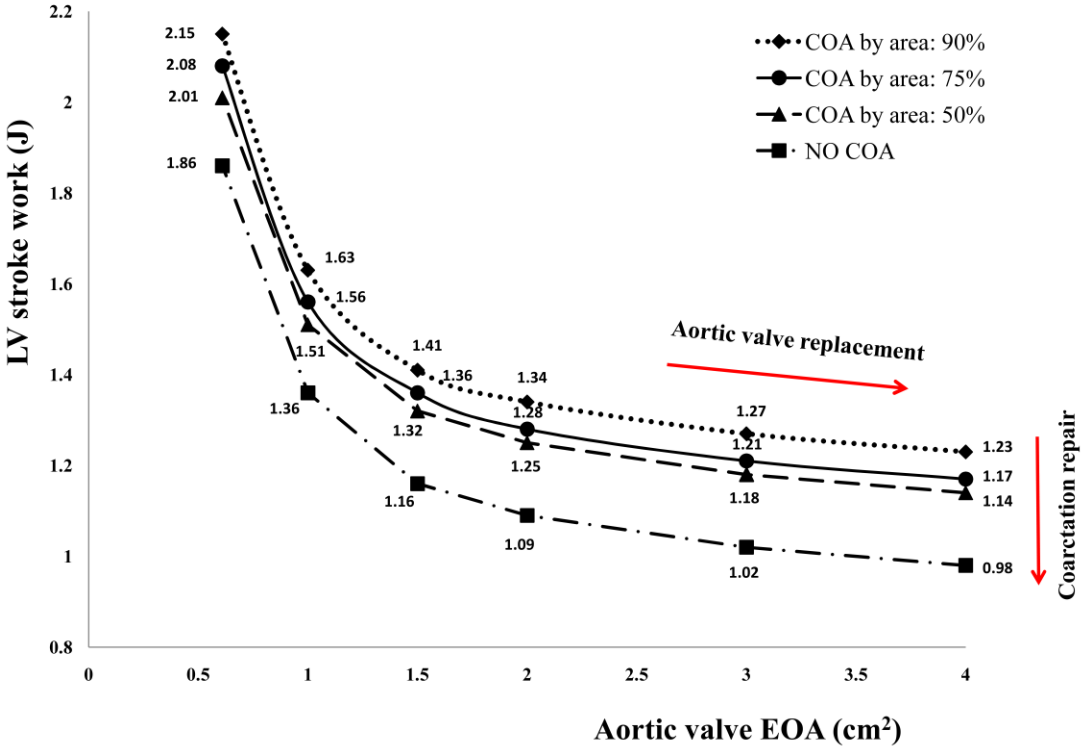

Figure 5.7. Variation of stroke work as a function of aortic stenosis effective orifice area for various coarctation severities. (*EOA*: effective orifice area). For all cases, stroke volume, heart rate and cardiac output are 75 ml, 70 beats/min and 5.2 l/min, respectively

For the two hypothetical cases, if both aortic valve replacement and COA repair are performed, LV stroke work will be reduced to1.09 J, representing an increase of 11% compared to the healthy case. This plot might be, therefore, of great interest when managing patients with COA and AS, in terms of suggesting the optimal sequence of lesion repair and providing potential outcome of the surgery.

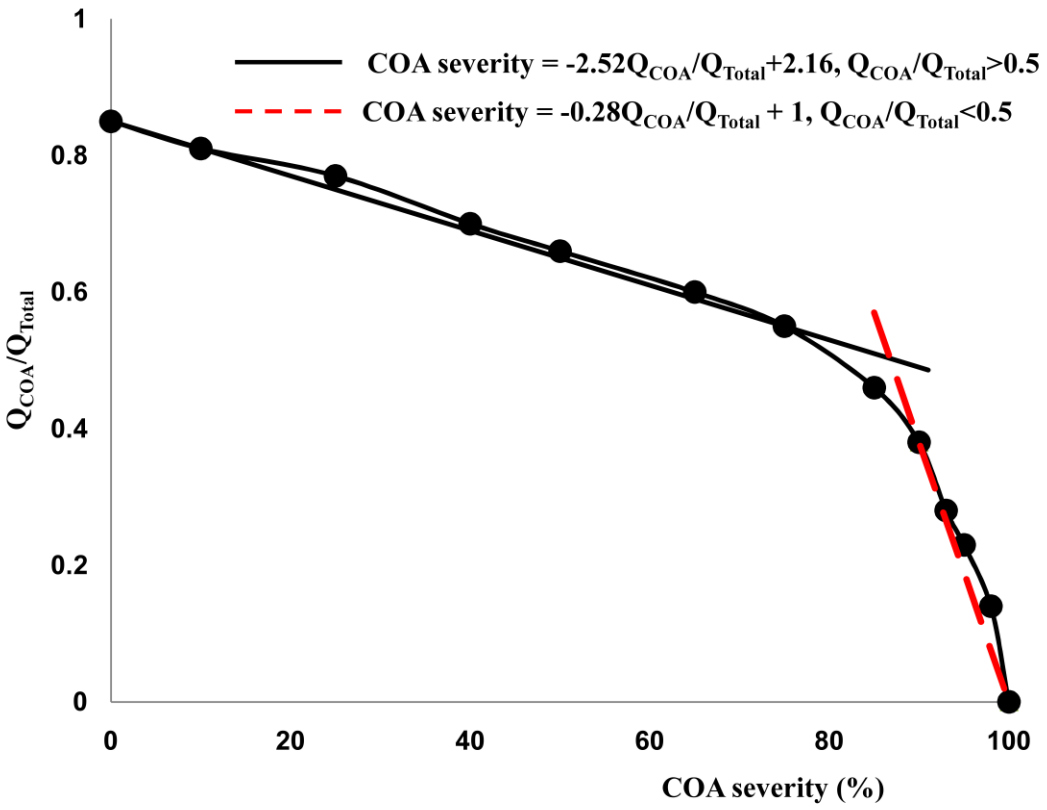

Figure 5.8. Ratio of flow crossing the coarctation of the aorta (Q_{COA}) to the total flow (Q_{Total}) ejected from the left ventricle through the aortic valve for different severities of the COA. For all cases, stroke volume, heart rate and cardiac output are 75 ml, 70 beats/min and 5.2 l/min, respectively

5.5. Potential clinical implications

Figure 5.8 displays predicted relationship between the severity of the COA and the ratio between the flow crossing the COA and the total flow in the ascending aorta (Q_{COA}/Q_{Total}). This relationship can be approximated, for simplicity (a 5th order polynomial fit gives the best results), using two straight lines (Figure 5.8) as follows:

$$COA_{Severity} = -2.52 Q_{COA}/Q_{Total} + 2.16 \qquad Q_{COA}/Q_{Total} \geq 0.5 \tag{5.5}$$

$$COA_{Severity} = -0.28 Q_{COA}/Q_{Total} + 1 \qquad Q_{COA}/Q_{Total} \leq 0.5$$

This is an interesting result as it can allow the estimation of the severity of the COA non-invasively by measuring the average flow rate in the COA region and simply divide it by the average flow rate crossing the aortic valve. These measurements (Q_{COA} and Q_{Total} in equation (5.5)) can be performed clinically by Doppler echocardiography (in patients with good echogenicity) or by MRI. In order to evaluate the accuracy of the COA severity predicted using this relationship, we used two recent works from literature (Kim et al., 2009; Hope et al., 2010). From these studies the ratio (Q_{COA}/Q_{Total}) can easily be obtained. However, unfortunately in none of these studies COA severity was explicitly mentioned. We had then to estimate the severity directly from their figures (with circular shape for the COA as an assumption): Hope et al., (2010): Figure (4)/page 715; Kim et al., (2009): Figures (8-9)/pages 2163-2164. There is very good agreement between the results, in Kim et al. (2009) the COA severity is 89% whereas the one calculated from equation (5.5) is 92%. A similar COA severity is obtained from Hope et al. (2010) and from our equation (94%). This shows that equation (5.5) has the potential to be used in clinical practice to non-invasively evaluate or confirm the severity of COA.

Finally, since the determination of LV stroke work using the lumped parameter model might be difficult to implement in clinic, we suggest a simple analytical formulation allowing the determination of left ventricular peak systolic pressure and then stroke

work non-invasively. Here, P_{LV}, P_S, $(TPG)_{AS}$, $(TPG)_{COA}$, SW and SV are left ventricular systolic pressure, aorta systolic pressure, mean transvalvular pressure gradient, mean trans-COA pressure gradient, stroke work and stroke volume, respectively.

$$P_{LV} = P_S + (\overline{TPG})_{AS} + (Q_{COA}/Q_{Total})(\overline{TPG})_{COA} \tag{5.6}$$

$$SW = P_{LV} \times SV \tag{5.7}$$

It should be noted that in clinical practice, all parameters included in the equations (5.6) and (5.7) can be determined non-invasively: P_S using a sphygmomanometer; $(TPG)_{AS}$ and, $(TPG)_{COA}$ using simplified Bernoulli equation, Q_{COA} and Q_{Total} using Doppler echocardiography (in patients with good echogenicity) or by MRI.

Figure 5.9 illustrates how the left ventricular peak systolic pressure calculated by equation (5.6) correlates with both results computed from the lumped parameter model and measured *in vitro*. There is a very good correlation and concordance between the results (lumped parameter model *vs.* predicted (eq. (5.6): R = 0.96; *in vitro* measurements *vs.* predicted (eq. (5.6): R = 0.98). Figure 5.10 shows that there is a very good correlation and concordance (R = 0.99) between the LV stroke work computed using the lumped parameter model and the one predicted using equations (5.7) (LV peak systolic pressure is predicted using equation (5.6)). Please note that the experimental setup did not allow the determination of *in vitro* LV stroke work. These formulations can be of great interest for the evaluation of patients with multiple lesions like COA and AS.

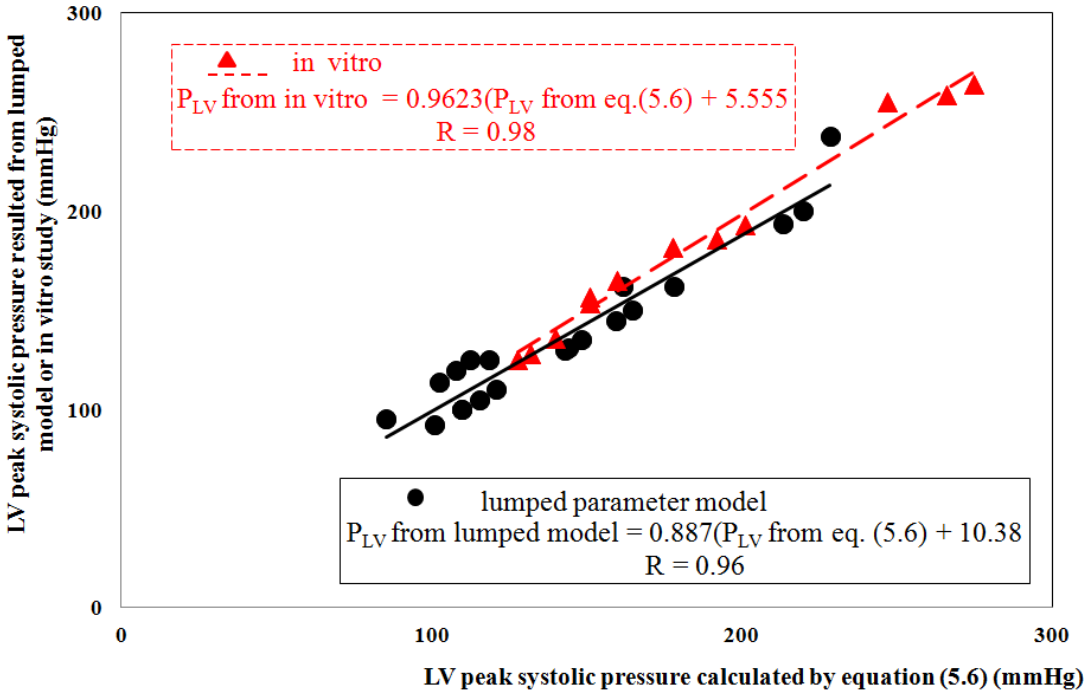

Figure 5.9. Correlations between peak systolic LV pressure calculated from equation (5.6) and the one computed from the lumped parameter model and measured *in vitro* for various severities of COA (50%, 75% and 90% by area) and different aortic valve conditions (*in vitro*: Normal, trileaflet AS and bicuspid AS; lumped parameter model: AS with *EOAs* of 0.61, 1, 1.5 cm^2)

5.6. Limitations of the study

Unfortunately, in the literature, contributions dealing with COA do not provide enough details about the lesion. This did not allow a rigorous validation of the model. We only found few studies by Markl et al. (2009), Kim et al. (2009) and Hope et al. (2010) in which enough information is provided. Thus this limitation should be acknowledged and further validations upon availability of data should be considered. Another potential limitation is that patients with severe COA are usually hypertensive and might exhibit physiological modifications like variation in the heart rate. These modifications have not been taken into account in this study in order to facilitate the

direct comparison between different cases. It should be also noted that the current version of the lumped parameter model does not include a separate compliance for the upper body. Further *in vivo* studies are still required then to determine the value of compliance in patients with COA and to investigate if it can be determined non-invasively. Furthermore, since the development of collaterals is very patient-dependent (some patients with severe COA do not even develop collaterals (Steffens et al., 1994)), we considered a combined resistance that includes both collaterals and aortic branches. It is important to note that, the flow through the combined resistance represents the flow that does not cross the COA. For example for a severe COA, the 60% of the total flow that does not cross the COA represents: the flow towards upper body (including aortic branches and collaterals). Furthermore, in order to better represent the pulmonary venous return flow and the atrio-ventricular interaction, a future model should ideally include a left atrium modeled using a time-varying elastance with a constant venous pressure as input. Finally, it has been reported that ejection fraction, heart rate, and stroke volume are usually normal in adequate concentric left ventricular hypertrophy (Berkin and Ball, 2001). Therefore, our simulations considered that all these parameters remained in the normal range and the ventricle response to the overload induced by AS and COA is through the variation of the peak elastance. Our simulations thus only cover hypertrophy for an ideal left ventricle, able to increase its E_{max} and maintain a constant stroke volume even for large global hemodynamic loads induced by both AS and COA. Although this approach can be less valid for severe AS, it allowed us to compare the stroke work induced by the LV under various COA and AS conditions. Future studies can

investigate the hypertrophic response of the LV to AS and COA in terms mainly of normalization of wall stress and increase in LV wall thickness.

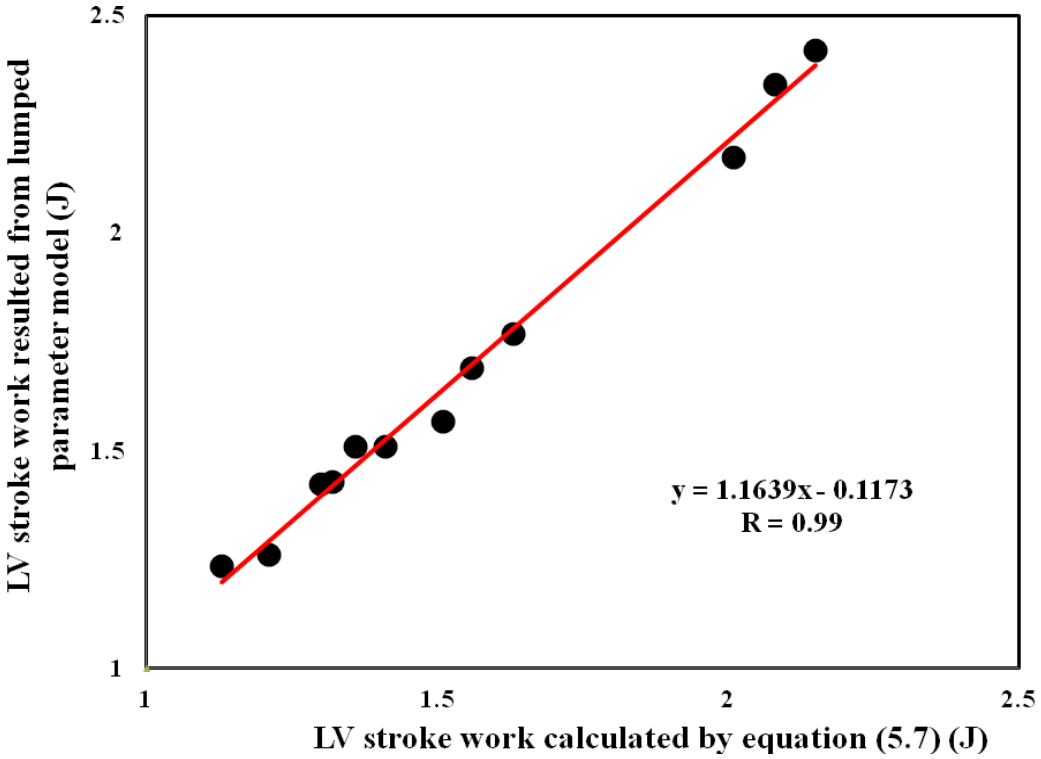

Figure 5.10. Correlation between LV stroke work determined by equation (5.7) and determined using the lumped model for various severities of COA (50%, 75% and 90% by area) and AS (EOA = 0.61, 1.0, 1.5 cm^2)

5.5. Conclusion

In this study, the respective impacts of aortic stenosis and coarctation of the aorta were investigated using a dedicated lumped parameter model. The lumped parameter model is able to estimate left ventricular stroke work using non-invasive data, which makes it suitable for clinical practice. It can be used to guide the choice of the optimal operative procedure (aortic valve replacement and/or COA repaired surgery) by providing potential outcomes of surgery in such patients. This is an important issue

since the benefit of a single procedure can be limited by the remaining overload from the untreated pathology. The interesting results obtained through this study need, however, to be further validated using *in vivo* animal experiments to investigate the effects of physiologic parameters such as heart rate variation, anatomical differences, collaterals, and upper body on pressure, flow, and ventricular function.

Early detection and accurate estimation of COA severity are the most important predictor of successful long-term outcome. However, current clinical parameters used for the evaluation of the severity of COA have several limitations. It is, then, difficult to accurately compare different patients with different COAs or the same patient between different follow ups for patients with both native and repaired coarctation. Therefore, there is a crucial need to introduce new parameters capable of accurately predicting the severity of the COA.

In the following chapter, the limitations of existing parameters for the evaluation of the severity of COA were evaluated and a new approach to predict COA severity was suggested.

Chapter 6

Article 4

6. A New Approach for the Evaluation of the Severity of Coarctation of the Aorta Using Doppler Velocity Index and Effective Orifice Area: *In vitro* Validation and Clinical Implications

Abstract

Early detection and accurate estimation of COA severity are the most important predictors of successful long-term outcome. However, current clinical parameters used for the evaluation of the severity of COA have several limitations and are flow dependent. The objectives of this study are to evaluate the limitations of current existing parameters for the evaluation of the severity of coarctation of the aorta (COA) and suggest two new parameters: COA Doppler velocity index and COA effective orifice area. Three different severities of COAs were tested in a mock flow circulation model under various flow conditions and in the presence of normal and stenotic aortic valves. Catheter trans-COA pressure gradients and Doppler echocardiographic trans-COA pressure gradients were evaluated. COA Doppler velocity index was defined as the ratio of pre-COA to post-COA peak velocities measured by Doppler echocardiography. COA Doppler effective orifice area was determined using continuity equation. The results show that Peak-to-peak trans-COA pressure gradient significantly increased with flow rate (from 83% to 85%). Peak Doppler pressure gradient also significantly increased with flow rate (80% - 85%). A stenotic or bicuspid aortic valve increased Peak Doppler pressure gradient by 20-50%

for a COA severity of 75%. Both COA Doppler velocity index and COA effective orifice area did not demonstrate significant flow dependence or dependence upon aortic valve condition. As a conclusion, COA Doppler velocity index and COA effective orifice area are flow independent and do not depend on aortic valve conditions. They can, then, more accurately predict the severity of COA.

6.1. Introduction

Coarctation of the aorta is a congenital heart disease characterized by narrowing of the isthmus zone, the section of the descending aorta distal to the left subclavian artery. COA is encountered in 0.1% of newborns (De Mey et al., 2001) and is the third most prevailing defect in infants and children (5 to 8% of all congenital heart disorders) (Rao, 1995). COA often coexists with aortic stenosis (AS) (between 30% to 50%) (Brickner et al., 2000; Braverman et al., 2005). Untreated COA, in adults, can result in serious complications such as hypertension, left ventricular hypertrophy, rupture of the aorta and premature coronary artery disease.

The most important predictor of successful long-term outcome in patients with COA is age at time of initial repair (Cohen et al., 1989). Early detection and accurate estimation of COA severity are then of primary importance. However, arm-to-leg blood pressure difference may not accurately represent COA severity and may significantly change with flow rate (Araoz et al., 2003; Swan et al., 2003). Doppler echocardiography and MRI trans-coarctation pressure gradients (TCPGs) are also highly dependent on flow rate and on collateral blood supply (Steffens et al., 1994;

Caravalho et al., 1990). Doppler echocardiography diastolic runoff, the magnitude of the antegrade diastolic flow, has also been suggested to evaluate the severity of COA. However, it is highly dependent on aortic compliance (DeGroff et al., 2003; Tacy et al., 1999). Invasively, catheter TPCGs are highly influenced by the flow rate and pressure recovery phenomena, and peak-to-peak pressure gradient also depends on compliant properties of the aorta (Kadem et al., 2006). Furthermore, using invasive cardiac catheterization might be problematic if multiple follow-up examinations after surgical repair are required knowing that recoarctation is a common occurrence (up to 40%) after COA repair (Araoz et al., 2003; Boxer et al., 1986; Parks et al., 1995).

In summary, the existing parameters to evaluate the severity of COA have significant limitations. It is, then, difficult to accurately compare different patients with different COA severities or a same patient between different follow ups. Therefore, there is a crucial need to introduce new parameters capable of accurately predicting the severity of COA and clinical outcomes. Our hypothesis is that a parameter like COA velocity index defined as the ratio between pre-COA velocity and COA jet velocity and defining a COA effective orifice area using continuity equation measured by Doppler echocardiography can accurately predict the severity of COA. In order to validate our hypothesis, an original *in vitro* study was performed using a mock flow circulation model with different COA severities (50%, 75% and 90% reduction in aortic cross-sectional area), and different aortic valve conditions (normal aortic valve, bicuspid AS and tricuspid AS) under 4 different total flow rates (3, 4, 5 and 6 L/min).

6.2. Methods

We designed and constructed a mock flow circulation model which consisted of a fluid reservoir, a gear pump, realistic elastic three-dimensional models of the aorta with out-of-plane curvature (including: ascending aorta, aortic branches and descending aorta), an adjustable systemic arterial resistance and compliance (Figure 6.1). The fluid (a mixture of 60% water and 40% glycerol, dynamic viscosity of 4 cP) is pumped from an open tank (reservoir), crosses the model of the aortic valve (bioprosthetic valve or silicone models of bicuspid and tricuspid stenoses (Blais et al., 2006)) and directed towards the arterial module (aortic arch arteries and the descending aorta). Under normal conditions (no COA) a small portion of the total flow rate (15%) is directed towards aortic arch branches. However, when a COA is present, it acts like a localized resistance obstructing flow towards the descending aorta. As a consequence, depending on its severity, a larger portion of the total flow rate bypasses the COA (forwarded towards the aortic branches and potential collaterals) (Markl et al., 2009; Hope et al., 2010). Including aortic arch branches is essential for the investigation of COA hemodynamics and represents a significant advantage compared to previous *in vitro* setups dedicated to COA (Seifert et al., 1999; De Mey et al., 2001). In this study, the proportion of the total flow directed towards aortic arch arteries was adjusted with respect to the severity of COA (Table 6.1) following a mathematical modeling of the flow through COA (Keshavarz-Motamed et al., 2011). Then, the flow in aortic arch arteries is redirected towards the main reservoir, while the flow in the descending aorta is directed towards the model of the arterial system. The compliance and the resistance of the systemic arterial

system can be adjusted to ensure physiological aortic pressure waveforms. Instantaneous flow rates were measured by two electromagnetic flowmeters (Carolina Medical Electronics, East Bend, NC, USA, 600 series, accuracy of 1% full scale) at the level of the ascending aorta and aortic arch arteries.

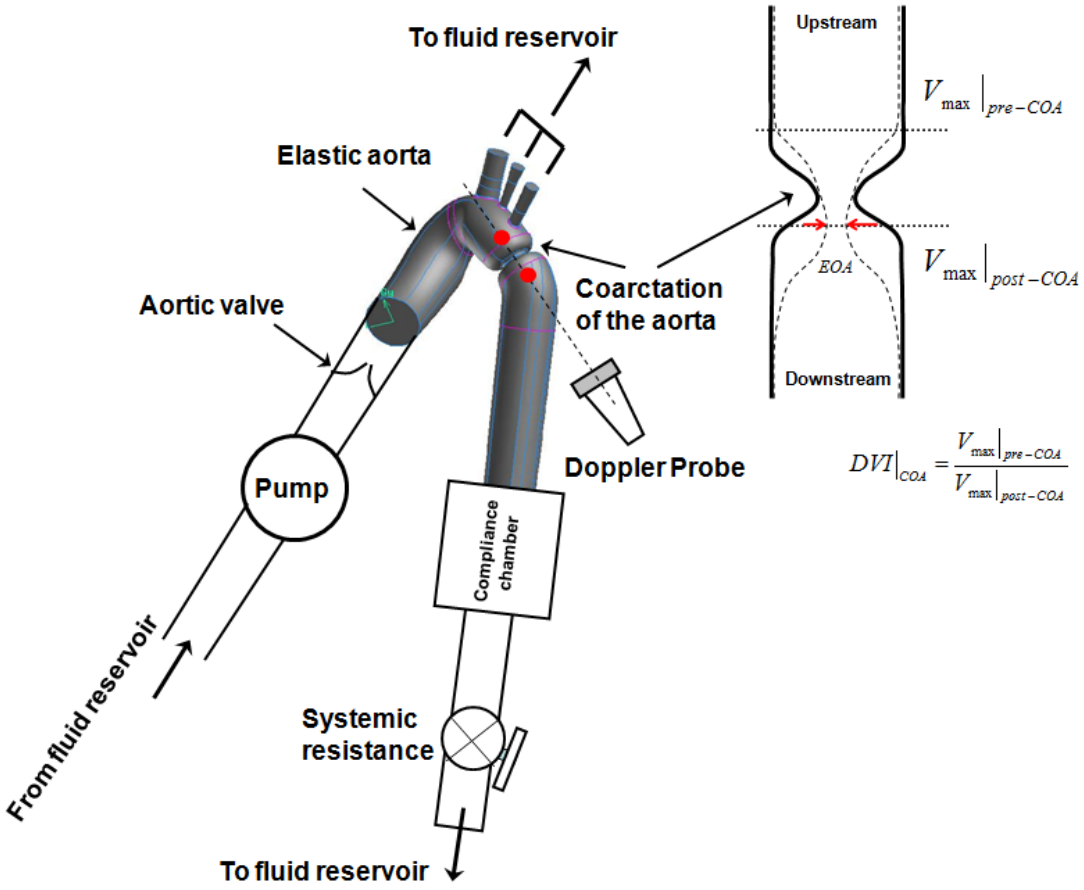

Figure 6.1. Schematic diagram of the *in vitro* flow model

The pressures in the left ventricle, aorta, upstream from the COA and downstream of COA were measured using Millar catheters (Millar Instruments, Houston, TX, USA, SPC 360S, accuracy 0.5% full scale) located 20 mm upstream of the valve, 20 mm downstream of the valve, 20 mm upstream of the COA and 20 mm downstream of

COA, respectively. Pressure measurements were used to determine: peak-to-peak, mean and maximal catheter TCPGs.

Doppler echocardiographic measurements were performed using a HP Sonos 5500 ultrasound machine (Philips healthcare, Best, The Netherlands) with a probe of 2.5 MHz. The probe was positioned on the elastic aorta and the ultrasound beam was oriented towards the COA. Both pre-COA and post-COA instantaneous velocities were measured. The measurements were performed three times and averaged. Doppler echocardiographic measurements included mean ($TCPG_{mean}$) and maximal ($TCPG_{max}$) trans-COA pressure gradients using simplified Bernoulli equation, with considering pre-COA velocity ($TCPG = 4[V^2 - V_P{}^2]$, where V is the velocity at COA vena contracta and V_P is the velocity proximal to COA) and without considering pre-COA velocity ($TCPG = 4V^2$) (De Mey et al., 2001). COA Doppler velocity index was defined as: $DVI|_{COA} = \frac{V_{\max}|_{pre-COA}}{V_{\max}|_{post-COA}}$; i.e., the ratio between upstream COA peak velocity (measured with pulsed-wave Doppler) and downstream COA peak velocity (measured with continuous-wave Doppler) (Figure 6.1). COA Doppler effective orifice area was determined using continuity equation as: $EOA_{COA} = \frac{SV_{COA}}{VTI_{COA}}$. Where SV_{COA} and VTI_{COA} are stroke volume crossing the COA (different from the stroke volume crossing the aortic valve) and velocity-time integral downstream of COA, respectively.

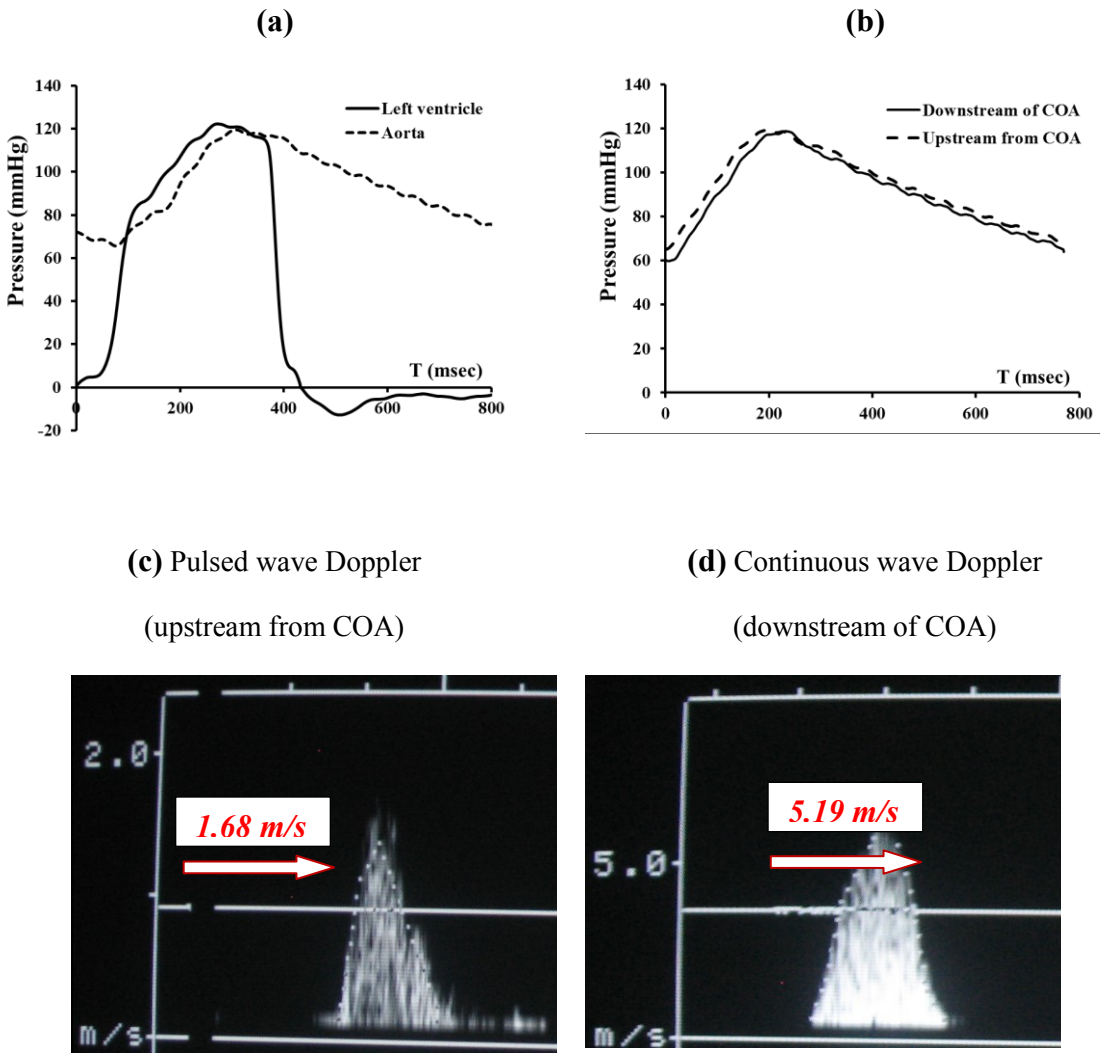

Figure 6.2. Unfiltered pressure wave forms obtained from in vitro model in normal condition (without COA and/or AS): (a) Left ventricle and ascending aorta (b) upstream and downstream of COA, Doppler echocardiographic measurements, (c) continuous wave Doppler measurements (downstream of COA), (d) pulsed wave Doppler measurements (upstream from the COA)

6.2.1 Experimental conditions

First, we validated the model under physiological conditions (Total stroke volume: 70 ml, heart rate: 70 bmp, systolic blood pressure: 120 mmHg, diastolic blood pressure: 70 mmHg).). Figure 6.2 shows the measurement of pressure waveforms in the left ventricle, ascending aorta, upstream and downstream of COA under normal condition (without COA and/or AS). Then, we examined the flow dependence of catheter and Doppler echocardiographic derived parameters with different severities of COA (50%, 75% and 90% reduction in aortic cross-sectional area), and various aortic valve conditions (normal aortic valve (no AS), bicuspid AS (valve effective orifice area = 1.3 cm^2) and tricuspid AS (valve effective orifice area = 1 cm^2)) under 4 different total flow rates (3, 4, 5 and 6 L/min), simulating low to high flow rate (under moderate exercise). Figure 6.2 shows an example of Doppler echocardiographic measurements. Table 6.1 shows the corresponding flow rate crossing the COA. COAs were simulated using small aspect-ratio rigid circular orifices to mimic discrete COAs found in humans.

6.3. Results

6.3.1 Analysis of current methods for the evaluation of the severity of COA

6.3.1.1 Peak-to-peak trans-coarctation pressure gradient (PtoP TCPG)

Figure 6.3 demonstrates that peak to peak trans-coarctation pressure gradient (PtoP TCPG) is significantly affected by the variation of trans-COA flow rate. Indeed, for a severe COA (90%), PtoP TCPG can almost vanish at low flow rate conditions (PtoP

TCPG at 6 L/min: 31 mmHg vs. PtoP TCPG at 3 L/min: 5 mmHg). Under such conditions, the severe COA (90%) will almost completely be masked by a decrease in trans-COA flow rate. These findings were also observed with COA severities of 50% (decrease from 9 mmHg to 1.5 mmHg) and 75% (decrease from 20 mmHg to 2.5 mmHg) (Figure 6.4(a)).

Figure 6.4(b) shows how aortic valve condition can affect PtoP TCPG (for simplicity, only a COA with severity of 75% is displayed). It can be noticed that whatever is aortic valve condition (normal, tricuspid AS or bicuspid AS), PtoP TCPG is significantly reduced when the flow rate is decreased from 6 L/min to 3 L/min. Furthermore, it appears that at a specific flow rate, aortic valve condition interacts with the COA and modifies PtoP TCPG: the presence of a AS reduces the PtoP TCPG value. This effect is more significant at higher flow rate.

6.3.1.2 Doppler echocardiography trans-coarctation pressure gradients (Doppler TCPG)

Figure 6.5(a) shows that peak Doppler TCPG is highly influenced by the variation of trans-COA flow rate. This trend was observed for all COA severities. Interestingly, this flow dependence is more important for severe COA (90%). Indeed, peak Doppler TCPG decreased from 34 mmHg to 5 mmHg for a decrease in flow rate from 6 L/min to 3 L/min. Under such conditions, the severity of COA can completely be masked due to variation of flow rate. For COA severities of 50% and 75%, the decrease in peak trans-COA pressure gradient was from 11 to 2 mmHg and from 23 to 3 mmHg, respectively (Figure 6.5(a)).

Furthermore, since peak Doppler TCPG is a function of the square of the peak trans-COA velocity, it is highly dependent on upstream conditions. This is what is highlighted in figure 6.5(b). The presence of a bicuspid or tricuspid aortic stenosis concomitant to a 75% COA can significantly modify the peak Doppler TCPG value compared to the case with normal aortic valve: the presence of a AS increase the PtoP TCPG value. This effect becomes more significant at higher flow rate. The same behavior was observed for mean Doppler TCPG using simplified Bernoulli equation with and without considering pre-COA velocity.

6.3.2 A new approach for evaluation of COA severity

6.3.2.1 COA Doppler velocity index (DVI_{COA})

Figure 6.6(a) shows that DVI_{COA} is independent from variations of flow rate (for a large range from 3 L/min to 6 L/min). Severity of COA is the only parameter determining DVI_{COA} (for 50% COA: DVI_{COA} = 0.50 ± 0.006; for 75% COA: DVI_{COA} = 0.33 ± 0.011 and for 90% COA: DVI_{COA} = 0.25 ± 0.003). Interestingly, DVI_{COA} is also independent from upstream conditions (valve condition: tricuspid or bicuspid AS). This is illustrated in figure 6.6(b) where for a 75% COA, DVI_{COA} is 0.33 ± 0.011, 0.33 ± 0.005 and 0.33 ± 0.006 for no-AS, tricuspid AS, and bicuspid AS, respectively. Moreover, the same measurements were performed on asymmetric COAs and there was a very good concordance between the results for DVI_{COA} (R = 0.99; SEE = 0.002).

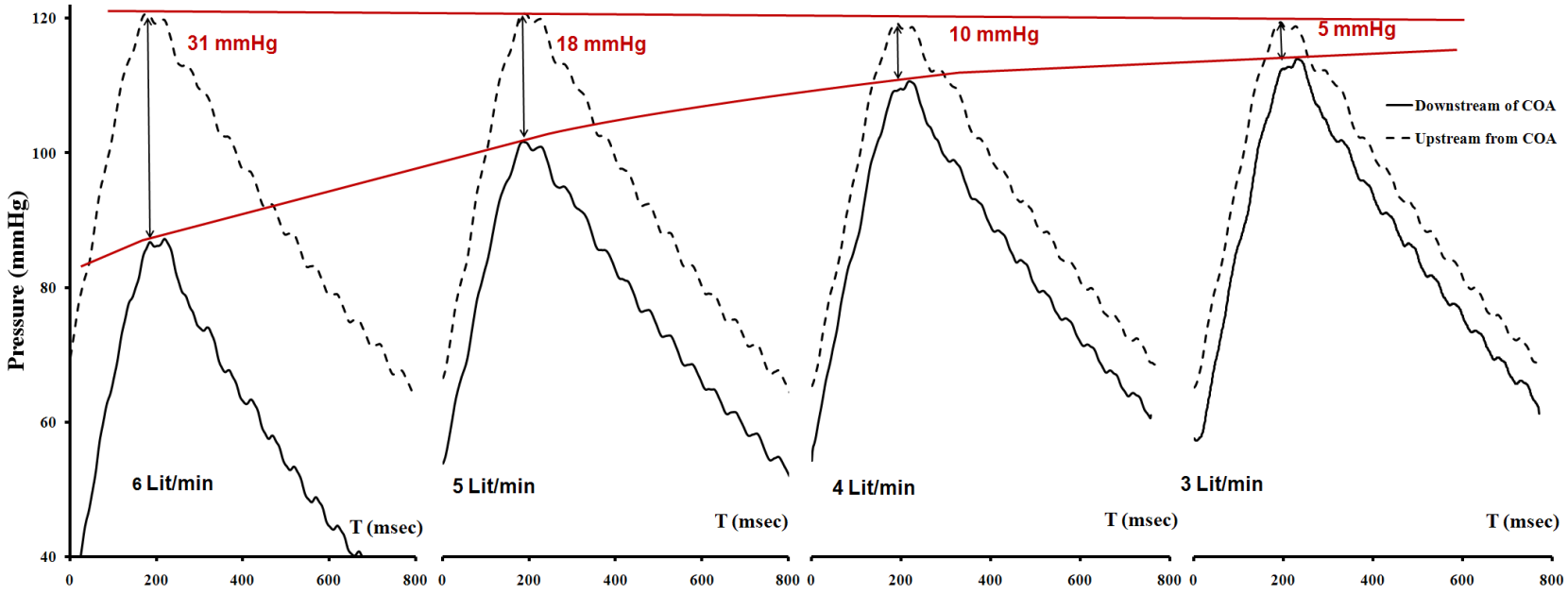

Figure 6.3. Illustration of the variation of peak-to-peak trans-coarctation pressure gradient for a fixed COA (90%) with different flow rates (3-6 L/min). Dotted line represents pressure measurement upstream from the COA and solid line represents pressure measurement downstream of the COA. It can be noticed the significant decrease in peak-to-peak trans-coarctation pressure gradient from 31 mmHg to 5 mmHg

(a)

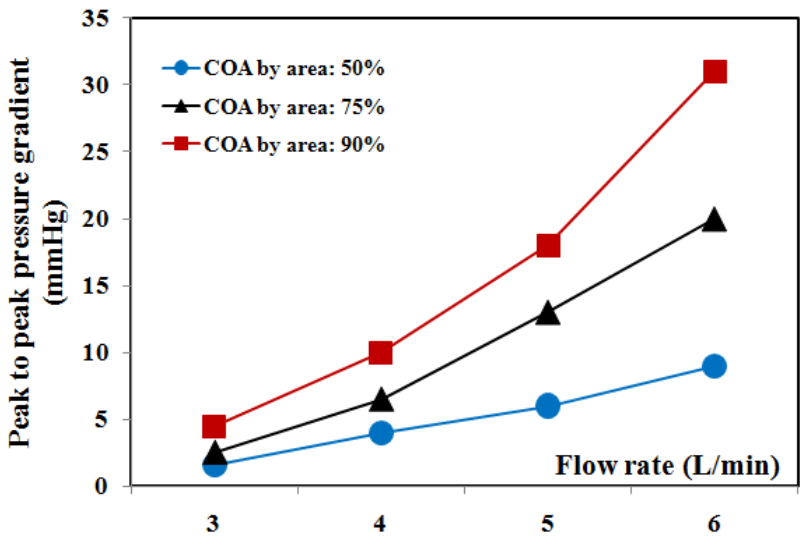

(b)

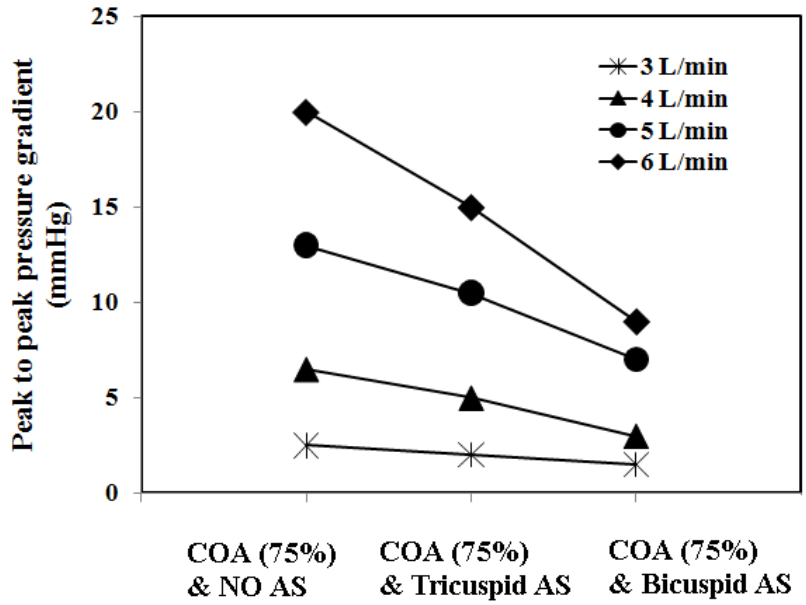

Figure 6.4. (a) Peak-to-peak trans-coarctation pressure gradient with respect to flow rate for different severities of COA (50%, 75% and 90%), (b) Peak-to-peak trans-coarctation pressure gradient with respect to flow rate for a fixed COA (75% by area) and various aortic valve conditions (normal aortic valve, bicuspid AS and tricuspid AS)

6.3.2.2 COA effective orifice area (EOA_{COA})

Figure (6.7(a)) shows that EOA_{COA} is not dependent on flow conditions for a large interval of flow rates (from 3 L/min to 6 L/min). EOA_{COA} is only determined by the severity of COA; 50% COA: EOA_{COA}= 2.67 ± 0.04 cm^2; 75% COA: EOA_{COA}= 1.38 ± 0.02 cm^2 and 90% COA: EOA_{COA}= 0.91 ± 0.02 cm^2. Similar to DVI_{COA}, upstream conditions (valve condition: tricuspid or bicuspid AS) do not influence COA effective orifice area as shown in figure (6.7(b)). This is illustrated in figure (6.7(b)) for a COA with a severity of 75%: No-AS: EOA_{COA}= 1.38 ± 0.02 cm^2; Tricuspid AS: EOA_{COA}= 1.38 ± 0.01 and Bicuspid AS: EOA_{COA}= 1.38 ± 0.02 cm^2. Furthermore, the same measurements were performed on asymmetric COAs and there was a very good correlation between the results for EOA_{COA} (R = 0.99; SEE = 0.05 cm^2).

6.4. Discussions

The most important predictor of successful long-term outcome in patients with COA is age at the time of the initial repair (Cohen et al., 1989). As a consequence, early detection and accurate estimation of COA severity are of primary importance. Several invasive and non-invasive parameters have been suggested in order to evaluate the severity of COA. However, most of these parameters have limitations (see Table 6.2 for summary). It is important, therefore, to develop simple non-invasive, and mainly flow independent, parameters allowing accurate estimation of COA severity.

As defined, COA Doppler velocity index introduced in this study takes into account the pre-COA velocity instead of the distal abdominal velocity as used in the

parameter introduced by Teien et al. (1993). The direct consequence of this choice is that DVI_{COA} is independent from the development of collateral flow, a common occurrence in patients with COA. It is also important to note that: 1) DVI_{COA} is analogous in its definition to the velocity ratio (peak LVOT velocity / Peak aortic velocity; LVOT: left ventricle outflow tract) introduced by Chafizadeh and Zoghbi (1991) in order to evaluate aortic stenosis severity and prosthetic heart valves; 2) DVI_{COA} correlates very well (in this study: R = 0.98) with Euler number (ratio of the pressure loss induces by the COA and the inertial force upstream from the COA) used by De May et al. (2001) to investigate the limitations of Doppler echocardiography in the evaluation of the severity of COA. The major advantage of DVI_{COA} is that it does not rely on the determination of the aortic area upstream from COA, since measuring this area using Doppler echocardiography might be difficult *in vivo*.

The results of this study are based on *in vitro* experiments; this has the advantage of allowing a closer control of the different parameters involved in the determination of COA severity. To be applicable *in vivo* both pre-COA and post-COA velocities have to be measured using Doppler echocardiography. Measuring post-COA velocity using continuous wave Doppler is now a clinical routine. Pre-COA velocity is less commonly measured in patients with COA, except when correcting Doppler trans-COA pressure gradients using pre-COA velocity. For this purpose, two different approaches can be considered: 1) using continuous wave Doppler measurements: by optimizing the gain and the gray scale, it is possible to obtain a Doppler signal including both pre-COA and post-COA velocities (double envelope) (Marx et al.,

1986; Aldousany et al., 1990); 2) using pulsed wave Doppler measurements upstream from the COA (Marx et al., 1986; Aldousany et al., 1990).

In order to evaluate the performance of DVI_{COA} *in vivo*, we used the data published in two previous studies: 1) Marx et al. (1986): prospective study of 32 patients (pre-COA velocity was not measured in 6 patients), catheter trans-COA pressure gradient included only Peak-to-Peak pressure gradient; 2) Aldousany et al. (1990): retrospective study of 11 patients, catheter trans-COA gradient included Peak-to-Peak pressure gradient, maximal instantaneous pressure gradient (not in 2 patients) and mean gradient (not in 1 patient). There was a good correlation between DVI_{COA} and peak-to-peak transvalvular pressure gradient: Aldousany et al. (R = -0.78); Marx et al. (R = -0.79); both studies: (R = -0.78). There was a moderate correlation between DVI_{COA} and catheter mean pressure gradient (R = -0.62). This moderate correlation can be explained by the fact that DVI_{COA} is an instantaneous parameter, while mean catheter pressure gradient is a time-averaged parameter. This argument is further reinforced by considering the very good correlation between DVI_{COA} and maximal catheter instantaneous pressure gradient (R = -0.89).

Although DVI_{COA} and EOA_{COA} behave in the same manner to determine the severity of COA, DVI_{COA} does not inform clinicians on the energy loss induced by the presence of the COA. This can be done using EOA_{COA} and aortic post-COA area. These two parameters can be used to determine an energy loss coefficient (Garcia et al., 2000).

(a)

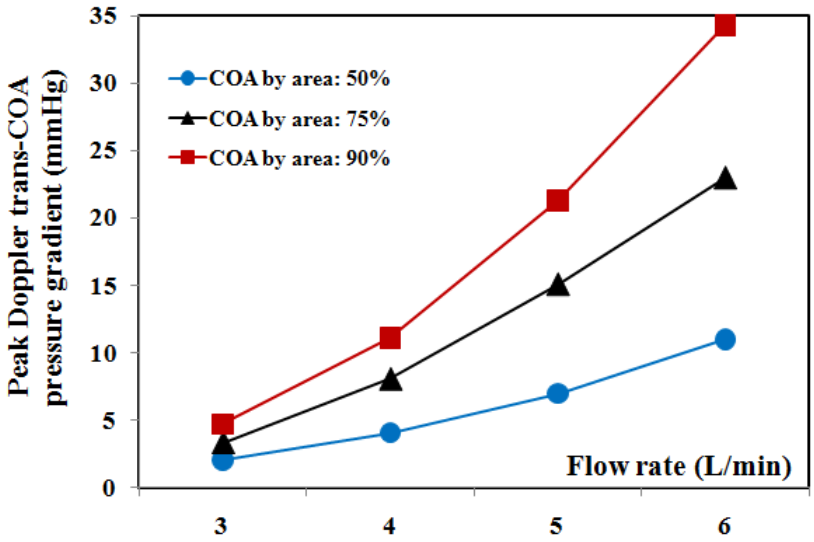

(b)

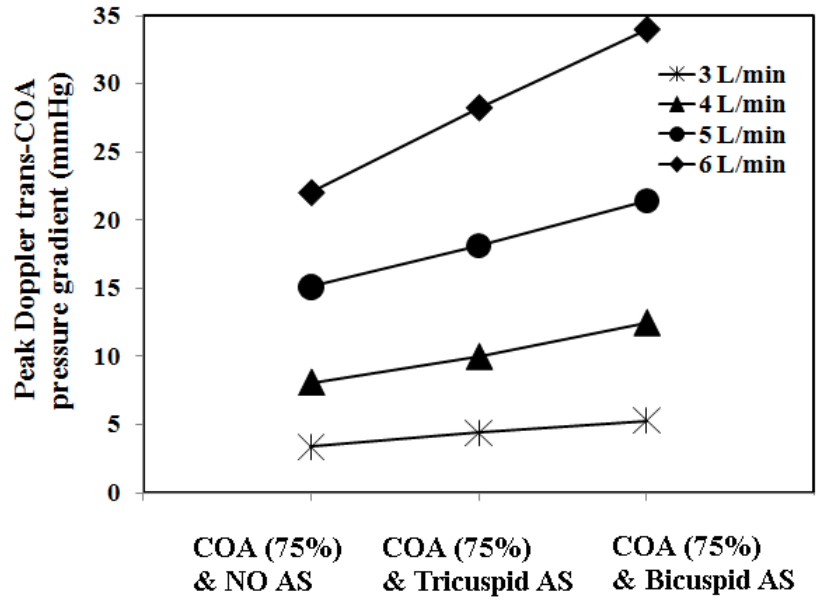

Figure 6.5. (a) Peak Doppler tans-coarctation pressure gradient with respect to flow rate for different severities of COA (50%, 75% and 90%), (b) Peak Doppler tans-coarctation pressure gradient with respect to flow rate for a fixed COA (75%) and different aortic valve conditions (normal aortic valve, bicuspid AS and tricuspid AS)

(a)

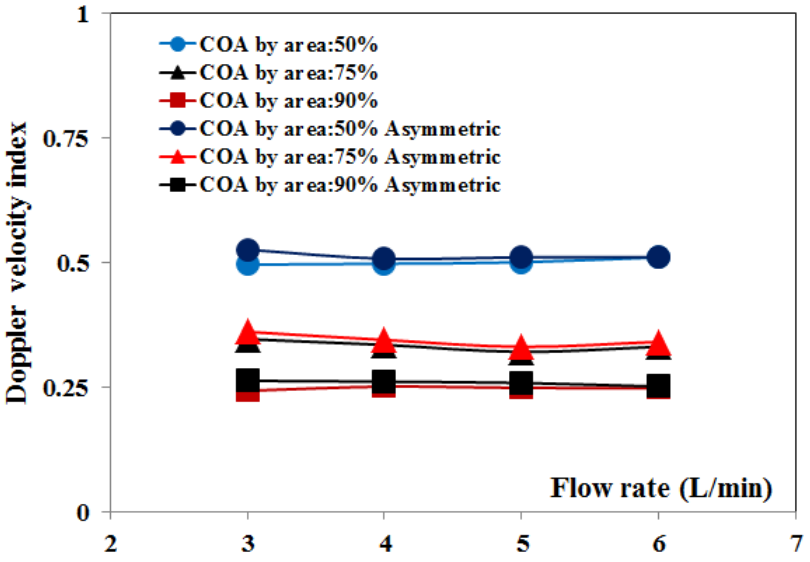

(b)

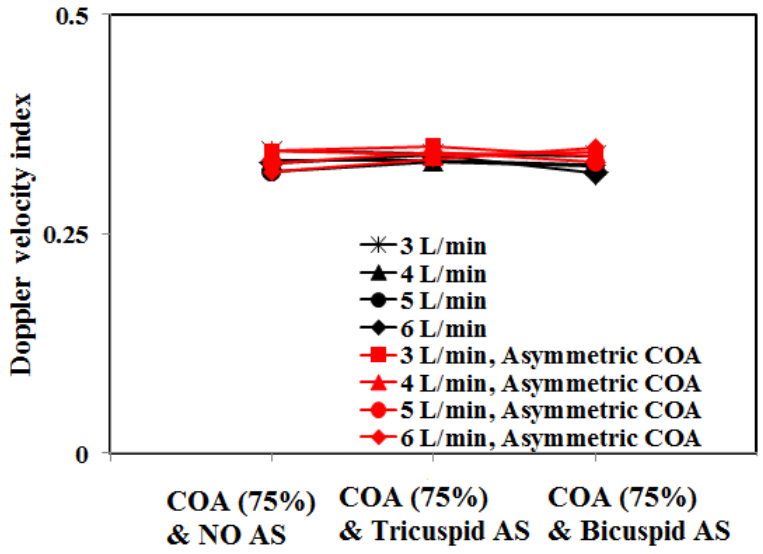

Figure 6.6. (a) Changes in the COA Doppler velocity index as a function of flow rate for different severities of COA (50%, 75% and 90%), (b) Changes in the COA Doppler velocity index as a function of flow rate for a fixed COA (75%) and different aortic valve conditions (normal aortic valve, bicuspid AS and tricuspid AS)

Finally, it should be mentioned that, for the sake of brevity, only the results for symmetric COAs were displayed and discussed. The same measurements were performed on asymmetric COAs and there was a very good correlation and concordance between the results for both DVI_{COA} (R = 0.99; SEE = 0.002) and EOA_{COA} (R = 0.99; SEE = 0.05 cm^2).

6.5. Limitations of the study

In this study, COA was simulated *in vitro* using thin rigid circular orifices. This is not always the case *in vivo* where the geometry of COA might be more complex. However, this correctly represents a discrete COA (one of the most common configurations of COA (Stern et al., 1991)). Also, the model does not consider collateral flows or aortic valve regurgitation. This however should not modify the findings since both DVI_{COA} and EOA_{COA} have been showed in this study to be flow independent. However, it should be mentioned that the determination of EOA_{COA}, *in vitro*, using Doppler echocardiography was feasible because the aortic area in the model was known. It might not be the case, *in vivo*, since measuring aortic area using Doppler echocardiography upstream of the COA is challenging. More accurate results for EOA_{COA} should be obtained using magnetic resonance imaging.

	Total flow rate							
	3 L/min		4 L/min		5 L/min		6 L/min	
	Flow through COA(L/min)	Flow through aortic arch arteries (L/min)	Flow through COA(L/min)	Flow through aortic arch arteries (L/min)	Flow through COA(L/min)	Flow through aortic arch arteries (L/min)	Flow through COA(L/min)	Flow through aortic arch arteries (L/min)
COA 50%	**2.25**	**0.75**	**3**	**1**	**3.5**	**1.5**	**4.5**	**1.5**
COA 75%	**1.8**	**1.2**	**2.4**	**1.6**	**2.85**	**2.15**	**3.6**	**2.4**
COA 90%	**1.5**	**1.5**	**2**	**2**	**2.3**	**2.7**	**2.7**	**3.3**

Table 6.1. Distribution of the flow rate directed toward aortic arch arteries and through COA for different severities of COA used in this study

	Invasive	Dependence			
		Arterial Compliance	Cardiac output	Aortic valve condition (Aortic stenosis)	Collateral flow
Catheter peak to peak pressure gradient	**YES**	**YES**	**YES**	**YES**	**YES**
Catheter maximum and mean pressure gradient	**YES**	**NO**	**YES**	**NO**	**YES**
Doppler maximum and mean pressure gradient	**NO**	**NO**	**YES**	**YES**	**YES**
Velocity ratio Teien et al. (1993)	**NO**	**NO**	**NO**	**YES**	**YES**
COA Doppler velocity index suggested in the current study	**NO**	**NO**	**NO**	**NO**	**NO**

Table 6.2. Summary of invasive and non-invasive parameters suggested to evaluate the severity of COA

(a)

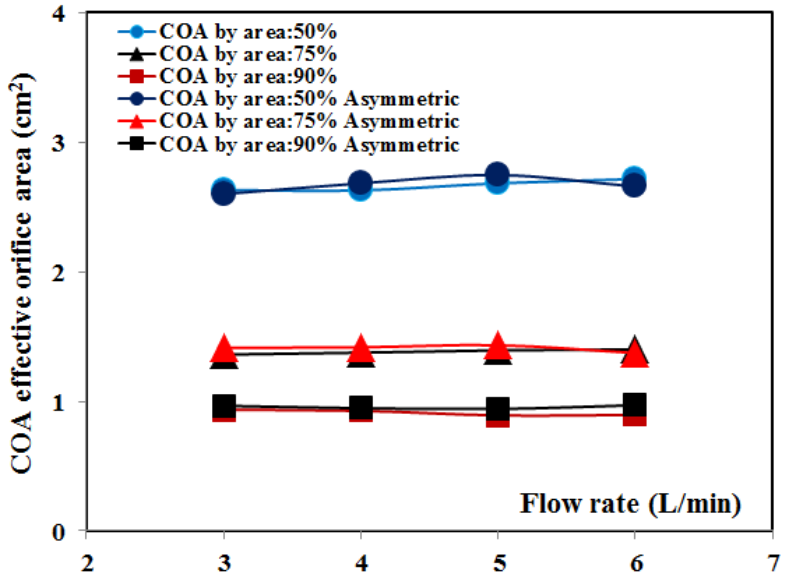

(b)

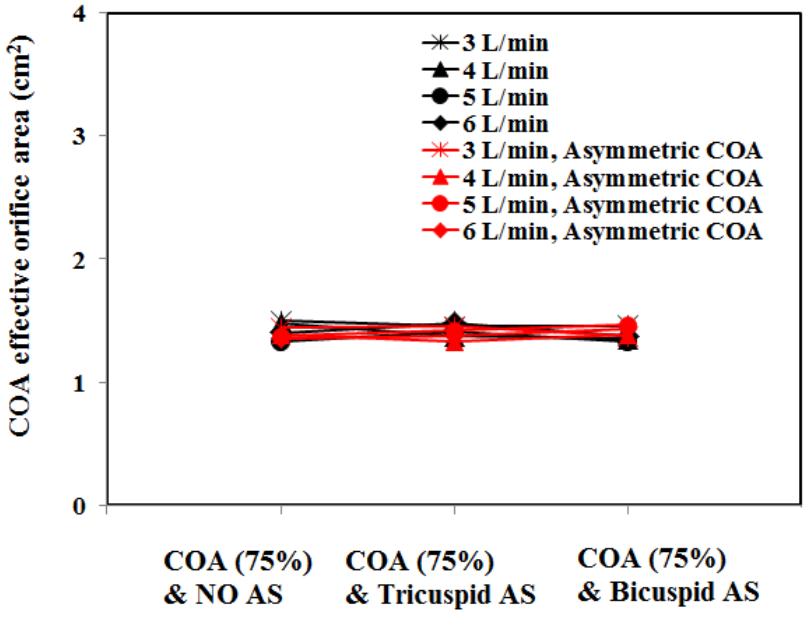

Figure 6.7. (a) Changes in COA effective orifice area as a function of flow rate for different severities of COA (50%, 75% and 90%), (b) Changes in COA effective orifice area as a function of flow rate for a fixed COA (75%) and various aortic valve conditions (normal aortic valve, bicuspid AS and tricuspid AS)

6.6. Conclusions

In this study, we introduced a simple and non-invasive method based on the ratio of pre-coarctation peak velocity and post-coarctation peak velocity measured by Doppler echocardiography. This parameter does not have the limitations of the current methods used to evaluate the severity of COA. Furthermore, we suggested the determination of COA effective orifice area in order to corroborate Doppler echocardiographic measurements and to allow the determination of the energy loss induced by the COA. More *in vivo* studies are still required to determine whether COA Doppler velocity index and COA effective orifice area are reliable in clinical practice.

Chapter 7

7. Conclusions and Future Work

The objective of this study was to understand the hemodynamic of coarctation of the aorta using a comprehensive approach including numerical simulations, mathematical lumped parameter modeling and experimental measurements.

In chapter 3, three dimensional numerical simulations were performed in a curved tube with two constrictions simulating aortic stenosis and coarctation of the aorta. The simple geometry in this study allowed us to explore the effects of coarctation of the aorta and aortic stenosis independent from sophisticated curvatures of the real aorta which impose difficulties in drawing clear conclusions.

In chapter 4, numerical simulations were performed in aortas with realistic geometries in healthy condition and when coarctation coexisted with normal tricuspid and bicuspid aortic valves.

The results of these two chapters indicated significant variation in flow characteristics across the coarctation lesion. This study also revealed that COA caused negative wall shear stress, low time-averaged wall shear stress, and high oscillatory stress index downstream of the COA which are all indicators of atherosclerosis. Furthermore, the presence of aortic stenosis and bicuspid aortic valve can lead to an overestimation of the severity of the coarctation of the aorta using catheterization and Doppler echocardiography.

In chapter 5, the impact of coexisting aortic stenosis and coarctaion of the aorta on the left ventricular workload was investigated by developing a lumped parameter model, based on non-invasive measurements. The results showed that left ventricular stroke work varied from 0.98 J (normal case: no aortic stenosis and no coarctation) up to 2.15 J (severe aortic stenosis :EOA = 0.61 cm^2 + severe coarctation: 90% by area) which means around 120% overload. Our results also showed that the proportion of the total flow rate that will cross the coarctation is significantly reduced when coarctation severity is increased. This model can also be used to optimize the management of patients with coarctation and aortic stenosis in terms of the sequence of lesion repair.

In chapter 6, the limitations of currently used clinical parameters for evaluation of the severity of coarctation were investigated and two new parameters were suggested: coarctation Doppler velocity index and coarctation effective orifice area. These two new parameters are flow independent and do not depend on aortic valve conditions. Therefore, they can more accurately predict the severity of coarctation.

Future work should include performing an experimental work using particle image velocimetry (PIV) to validate the numerical results.

Fluid-solid interaction is another point that should be taken into account in future directions, in order to study the effect of the aortic valve's opening and closing phases.

Furthermore, in cases of severe coarctation of the aorta, the body usually responds by developing a complex pattern of collaterals to limit the impact of the coarctation on

the amount of blood towards the lower parts of the body. It would, therefore, be interesting to model coarctation with collaterals.

Our hypothesis is that COA Doppler velocity index and COA effective orifice area can more accurately predict the severity of coarctation of the aorta. However, *in vivo* studies are required to determine their reliability in clinical practice. Therefore, future plans can be targeted more specifically towards collaboration with clinicians to have further validation *in vivo*.

Furthermore, since the development of collaterals is patient-dependent, in this thesis, a combined resistance that includes both collaterals and aortic branches was considered in a lumped parameter model. It would, therefore, be interesting to model collaterals and aortic branches separately.

Additionally, in order to better represent the pulmonary venous return flow and the atrio-ventricular interaction, a future model should ideally include a left atrium modeled using a time-varying elastance with a constant venous pressure as input.

Current simulations presented in this thesis cover only hypertrophy for an ideal left ventricle, able to increase its E_{max} and maintain a constant stroke volume even for large global hemodynamic loads induced by both AS and COA. Some plans can be targeted for investigation of the hypertrophic response of the LV to AS and COA in terms mainly of normalization of wall stress and increases in LV wall thickness.

References

Aldousany, A.W., DiSessa, T.G., Alpert, B.S., Birnbaum, S.E., Willey, E.S., 1990. Significance of the Doppler-derived gradient across a residual aortic coarctation. Pediatr Cardiol 11, 8--14.

Abbott, M.E., 1928. Coarctation of the aorta of adult type; statistical study and historical retrospect of 200 recorded cases with autopsy; of stenosis or obliteration of descending arch in subjects above age of two years. AM Heart J 3, 574.

Abbruzzese, P.A., Aidala, E., 2007. Aortic coarctation: An Overview. J Cardiovas Med (Hagerstown) 8, 123-128.

Agrawal, Y., Talbot, L., Gong, K., 1978. Laser anemometer study of flow development in curved circular pipes. J Fluid Mech 85, 497-518.

Araoz, P.A., Reddy, G.P., Tarnoff, H., Roge, C.L., Higgins, C.B., 2003. MR findings of collateral circulation are more accurate measures of hemodynamic significance than arm-leg blood pressure gradient after repair of coarctation of the aorta. J Magn Reson Imaging 17, 177-183.

Barton, C.H., Ni, Z., Vaziri, N.D., 2001. Enhanced nitric oxide inactivation in aortic coarctation-induced hypertension. Kidney 60, 1083-1087.

Berger, S.A., Jou, L.D., 2000. Flow in stenotic vessels. Ann Rev Fluid Mech 32, 347-382.

Berkin, K.E., Ball, S.G., 2001. Essential hypertension: the heart and hypertension. Heart 86, 467-475.

Blais, C., Burwash, I.G., Mundigler, G., Dumesnil, J.G., Loho, N., Rader, F., Baumgartner, H., Beanlands, R.S., Chayer, B., Kadem, L., Garcia, D., Durand,

L.G., Pibarot, P., 2006. The Projected valve area at normal flow rate improves the assessment of stenosis severity in patients with low flow, low gradient aortic stenosis. The Multicenter TOPAS Study. Circulation 113, 711-721.

Bluestein, D., Rambod, E., Gharib, M., 2000. Vortex shedding as a mechanism for free emboli formation in mechanical heart valves. J Biomech Eng 122, 125-134.

Boxer, R.A., LaCorte, M.A., Singh, S., Cooper, R., Goldman, M.M., Stein, H.L., 1986. Nuclear magnetic resonance imaging in evaluation follow-up of children treated for coarctation of the aorta. J Am Coll Cardiol 7, 1095-1098.

Borow K.M., Colan S.D., Neumann A., 1985. Altered left ventricular mechanics in patients with valvular aortic stenosis and coarctation of the aorta: effect on systolic performance and late outcome. Circulation 72, 515-522.

Boiron, O., Deplano, V., Pelissier, R., 2007. Experimental and numerical studies on the starting effect on the secondary flow in a bend. J Fluid Mech 574, 109-129.

Bogren, H.G., Buonocore, M.H., 1994. Blood flow measurements in the aorta and major arteries with MR velocity mapping. J Magn Reson Imaging 4, 119-130.

Braverman, A.C., Guven, H., Beardslee, M.A., Makan, M., Kates, A.M., Moon, M.R., 2005. The bicuspid aortic valve. Journal of Current Problems in Cardiology 30, 470-522.

Brickner, M.E., Hillis, L.D. Lange, R.A., 2000. Congenital heart disease in adults. New Engl J Med 342, 256-263.

Brickner, M.E., Hillis, L.D., Lange, R.A., 2000. Congenital heart disease in adults. New Engl J Med 342, 256-63.

Brili, S., Dernellis, J., Aggeli, C., Pitsavos, C., Hatzos, C., Stefanadis, C., Toutouzas, P., 1998. Aortic elastic properties in patients with repaired coarctation of aorta. Am J Cardiol 82, 1140-1143.

Bierman, E.L., 1994. Atherosclerosis and other forms of artherosclerosis, Harrison's Principles of Internal Medicine. 13th ed. New York, NY: McGraw-Hill Book Co., 1106-1116.

Burkhoff, D., Mirsky, I., Suga, H., 2005. Assessment of systolic and diastolic ventricular properties via pressure-volume analysis: A guide for clinical, translational, and basic researchers. Am J Physiol Heart Circ Physiol 289, 501-512.

Caruthers, S.D., Lin, S.J., Brown, P., Watkins, M.P., Williams, T.A., Lehr, K.T., Wickline, S.A., 2003. Practical value of cardiac magnetic resonance imaging for clinical quantification of aortic valve stenosis: comparison with echocardiography. Circulation 108, 2236-2243.

Caravalho, J.S., Redington, A.N., Shinebourne, E.A., Rigby, M., Gibson, D., 1990. Continuous wave Doppler echocardiography and coarctation of the aorta: gradients and flow patterns in the assessment of severity. Heart 64, 133-137.

Cape, E.G., Kelly, D.L., Ettedgui, J.A., Park, S.C., 1996. Influence of stenotic valve geometry on measured pressure gradients and ventricular work: the relationship between morphology and flow. Pediatr Cardiol 17, 155-162.

Caro, C.G., Doorly, D.J., Tarnawski, M., Scott, K.T., Long, Q., Dumoulin, C.L., 1994. Non-Planar Curvature and Branching of Arteries. J Physiol 475, 60.

Celik, I.B., Ghia, U., Roache, P.J., Freitas, C.J., Coleman, H., Raad, P.E., 2008. Procedure for estimation and reporting of uncertainty due to discretization in CFD applications. ASME J Fluids Eng 130, 078001-1-07800, 1-4.

Chafizadeh, E.R., Zoghbi, W.A., 1991. Doppler echocardiographic assessment of the St. Jude Medical prosthetic valve in the aortic position using the continuity equation. Circulation 83, 213-223.

Chang, L.J., Tarbell, J.M., 1985. Numerical simulation of fully developed sinusoidal and pulsatile flow in curved tubes. J Fluid Mech 161, 175-198.

Chambers, J., Rajani, R., Hankins, M., Cook, R., 2005. The peak to mean pressure decrease ratio: a new method of assessing aortic stenosis. Journal of the American Society of Echocardiography 18, 674-678.

Chemla, D., Hébert, J.L., Coirault, C., Zamani, Z., Suard, I., Colin, P., Lecarpentier, Y., 1998. Total arterial compliance estimated by stroke volume-to-aortic pulse pressure ratio in humans. American Journal of Physiology-Heart and Circulatory Physiology 274, 500-505.

Cohen, M., Fuster, V., Steele, P.M., Driscoll, D., McGoon, D.C., 1989. Coarctation of the aorta. Long-term follow-up and prediction of outcome after surgical correction. Circulation 80, 840-845.

Cuming, H.G., 1952. The secondary flow in curved pipes. Aeronautical Research Council Reports and Memoranda 1952, 1-17.

Chu, M.W.A., Adams, C., Torres, P., 2011. Ascending-to-descending aortic bypass and aortic valve replacement for concomitant severe aortic coarctation and

aortic stenosis. Vasc Endovasc Surg, in presss. DOI: 10.1177/1538574410396589.

D'Abreu, A.L., Parsons, C., 1956. Surgical treatment of children with coarctation of the aorta. Br Med J 2 :390-393.

Dash, R.K., Jayaraman, G., Mehta, K.N., 1999. Flow in a catheterized curved artery with stenosis. J Biomech 32, 49-61.

Dazu, V.J., Gibbons, G.H., 1993. Vascular remodeling: mechanisms and implications. J Card Pbar 21, 1-5.

Dean, W.R., 1927. Note on the motion of fluid in a curved pipe. Philos Mag 20, 208-223.

Dean, W.R., 1928. The streamline motion of fluid in a curved pipe. Philos Mag 30, 673-693.

DeGroff, C.G., Orlando, W., Shandas, R., 2003. Insights into the effect of aortic compliance on Doppler diastolic flow patterns seen in coarctation of the aorta: a numeric study. JASE 16, 162-169.

De Mey, S., Segers, P., Coomans, I., Verhaaren, H., Verdonck, P., 2001. Limitations of Doppler echocardiography for the post-operative evaluation of aortic coarctation. J Biomech 34, 951-960

Doby, T., Lowman, R.M., 1961. Demonstration of blood currents with radiopaque streamers. Acta. Radio 55, 272-275.

Engvall, J., Ask, P., Loyd, D., Wranne, B., 1991. Coarctation of the aorta-a theoretical and experimental analysis of the effects of a centrally located arterial stenosis. J Med Biol Eng Comput 29, 291-296.

Engvall, J., Karisson, M., Ask, P., Loyd, D., Nylander, E., Wranne, B., 1994. Importance of collateral vessels in aortic coarctation: computer simulation at rest and exercise using transmission line elements. . J Med Biol Eng Comput 32, 115-122.

Eustice, J., 1910. Flow of water in curved pipes. Proc. R. Soc. London Ser. A. 84, 107-118.

Fawzy, M.E., Awad, M., Hassan, W., Al Kadhi, Y., Shoukri, M., Fadley, F., 2004. Long-term outcome (up to 15 years) of balloon angioplasty of discrete native coarctation of the aorta in adolescents and adults. J Am Coll Cardiol 43, 1062-1067.

Fisher, A.B., Chien, S., Barakat, A.I., Nerem, R.M., 2001. Endothelial cellular response to altered shear stress. American Journal of Physiology. Lung Cellular and Molecular Physiology 281, 529-533.

Friedman, M.H., Hutchins, G.M., Bargeron, C.B., Deters, O.J., Mark, F.F., 1981. Correlation between intimal thickness and fluid shear in human arteries. Atherosclerosis 39, 425-436.

Frouin, F., Mousseaux, E., 2011. Automated estimation of aortic strain from steady-state free-precession and phase contrast MR images. Magn Reson Med 65, 986–993.

Fry, D.L., 1969. Certain histological and chemical responses of the vascular interface to acutely induced mechanical stress in the aorta of the dog. Circ Res. 24, 93-108.

Fung, Y.C., 1981. Mechanical properties of living tissues. New York: Springer.

Frazin, L.J., Lanza, G., Vonesh, M., Khasho, F., Spitzzeri, C., McGee, S., Mehlmann, D., Chandran, K.B., Talano, J., McPherson, D., 1990. Functional chiral asymmetry in the descending thoracic aorta. Circulation 82, 1985-1994.

Gaca, A.M., Jaggers, J.J., Dudley, L.T., Bisset, G.S., 2008. Repair of congenital heart disease: A primer-part 2. Radiology 248, 44-60.

Galt, S.W., Zwolak, R.M., Wanger, R.J., Gilbertson, J.J., 1993. Differential response of arteries and vein grafts to blood flow reduction. J Vasc Surg 17, 563-570.

Gao, F, Watanabe, M, Matsuzawa, T., 2006. Stress analysis in a layered aortic arch model under pulsatile blood flow. Biomed Eng 5, 1-11.

Garcia, D., Pibarot, P., Dumesnil, J.G., Sakr, F., Durand, L.G., 2000. Assessment of aortic valve stenosis severity: A new index based on the energy loss concept. Circulation 101, 765-771.

Garcia, D., Barenbrug, P.J.C., Pibarot, P., Dekker, A.L.A.J., Van Der Veen, F.H., Maessen, J.G., Dumesnil, J.G., Durand, L.G., 2005. A ventricular-vascular coupling model in presence of aortic stenosis. Am J Physiol Heart Circ Physiol 288, 1874-1884.

Garcia, D., Pibarot, P., Durand, L.G., 2005. Analytical modeling of the instantaneous pressure gradient across the aortic valve. J Biomech 38, 1303-1311.

Garcia, D., Durand, L.G., 2006. Aortic stenosis and systematic hypertension, modeling of. Wiley Encyclopedia of Biomedical Engineering, John Wiley & Sons, Inc. 1-13.

Ghalichi, F., Deng, X., Champlain, A.D., Douville, Y., King, M., Guidoin, R., 1998. Low Reynolds number turbulence modeling of blood flow in arterial stenosis. Biorheology 35, 281-294.

Gosman, A.D., Ioannides, E., 1981. Aspects of computer simulation of liquid-fueled combustors. AIAA J 7, 482-490.

Grotenhuis, H.B., Roos, A.D., 2011. Structure and function of the aorta in inherited and congenital heart disease and the role of MRI. Heart 97, 66-74.

Gunthard, J., Buser, P.T., Miettunen, R., Hagmann, A., Wyler, F., 1996. Effects of morphologic restonosis, defined by MRI after coarctation repair on blood pressure and arm-leg and Doppler gradients. Angiology 47, 1073-1080.

Hamakiotes, C.C., Berger, S.A., 1998. Fully developed pulsatile flow in a curved pipe. J Fluid Mech 195, 23-55.

Hamakiotes, C.C., Berger, S.A., 1990. Periodic flows through curved tubes-the effect of the frequency parameter. J Fluid Mech 210, 353-370.

Haldane, J.H., 1983. Coarctation of the aorta in an elderly man. Can Med Assoc J 128, 1298-1299.

Hamdan, M., 2006. Coarctation of the aorta: a comprehensive review. Journal of Arab Neonatology Forum 3, 5-13.

Harreveld, A.V., Feigen, G.A., Lerman, L.S., 1949. Hemodynamics of aortic occlusion. Am J Physiol 157, 168-176.

Herment, A., Lefort, M., Kachenoura, N., Cesare, D.A., Taviani, V., Graves, M.J., Pellot-Barakat, C., Frouin, F., Mousseaux, E., 2011. Automated estimation of

aortic strain from steady-state free-precession and phase contrast MR images. Magn Reson Med 65, 986-993.

Herment, A., Lefort, M., Kachenoura, N., Cesare, D.A., Taviani, V., Graves, M.J., Pellot-Barakat, C., O'Rourke, M., Farnsworth, A., O'Rourke, J., 2008. JACC 1, 749-751.

Hope, M.D., Meadows, A.K., Hope, T.A., Ordovas, K.G., Saloner, D., Reddy, G.P., Alley, M.T., Higgins, C.B., 2010. Clinical evaluation of aortic coarctation with 4D flow MR imaging. J Magn Reson Imaging 31, 711-718.

Hoogstraten, H.W., Kootstra, J.G., Hillent, B., 1996. Numerical simulation of blood flow in an artery with two successive bends. J Biomech 29, 1075-1083.

Hoogstraten, H.W., Kootstra, J.G., Hillent, B., 1996. Numerical simulation of blood flow in an artery with two successive bends. J Biomech 29, 1075-1083.

Hsiai, T.K., Cho, S.K., Honda, H.M., Hama, S., Navab, M., Demer, L.L., Ho, C.M., 2002. Endothelial cell dynamics under pulsating flows: significance of high versus low shear stress slew rates. Ann Biomed Eng 30, 646-656.

Hunt, J.C.R., Wray, A.A., Moin, P., 1988. Eddies, stream, and convergence zones in turbulent flows. Center for Turbulent Research Report CTR-S88 193-208.

Huo, Y., Guo, X., Kassab, G.S., 2008. The flow field along the entire length of mouse aorta and primary branches. Ann Biomed Eng 36, 685-699.

Jin, S., Oshinski, J., Giddens, P.D., 2003. The effects of wall motion and compliance on flow pattern in the ascending aorta. J Biomech Eng 125, 347-354.

Kadem, L., Garcia, D., Durand, L.G., Rieu, R., Dumesnil, J.G., Pibarot, P., 2006. Value and limitations of peak-to-peak gradient for evaluation of aortic stenosis. J Heart Valve Dis 15, 609-616.

Kerber, C.W., Hecht, S.T., Knox, K., Buxton, R.B., Meltzer, H.S., 1996. Flow dynamics in a fatal aneurysm of the basilar artery. AJNR Am J Neuroradiol. 17, 1417-1421.

Keshavarz-Motamed, Z., Garcia, J., Pibarot, P., Larose, E., Kadem, L., 2011. Modeling the impact of concomitant aortic stenosis and coarctation of the aorta on left ventricular workload. J Biomech 16, 2817-2825.

Keshavarz-Motamed, Z., Kadem, L., 2010. 3D pulsatile flow in a curved tube with coexisting model of aortic stenosis and coarctation of the aorta. Med Eng Phys 3, 315-324.

Keshavarz-Motamed, Z., Garcia, J., Maftoon, N., Bedard, E., Chetaille, P., 2011. A new approach for the evaluation of the severity of coarctation of the aorta using Doppler velocity index and effective orifice area: *in vitro* validation and clinical implications. J Biomech, under second review.

Kim, H.J., Vignon-Clementel, I.E., Figueroa, C.A., Ladisa, J.F., Jansen, K.E., Feinstein, J.A., Taylor, C.A., 2009. On coupling a lumped parameter heart model and a three-dimensional finite element aorta model. Ann Biomed Eng 37, 2153-2169.

Kilner, P.J., Yang, G.Z., Mohiaddin, R.H., Firmin, D.N., Longmore, D.B., 1993. Helical and retrograde secondary flow patterns in the aortic arch studied by three-directional magnetic resonance velocity mapping. Circulation 88, 2235-2247.

Klipstein, R.H., Firmin, D.N., Underwood, S.R., Rees, R.S., Longmore, D.B., 1987. Blood flow patterns in the human aorta studied by magnetic resonance. Br Heart J 58, 316-323.

Kligfield, P., Okin, P., Devereux, R.B., Goldberg, H., Borer, J.S., 1984. Duration of ejection in aortic stenosis: effect of stroke volume and pressure gradient. JACC 3, 157-161.

Komai, Y., Tanishita, K., 1997. Fully developed intermittent flow in a curved tube. J Fluid Mech 347, 263-287.

Ku, D.N., Giddens, D.P., Zarins, C.K., Glagov, S., 1985. Pulsatile flow and atherosclerosis in the human carotid bifurcation: positive correlation between plaque location and low and oscillating stress. Arteriosclerosis 5, 292-302.

Kupferminc, M.J., Lessing, J.B., Jaffa, A., Vidne, B.A., Peyser, M.R., 1993. Fetomaternal blood flow measurements and management of combined coarctation and aneurysm of the thoracic aorta in pregnancy. J Acta Obstet Gyn Scan 72, 398-402.

Ku, D.N., Giddens, D.P., Zarins, C.K., Glagov, S., 1985. Pulsatile flow and atherosclerosis in the human carotid bifurcation: positive correlation between plaque location and low and oscillating stress. Arteriosclerosis 5, 292-302.

Li, Y.J., Haga, J.H., Chien, S., 2005. Molecular basis of the effects of shear stress on vascular endothelial cells. J Biomech 38, 1949-1971.

Liu, B., 2007. The influences of stenosis on the downstream flow pattern in curved arteries. Med Eng Phys 29, 868-876.

Lind, L., 2003. Circulating markers of inflammation and atherosclerosis. Atherosclerosis, 169, 203-214.

Lotz, J., Meier, C., Leppert, A., Galanski, M., 2002. Cardiovascular flow measurement with phase-contrast MR. RadioGraphics 22, 651-671.

Lynch, P.R, Bove, A.A., 1969. Patterns of blood flow through the intact heart and its valves. In; LA Brewer III (ed). Prosthetic Heart Valves. Charles C Thomas, Springfield, DL.

Mahadevan, V., Mullen, M.J., 2004. Endovascular management of aortic coarctation, Int J Cardiol 97, 75-78.

Maia, M.M., Aiello, V.D., Barbero-Marcial, M., 2000. Coarctation of the aorta corrected during childhood. Clinical Aspects during Follow-Up. Arquivos Brasileiros De Cardiologia 74, 167-180.

Malek, A.M., Alper, S.L., Izumo, S., 1999. Hemodynamic shear stress and its role in atherosclerosis. AM Med Assoc 282, 2035-2042.

McDonald, D.A., 1974. Blood flow in arteries. Williams and Wilkins, Baltimore, USA.

Marx, G.R., Allen, H.D., 1986. Accuracy and pitfalls of Doppler evaluation of the pressure gradient in aortic coarctation. J Am Coll Cardiol 7, 1379-85.

Markl, M., Arnold, R., Hirtler, D., Muhlen, C.V.Z., Harloff, A., Langer, M., Hennig, J., Frydrychowicz, A., 2009. Three-dimensional flow characteristics in aortic coarctation and poststenotic dilatation. Comput Assist Tomog 33, 776-778.

Miller, P.R., 2007. *In vitro* flow study of a coarctation in an artificial model of the aortic arch and descending aorta. Master thesis, University of Colorado.

Morris, L., Delassus, P., Callanan, A., Walsh, M., Wallis, F., Grace, P., McGloughlin, T., 2005. 3-D Numerical simulation of blood flow through models of the human aorta. J Biomech Eng 127, 767-775.

Mori, D., Yamaguchi, T., 2002. Computational fluid dynamics modeling and analysis of the effect of 3-D distortion of the human aortic arch. Comput Method Biomec 5, 249-260.

Nanton, M.A., Olley, P.M., 1976. Residual hypertension after coarctectomy in children. Am J Cardiol 37, 769-772.

Naruse, T., Tanishita, K., 1996. Large curvature effect of pulsatile flow in a curved tube. J Biomech, 118, 333-340.

Nerem, R.M., 1992. Vascular fluid mechanics, the arterial wall, and atherosclerosis. J Biomech Eng 114, 274-282.

Niederberger, J., Schima, H., Maurer, G., Baumgartner, H., 1996. Importance of pressure recovery for the assessment of aortic stenosis by Doppler ultrasound: role of aortic size, aortic valve area, and direction of the stenotic jet *in vitro*. Circulation 94, 1934-1940.

Oliver, J.M., Gallego, P., Gonzalez, A., Aroca, A., Brett, M., Mesa, J.M., 2004. Risk factors for aortic complications in adults with coarctation of the aorta. J Am Coll Cardiol 44, 1641-1647.

O'Rourke, M., Farnsworth, A., O'Rourke, J., 2008. Aortic dimensions and stiffness in normal adults. Journal of the American College of Cardiology: Cardiovasc Imag 1, 749-751.

Parks, W.J., Ngo, T.D., Plauth, W.H., Bank, E.R., Sheppard, S.K., Pettigrew, R.I., Williams, W.H., 1995. Incidence of aneurysm formation after Dacron patch aortoplasty repair for coarctation of the aorta: long-term results and assessment utilizing magnetic resonance angiography with three dimensional surface rendering. J Am Coll Cardiol 26, 266-271.

Pedersen, E.M., Agerbaek, M., Kristensen, I.B., Yoganathan, A.P., 1997. Wall shear stress and early atherosclerotic lesions in the abdominal aorta in young adults. Eur J Vasc Endovasc Surg 13, 443-451.

Qiu, Y., Tarbell, J.M., 2000. Numerical simulation of pulsatile flow in a compliant curved tube model of a coronary artery. J Biomech 122, 77-85.

Rao, P.S., 1995. Coarctation of the aorta. Seminars in Nephrology 15, 87-105.

Rosenthal, L., 1995. Coarctation of the aorta and pregnancy: report of five cases. Brit Med J 1, 16-18.

Rao, P.S., Galal, O., Smith, P.A., Wilson, A.D., 1996. Five- to 9-year follow-up results of balloon angioplasty of native aortic coarctation in infants and children. J Am Coll Cardiol 27, 462-470.

Riehle, T.J., Oshinski, J.N., Brummer, M.E., Favaloro-Sabatier, J., Mahle, W.T., Fyfe, D.A., Kanter, K. R., Parks, W. J., 2006. Velocity-encoded magnetic resonance image assessment of regional aortic flow in coarctation patients. Ann Thorac Surg 81, 1002-1007.

Ryval, J., Straatman, A.G., Steinman, D.A., Two-equation turbulence modeling of a pulsatile flow in a stenosed tube. J Biomech Eng 126, 625-635.

Sakalihasan, N., Limet, R., Defawe, O.D., 2005. Abdominal aortic aneurysm. Lancet 365, 1577-1589.

Saidi, A.S., Bezold, L.I., Altman, C.A., Ayres, N.A., Bricker, J.T., 1998. Outcome of pregnancy following intervention for coarctation of the aorta. AM J Cardiol 82, 786-788.

Sciolaro, C., Copeland, J., Cork, R., Barkenbush, M., Donnerstein, R., Goldberg, S., 1991. Longterm follow-up comparing subclavian flap angioplasty to resection with modified oblique end-to-end anastomosis. Thorac Cardiovasc Surg 101, 1-13.

Secchi, F., Iozzelli, A., Papini, G.D.E., Aliprandi, A., Di Leo, G., Sardanelli, F., 2009. MR imaging of aortic coarctation. Radiol med 2009; 114, 524-537.

Senzaki, H., Iwamoto, Y., Ishido, H., Masutani, S., Taketazu, M., Kobayashi, T., Katogi, T., Kyo, S., 2008. Ventricular-vascular stiffening in patients with repaired coarctation of aorta: integrated pathophysiology of hypertension. Circulation 118, 191-198.

Shahcheraghi, N., Dwyer, H.A., Cheer, A.Y., Barakat, A.I., and Rutaganira, T., 2002. Unsteady and three-dimensional simulation of blood flow in the human aortic arch. J Biomech 124, 378-387.

Seifert, B.L., DesRochers, K., Ta, M., Giraud, G., Zarandi, M., Gharib, M., Sahn, D.J., 1999. Accuracy of Doppler methods for estimating peak-to-peak and peak instantaneous gradients across coarctation of the aorta: An *in vitro* Study. J AM SOC Echocardiog 12, 744-753.

Segadal, L., and Matre, K., 1987. Blood velocity distribution in the human ascending aorta. Circulation, 77, 90-100.

Suarez de Lezo, J., Pan, M., Romero, M., et al., 1999. Immediate and follow-up findings after stent treatment for severe coarctation of aorta. Am J Cardiol 83, 400-406.

Segers, P., Stergiopulos, N., Westerhof, N., Wouters, P., Kolh, P., Verdonck, P., 2003. Systemic and pulmonary hemodynamics assessed with a lumped-parameter heart-arterial interaction model. J Eng Math 47, 185-199.

Segers, P., Steendijk, P., Stergiopulos, N., Westerhof, N., 2001. Predicting systolic and diastolic aortic blood pressure and stroke volume in the intact sheep. J Biomech 34, 41-50.

Segers, P., Stergiopulos, N., Westerhof, N., 2000. Quantification of the contribution of cardiac and arterial remodeling to hypertension. Hypertension 36, 760-765.

Segers, P., Stergiopulos, N., Westerhof, N., 2002. Relation of effective arterial elastance to arterial system properties. AM J Physiol Heart C 282, 1041-1046.

Senzaki, H., Chen, C.H., Kass, D.A., 1996. Single-beat estimation of end-systolic pressure-volume relation in humans. A new method with the potential for noninvasive application. Circulation 94, 2497-2506.

Steffens, J.C., Bourne, M.W., Sakuma, H., O'Sullivan, M., Higgins C.B., 1994. Quantification of collateral blood flow in coarctation of the aorta by velocity encoded cine magnetic resonance imaging. Circulation 90, 937-943.

Suga, H., Sagawa, K., Shoukas, A.A., 1973. Load independence of the instantaneous pressure-volume ratio of the canine left ventricle and effects of epinephrine and heart rate on the ratio. Circulation Research 32, 314-322.

Sun, Y., Sjoberg, B.J., Ask, P., Loyd, D., Wranne, B., 1995. Mathematical model that characterizes transmitral and pulmonary venous flow velocity patterns. American Journal of Physiology-Heart and Circulatory Physiology 268, 476-489.

Suzuki, J., Shimamoto, R., Nishikawa, J., Tomaru, T., Nakajima, T., Nakamura, F., Shin, W.S., Toyo-oka, T., 1998. Vector analysis of the hemodynamics of atherogenesis in the human thoracic aorta using MR velocity mapping. AJR 171, 1285-1290.

Swan, L., Goyal, S., Hsia, C., Hechter, S., Webb, G., Gatzoulis, M.A., 2003. Exercise systolic blood pressures are of questionable value in the assessment of the adult with a previous coarctation repair. Heart 89, 189-192.

Stern, H.C., Locher, D., Wallnofer, K., Weber, F., Scheid, K.F., Emmrich, P., Buhlmeyer, K., 1991. Noninvasive assessment of coarctation of the aorta: comparative measurements by two-dimensional echocardiography, magnetic resonance, and angiography. Pediatr Cardiol 12, 1-5.

Sturm, C., Li, W., Woodard, J., Hwang, N., 1992. Fluid mechanics of left ventricular assist system outflow housings. ASAIO J 38, 225-227.

Tan, F.P.P., Borghi, A., Mohiaddin, R.H., Wood, N.B., Thom, S., Xu, X.Y., 2009. Analysis of flow patterns in a patient-specific thoracic aortic aneurysm model. Comput Struct 87, 680-690.

Tanné, D., Kadem, L., Rieu, R., Pibarot, P., 2008. Hemodynamic impact of mitral prosthesis-patient mismatch on pulmonary hypertension: an in silico study. J Appl Physiol 295, 1916-1926.

Tadros, T.M., Klein, M.D., Shapira, O.M., 2009. Ascending aortic dilatation associated with bicuspid aortic valve: pathophysiology, molecular biology, and clinical implications, Circulation 119, 880-890.

Tacy, T.A., Baba, K., Cape, E.G., 1999. Effect of aortic compliance on Doppler diastolic flow pattern in coarctation of the aorta. J Am Soc Echocardiogr 12, 636-642.

Teien, D.E., Wendel, H., Bjornebrink, j., Ekelund, L., 1993. Evaluation of anatomical obstruction by Doppler echocardiography and magnetic resonance imaging in patients with coarctation of the aorta. Heart 69, 352-355.

Thomson, J., 1876. On the origin of windings of rivers in alluvial plains, with remarks on the flow of water around bends in pipes. Proc. R. Soc. London Ser. A. 25, 5-8.

Thanopoulos, B.D., Hadjinikolaou, L., Konstadopoulou, G.N., Tsaousis, G.S., Triposkiadis, F., Spirou, P., 2000. Stent treatment for coarctation of the aorta: intermediate term follow up and technical considerations. Heart 84, 65-70.

Tse, K.M., Chiu, P., Lee, H.P., Ho, P., 2011. Investigation of hemodynamics in the development of dissecting aneurysm within patient-specific dissecting aneurismal aortas using computational fluid dynamics (CFD) simulations. J Biomech 44, 827-836.

Voelker, W., Reul, H., Ing, G.N., Ing, T.S., Ing, B.S., Ing, A.S., Karsch, K.R., 1995. Comparison of valvular resistance, stroke work loss, and Gorlin valve area for quantification of aortic stenosis: an *in vitro* study in a pulsatile aortic flow model. Circulation 91, 1196-1204.

Vitarelli, A., Conde, Y., Cimino, E. et al., 2007. Assessment of ascending aorta distensibility after successful coarctation repair by strain Doppler echocardiography. JASE 21, 729-736.

Vogt, M., Kühn, A., Baumgartner, D., Baumgartner, C., Busch, R., Kostolny, M., Hess, J., 2005. Impaired elastic properties of the ascending aorta in newborns before and early after successful coarctation repair: proof of a systemic vascular disease of the prestenotic arteries. Circulation 111, 3269-3273.

Ward, C., 2000. Clinical significance of the bicuspid aortic valve. Heart 83, 81-85.

Wen, C. Y., Yang, A. S., Tseng, L. Y., Chai, J. W., 2010. Investigation of pulsatile flowfield in healthy thoracic aorta models. Ann Biomed Eng 38, 391-402.

Williams, G.S., Hubbell, C.W., Fenkell, G.H., 1902. Experiments at Detroit. Mich., on the effect of curvature upon the flow of water in pipes. Trans ASCE, 471-196.

Womersley, J.R., 1957. The mathematical study of the arterial circulation in a state of oscillatory motion. Tech. Rep. WADC-TR, Wright Air Dev. Cent, 56-614.

Wood, N.B., Weston, S.J., Kilner, P.J., Gosman, A.D., Firmin, D.N., 2001. Combined MR imaging and CFD simulation of flow in the human descending aorta. J Magn Reson Imaging 13, 699-713.

Xu, J., Shiota, T., Omoto, R., Zhou, X., Kyo, S., Ishii, M., Rice, M.J., Sahn, D.J., 1997. Intravascular ultrasound assessment of regional aortic wall stiffness, distensibility, and compliance in patients with coarctation of the aorta. American Heart Journal 134, 93-98.

Yao, H. Ang, K.C., Yeo, J.H., Sim, K.W., 2000. Computational modeling of blood flow through curved stenosed arteries", Med Eng Phys 24, 163-168.

Yao, L.S., Berger, S.A., 1975. Entry flow in a curved pipe. J Fluid Mech 67, 177-210.

Zarandi, M., Gharib, M., 2000. Pulsatile flow in curved vessels. Proc 22nd annual EMBS international conference 249-250.

Zarandi, M.M., 2000. Steady and pulsatile flow in curved vessels. PhD thesis, California Institute of Technology, California.

Zarins, C.K., Giddens, D.P., Bharadvaj, B.K., Sottiurai, V.S., Mabon, R.F., Glagov, S., 1983. Carotid bifurcation atherosclerosis: quantitative correlation of plaque localization with flow velocity profiles and wall shear stress. Circ Res. 53, 502-514.

Zalosh, R.G., Nelson, W.G., 1991. Pulsating flow in a curved tube. J Fluid Mech 59, 693-705.

Zoghbi, W.A., et al., 2009. Recommendations for evaluation of prosthetic valves with echocardiography and Doppler ultrasound. JASE 22, 975-1014.